We are grateful to the referees for their constructive feedback and the time they spent reviewing our manuscript. This helped us to improve the presentation, while results and conclusions remain unchanged. Below are our responses (in **bold**) to the referee comments (in *italics*). The list of relevant changes made in the manuscript are in red. Line numbers refer to the originally submitted manuscript.

Referee #1

Fundamental remarks:

1. Weathering vs sedimentation: It is said that when sedimentation is included in the model the atmospheric Δ14C strongly decreases in comparison to an atmosphere-ocean model version only. I believe this is naming the wrong process. My understanding of the model description is, that weathering is the process that brings 14C-free C into the system, so it is carbonate weathering, that is fundamental for the 14C cycle. It is clear that once weathering input (of alkalinity and DIC to the ocean) is considered also sedimentation as sink needs to be implemented (otherwise the carbon cycle would run away with an ocean accumulating alkalinity, and subsequent changes to atmospheric CO2 levels), but sedimentation is not the important process here that changes Δ14C. This might then also lead to a different name of the model configuration now called OCN-SED.

Weathering fluxes are an important component of the global carbon cycle and input to the ocean from terrestrial weathering of carbonate and silicate rocks and volcanic emissions is included in our model to balance material loss by burial of particulate organic matter, calcium carbonate, and opal at the sea floor. See also our response to the following comment #2. Potential further changes in weathering fluxes may have been very important for past changes in $\delta^{13}C$ but are largely irrelevant for the present study with its focus on $\Delta^{14}C$. What we are interested in demonstrating here is that a change in the global ocean carbon inventory linked with the weathering/sedimentation balance is a potentially important factor affecting atmospheric $\Delta^{14}C$ levels. Also note that the nomenclature of the model configurations is meant to describe the global carbon reservoirs (model components) under consideration, so, e.g., model configuration OCN-SED includes the ocean model and the sediment model. We will modify the text to make this clearer.

We have modified the discussion in Sect. 3.1 such that it is now clear that what's important for the long-term response of $\Delta^{14}C$ to perturbations in the ocean carbon cycle is the interaction with the ocean sediments and the imbalance between weathering and sedimentation, e.g., on lines 336-338:

The response of $\Delta^{14}C_{atm}$ to various perturbations depends on the magnitude of the change in the ocean carbon inventory, with a larger change achieved by considering the interaction with the ocean sediments and the imbalance between weathering and sedimentation (see Fig. 5e,f).

We have also added a more detailed description of the model's representation of weathering fluxes in Appendix A (see next point).

2. No details on weathering are given, but since it is said, that 14C-free C is entered via weathering I have to assume, this implies carbonate weathering. However, it need to be clarified (and maybe corrected?), that in carbonate weathering, 50% of the carbon that enters the ocean as weathering product (bicarbonate ion, HCO−3 , which changes DIC and alkalinity in the ocean) comes from rocks (14C-free), and 50% has its origin in atmospheric CO2 with its atmospheric 14C-signature. For silicate weathering, also bringing HCO−3 to the ocean, 100% of the carbon has its origin in the atmosphere. Is silicate weathering considered? For details see, for example, Colbourn et al. (2013). Without checking on recent updates, I believe both silicate and carbonate weathering contributed about a similar amount of HCO−3 input into the ocean. At least in a study some years ago (Hartmann et al., 2009) in present day weathering the CO2 consumption is twice as big in silicate than in carbonate weathering, but since in carbonate weathering 50% of the C has its origin from rocks, both processes should contribute about the same. Since weathering is the relevant process for this paper more details on its implementation in the model should be included. From the Appendix I understood, that weathering rates are constant in time, but please give their numbers, which would be especially of interest to other modellers doing similar things. Also consider in a discussion, that missing temporal changes in weathering rate might be one reason why reconstructed Δ14C (and CO2) is not met with simulations. Having found, that the input of 14C-free carbon to the system is so important for an understanding of Δ14C brings me also to the quesion if 14C-free CO2 outgassing from volcanos is considered, which might have similar effects on 14C. I understand that this has been investigated previously with the Bern3D model (Roth and Joos, 2012), but with focus on 13C. Maybe some more insights from previous simulations are possible here, at least in a discussion. At least please mention the applied CO2 volcanic outgassing rates. Note, that there is a fundamental, analytical derived solution from the steady state assumption on volcanic CO2 input being 50% of the CO2 consumption by silicate weathering, which is of relevance for times longer than 100 kyr (briefly mentioned in Munhoven and François (1996) or in depth discussed on pages 80-81 of Munhoven (1997), http://www.astro.ulg.ac.be/~munhoven/en/PhDIndex.html). For shorter periods such as the last 50 kyr considered here, differences from this numbers are certainly possible, but this relationship gives a rough guideline, and might explain long-term drifts in the C cycle, if not obeyed. Taken together, I have the impression, that no silicate weathering, and also no volcanic outgassing of CO2 is considered here, which would indicate according to this theory no drift in the system, but also the missing of two important processes. If so, I am not saying, these should be implemented in the revision, but it needs to be stated clearly if and how they are (not) included. How does your weathering flux compare to others, e.g. Fig 7 in Brovkin et al. (2012) or Colbourn et al. (2013)?

We are afraid that there has been a misunderstanding with regard to the model representation of terrestrial weathering fluxes. Apparently the referee missed the

description of the sediment model and weathering fluxes given in Appendix A (lines 756-771). We will include the preindustrial steady-state values for weathering rates in Sect. 2.2 and provide additional details on the representation of terrestrial weathering in Appendix A. For convenience, the approach is described here in detail.

The Bern3D model simulates net ocean-sediment exchange, sediment stocks, and burial fluxes from the ocean sediments to the lithosphere of P, Si, Alk, DIC, $DI^{14}C$, and $DI^{13}C$ using a 10-layer ocean sediment model. In steady state, the net loss fluxes from the ocean to the sediments and lithosphere are compensated by corresponding input fluxes to the ocean, termed "weathering fluxes". These input fluxes are thought to represent the fluxes from weathering (dissolution) of carbonate and silicate rocks on land, of phosphorous release by rock weathering, and from CO_2 emissions from volcanic activity. The ocean inventories of P, Si, and Alk and atmospheric CO_2 and its isotopic signature are prescribed during the atmosphere-ocean-sediment spin-up. Any loss of P, Si, Alk, DIC and $DI^{13}C$ by net fluxes to the sediments is compensated by a corresponding input flux during the spin-up phase. Input fluxes are added uniformly to the coastal surface ocean. At the beginning of transient simulations, the global input fluxes of P, Si, Alk, DIC and $DI^{13}C$ are set equal to the burial fluxes diagnosed at the end of the model spin-up. These input fluxes are jointly denoted as "weathering fluxes". Radiocarbon is transferred from the ocean to the sediments and lithosphere where it decays, but no radiocarbon is added to the ocean from "weathering" as old rocks are radiocarbon free (or "radiocarbon dead").

The preindustrial spin-up results in steady-state values for weathering-derived inputs (and hence steady-state burial rates) of DIC, Alk, P, and Si of 0.46 Gt C per year, 34.37 Tmol HCO_3^- per year, 0.17 Tmol P per year, and 6.67 Tmol Si per year, respectively. These values are within the range of observational estimates (see, e.g., Jeltsch-Thömmes et al., 2019, Table 1). The weathering input of Alk as HCO_3^- is also comparable to the global riverine bicarbonate flux presented in Brovkin et al. (2012), very close to their interglacial estimates (36 to 38 Tmol per year) but lower than their LGM estimates (almost 50 Tmol per year).

These input fluxes may be further attributed to the weathering of organic material, $CaCO_3$, and $CaSiO_3$ on land, and to volcanic CO_2 outgassing. The flux of phosphorus (P) is assigned to weathering of organic material, and the related carbon (C) and Alk fluxes are computed by multiplication of the P flux with the Redfield ratio for organic matter stoichiometry (C:P:Alk = 117:1:-17). Similarly, the silicon (Si) flux is assigned to $CaSiO_3$ weathering, and the related Alk flux is computed using Si:Alk = 1:2 based on the simplified $CaSiO_3$ weathering reaction: $2CO_2 + CaSiO_3 + H_2O \rightarrow 2HCO_3^- + Ca^{2+} + SiO_2$ (Colbourn et al., 2013). As Colbourn et al., we sidestep the carbon flux from the atmosphere to the ocean. The remaining Alk flux is attributed to $CaCO_3$ weathering with the stoichiometric ratio C:Alk = 1:2 based on the $CaCO_3$ dissolution reaction: $CO_2 + H_2O + CaCO_3 \rightarrow Ca^{2+} + 2HCO_3^-$. The volcanic outgassing flux is the remaining flux needed to balance the C input flux. The diagnosed fluxes at the end of the spin-up are 0.24 Gt C per year for terrestrial weathering

of organic material, 0.13 Gt C per year for terrestrial $CaCO_3$ weathering, 0.09 Gt C per year for volcanic CO_2 outgassing, and 6.67 Tmol Si per year for terrestrial $CaSiO_3$ weathering.

For simplicity, we kept weathering fluxes constant during transient simulations, and weathering feedbacks (Jeltsch-Thömmes and Joos, 2020; Colbourne et al., 2013) were not enabled in this study. This does not affect our results and conclusions. First, changes in weathering fluxes have no influence on the ocean radiocarbon inventory as weathering fluxes are "radiocarbon dead". Second, the impact of potential changes in weathering fluxes on atmospheric CO_2 and the ocean and sediment carbon inventories, which would influence atmospheric $\Delta^{14}C$, is implicitly considered in our sensitivity experiments where CO_2 and carbon inventories are forced to vary. Third, we note that there is a large uncertainty in the dissolution rates of carbonate and silicate rocks on land (terrestrial weathering) over time, and that these weathering reactions represent a very long-term sink of atmospheric CO_2. In particular, weathering of silicate rocks on land is occurring too slowly (on a time scale of hundreds of thousands of years) to be important on the time scale relevant for this study (~50,000 years). Furthermore, Roth and Joos (2013) demonstrated that even massive changes in volcanic emissions cause changes in atmospheric $\Delta^{14}C$ that are much smaller than the discrepancies between reconstructed and modelled $\Delta^{14}C$.

Finally, we would like to point out that because DIC and Alk are conservative with respect to changes in state (temperature, salinity, and pressure) during mixing, both are carried as tracers in ocean carbon cycle models like the Bern3D. Together they completely determine the CO_2 system in seawater ($\mathbf{H^+}$, $\mathbf{pCO_2}$, $\mathbf{H_2CO_3^*}$, $\mathbf{HCO_3^-}$, and $\mathbf{CO_3^{2-}}$), using the well-known carbonate chemistry routines. These parameters can be used to compute, e.g., air-sea CO_2 and $^{14}CO_2$ fluxes or the saturation state of seawater with respect to $CaCO_3$.

We have added the preindustrial steady-state values for weathering-derived inputs to Sect. 2.2, line 194:

Note the preindustrial spin-up results in steady-state values for weathering-derived inputs of DIC, Alk, P, and Si of 0.46 Gt C per year, 34.37 Tmol HCO_3^- per year, 0.17 Tmol P per year, and 6.67 Tmol Si per year, respectively. These terrestrial weathering rates were chosen to balance the sedimentation rates on the sea floor and are held fixed and constant throughout the simulations.

We have also added more detailed description of the model's representation of weathering fluxes in Appendix A:

Weathering (dissolution) of carbonate and silicate rocks on land, phosphorous release by chemical weathering of rocks, and volcanic outgassing of CO_2 are simulated as constant inputs of DIC, Alk (as bicarbonate ion, HCO_3^-), phosphate (P), and silicate (Si) to the ocean at rates intended to balance their removal from the ocean by sedimentation on the sea floor. These weathering inputs are added as a constant increment to each surface ocean grid cell along the coastlines. The preindustrial steady state of the model is used to diagnose the weathering rates that are held fixed and constant throughout the simulations. Note that the preindustrial spin-up results in steady-state values for weathering-derived inputs of DIC, Alk, P, and Si of 0.46 Gt C per year, 34.37 Tmol HCO_3^- per year, 0.17 Tmol P per year, and 6.67 Tmol Si per year, respectively. These values are within the range of observational estimates (see, e.g., Jeltsch-Thömmes et al., 2019). Additional details concerning the sediment model are provided in Tschumi et al. (2011), while the appendix of Jeltsch-Thömmes et al. (2019) gives a detailed description of the atmosphere–ocean–sediment spin-up.

3. Earlier simulation studies have shown, that to get the 14C cycle right, one needs to have the C cycle right as well. Köhler et al. (2006) has shown that previous studies (Beck et al., 2001; Hughen et al., 2004) focusing only on 14C, but showing no simulated CO2, they therefore have very likely some deficits. For atmospheric Δ14C especially the air-sea gas exchange is important, which depends similarily on the gas exchange velocity (kw, which is considered here in sensitivity experiments), but also on the CO2 gradient between atmosphere and surface ocean. This implies that whenever simulated CO2 differs from reconstructions there will also be an offset in simulated Δ14C from data. In a recent simulation effort for IntCal20 (the successor of IntCal13) the marine surface Δ14C has been simulated (Heaton et al., submitted). There, the importance of time-dependent changes in CO2 has been as important for the simulated surface ocean Δ14C as that of climate change (temperature change, ocean circulation change etc), which via gas exchange would also feedback to atmosheric Δ14C. This is unpublished so far, but since it is submitted and will probably be available in due time I nevertheless mention it here.

We thank the referee for bringing this very interesting-sounding work to our attention. We look forward to reading it once it becomes publicly available.

It is well known that gross isotopic air-sea fluxes scale with atmospheric CO_2 and the $^{14}C/C$ ratio. In 6 of our 8 model carbon cycle scenarios, parameter values were selected to reproduce low glacial atmospheric CO_2 concentrations. Note also that atmospheric CO_2 was prescribed in the model runs where the ^{14}C production rate is deconvolved from the model results (i.e., Sect. 3.4). Thus, temporal changes in atmospheric CO_2 are taken into account by our model simulations.

We have added the following text after the second paragraph in Sect. 2.4:

Variations in atmospheric CO_2 govern how fast $\Delta^{14}C$ signatures are passed between the atmosphere and ocean. Gross fluxes of ^{14}C between the atmosphere and ocean, and vice versa, scale with atmospheric pCO_2 and its $^{14}C/C$ ratio. It is therefore important to reproduce low glacial atmospheric CO_2 concentrations in at least some of the model scenarios, thereby capturing the influence of temporal changes in CO_2 on the air-sea exchange of ^{14}C.

4. The coauthor Florian Adolphi is also coauthor of the nows ubmitted IntCal20 effort (updating the atmospheric Δ14C record), (Reimer et al., submitted) and should therefore be aware of the large changes which occur between IntCal13 and IntCal20, namely the amplitude of the Δ14C maxima around 40 kyr increases in IntCal20 towards the Hulu Cave numbers. Maybe this should be briefly discussed in an outlook.

The backbone of the new IntCal20 calibration curve is the Hulu Cave $\Delta^{14}C$ dataset from Cheng et al. (2018) that we use in this work, since IntCal20 is not yet published. Essentially all datasets underlying the IntCal20 curve are tied to the Hulu Cave record, either via time scales (Lake Suigetsu plant macrofossil data) or marine reservoir corrections (marine records). Hence, IntCal20 looks more or less like the Hulu record. Since we are not discussing the fine-scale structure of the record but rather the large-scale changes in $\Delta^{14}C$, using IntCal20 would not significantly impact our conclusions.

We have added the following text to the third paragraph in Sect. 2.5:

Note that although the forthcoming IntCal20 calibration curve (Reimer et al., in press) will be the new standard atmospheric radiocarbon record for the last 55,000 years, essentially all data underlying IntCal20 before 13.9 kyr BP are tied to the Hulu Cave dataset, either via time scales (Lake Suigetsu plant macrofossil data) or marine reservoir corrections (marine records). Hence, the IntCal20 and Hulu Cave $\Delta^{14}C_{atm}$ records are very similar and using IntCal20 would not impact our conclusions.

Minor issues in chronological order:

1. The decay constant of 14C used here is based on a halflife of 14C of 5700 yr (here) but of 5730 yr in Intcal13 (and IntCal20) which produced the atmospheric Δ14C record. If you consider the decay of 14C over 40 kyr (the time of the maximum in atm Δ14C) with either 5700 vs 5730 yr you get a 2.5% smaller number when based on 5700 yr, although the halflife time differed only by 0.5%. This difference is small when compared to the difference of IntCal13 and the Hule Cave data, but should nevertheless be mentioned.

As mentioned in Fig. 1 caption, reconstructed $\Delta^{14}C$ values taken from the IntCal13 calibration curve and the Hulu Cave dataset were adjusted to the presently accepted value of the radiocarbon half-life (5700 years), allowing comparison with our modelled $\Delta^{14}C$ values.

2. line 173: Please be specific, how 14C is fractionation corrected.

Radiocarbon measurements are generally reported as $\Delta^{14}C$ which includes a correction for fractionation effects. The measured $\delta^{13}C$ value is used to remove the effects of isotopic fractionation. As indicated in Sect. 2.2, this model study simulates a ^{14}C concentration that is "fractionation corrected". What we mean by this is as follows. To model ^{14}C, the Bern3D

neglects effects due to fractionation during gas exchange and photosynthesis, which means that model results for $\Delta^{14}C$ are directly comparable to measurements reported as $\Delta^{14}C$. If we were interested in dealing with absolute values of the ^{14}C concentration over time, then a correction is needed to account for fractionation effects, using the following equation (see Orr et al., 2017, Eq. A3 and associated discussion in the Appendix):

$$^{14}C = \left(^{14}C_{model} \,/\, \left[1 - 2\left(\frac{\delta^{13}C + 25}{1000}\right)\right]\right)\, ^{14}r_{std} \qquad (1)$$

For ^{13}C, the Bern3D includes fractionation effects during gas exchange and photosynthesis. Eq. 1 together with modelled $\delta^{13}C$ values could be used to compute corrections for atmospheric and oceanic ^{14}C, were we interested in looking at absolute values of the ^{14}C concentration.

The text near line 173 is modified to read:

In this model study, $\Delta^{14}C$ is treated as a diagnostic variable using the two-tracer approach of OCMIP-2. Rather than treating the $^{14}C/C$ ratio as a single tracer, fractionation-corrected ^{14}C is carried independently from the carbon tracer.

3. line 180-181: Weathering is prescribed as constant input of DIC, but no 14C. See fundamental comment above, but no matter where the C of weathering comes from the input in the ocean should be a HCO−3 , changing both DIC and alkalinity in the ocean. I hope this is only a too simplified description here, but has implemented correctly in the model. Please revise.

This comment has already been addressed in our response to comment #2 of the referee's "fundamental remarks".

4. line 184: For the preindustrial spin-up CO2 is fixed to 278.05 ppm. Why this number, would not 278 ppm do the same job? Is this OCMIP protocol? Also: What would be the internally calculated preindustrial CO2? By prescribing CO2 concentration during spin-up C is added or extracted from the simulated system, which might be a potential source of bias. How long is the spin-up time?

This is irrelevant. The reason for this atmospheric CO_2 value is that it is the nominal value for year 1750 in one of our in-house CO_2 data compilations, but yes, holding atmospheric CO_2 constant at 278 ppm would do the same job. In the preindustrial spin-up simulation, the model is run to equilibrium over a ~50,000-year integration, as mentioned in line 186. During this spin-up, atmospheric CO_2 is held constant at 278.05 ppm and $\Delta^{14}C$ at 0 permil. These are the values that the atmospheric carbon and ^{14}C tracers see. The ocean carbon and radiocarbon inventories change in response to this forcing. After spin-up the ocean is in equilibrium with the atmosphere.

5. line 229: Consider citing the underlying ice core paper, from which the greenhouse gases splines provided by Köhler et al (2017) have been calculated.

Agreed. We will cite Enting (1987) for the spline smoothing method.

We have now cited Enting (1987):

(data compilation of Köhler et al., 2017, as splined using the spline smoothing method of Enting, 1987)

6. line 232: Global benthic δ18O is not only a global ice volume proxy, but has also a considerable contribution from deep ocean temperature, see papers of the van de Wal group from Utrecht Universitiy on the deconvolution (e.g. Bintanja and van de Wal, 2008). Taken this knowledge into consideration, would this change your approach how sea level is changing? You might also discuss how different sea level reconstructions vary, e.g. see three different sea level reconstructions in Fig 1f of Hasenclever et al. (2017), and what this uncertainty in sea level might introduce into your approach.

No, this would not significantly change our approach or our results. As explained in the manuscript, we use the global benthic $\delta^{18}O$ stack to scale the ice sheet size for periods where no reconstructions are available. The tie points of this scaling, i.e., the LGM and preindustrial ice sheet reconstructions, remain unaffected by the scaling method, i.e. whether the scaling is done with $\delta^{18}O$ corrected for deep ocean temperature or not. Ice sheet size is important for albedo, salinity and latent heat fluxes, but has little influence on modelled atmospheric $\Delta^{14}C$ (e.g., the small difference between scenarios MOD and PAL in Fig. 8).

7. lines 223-236: Model description says that greenhouse gas radiative forcing has been taken from data, thus I assume that CO2 seen by the carbon cycle is never prescribed, but always model-internally calculated. Please state this explicitly (or the correct version of this sentence, if this was not the case). However, you might also consider one scenario in which CO2 is prescribed for the C cycle from data (similar as in Butzin et al., 2017, in which atmospheric CO2 and Δ14C has been prescribed by data), since this would bring your simulated C cycle as close to observations as probably possible, which might further reduce the bias in 14C (see also fundamental remarks above).

Although the radiative forcing for CO_2 is prescribed, the atmospheric CO_2 concentration is allowed to evolve freely, except in the simulations described in Sect. 2.5. We will clarify this point in Sect. 2.4.

As discussed in lines 302-315, our approach to estimating the ^{14}C production rate over the last 50 kyr relies on model simulations forced by reconstructed changes in atmospheric $\Delta^{14}C$

and CO_2 as well as 7 different carbon cycle scenarios. None of the model runs are able to reproduce the reconstructed variations in ^{14}C production during the last glacial, especially between 32 and 22 kyr BP (see Sect. 3.4 and Fig. 10 and 11). Thus, the discrepancy between reconstructions and model results remains even when prescribing atmospheric CO_2.

We have clarified in Sect. 2.4 that atmospheric CO_2 is allowed to evolve freely:

Note that, although the radiative forcing for CO_2 is prescribed, the atmospheric CO_2 concentration is allowed to evolve freely, except in the simulations described in Sect. 2.5.

8. Obtained surface reservoir ages (Fig 8c) might be compared with data and other models, e.g. see Butzin et al. (2017); Skinner et al. (2019). Benthic-atmospheric offsets (Fig 8d) might be compared for the LGM with the data compilation of Skinner et al. (2017). Note, surface reservoir ages might vary a lot as function of latitude, so this Fig 8c needs more information on averaging; even better: might be revised and thus restricted to sea ice-free areas only.

We agree comparison with measurement- and model-based estimates of radiocarbon reservoir age offsets from, e.g., Skinner et al. (2017) and Butzin et al. (2017), is a missed opportunity. It was a sacrifice made to reduce the length of an already very lengthy manuscript. Nonetheless, some intriguing points can be made by such a comparison, so we will incorporate it into Sect. 3.3 and Fig. 8.

Comparison of our LGM B-Atm age offset estimates from runs CIRC, VENT, and VENTx (range of 3682 to 3962 ^{14}C years) with the compiled LGM marine radiocarbon data of Skinner et al. (2017) demonstrate that the carbon cycle scenarios are extreme, although it should be noted that they consider a wider depth range (~500 to 5000 m) of the ocean than we do. Skinner et al. (2017) predict a global average LGM B-Atm value of ~2048 ^{14}C years, an increase of ~689 ^{14}C years relative to preindustrial. Turning our comparison to surface reservoir ages, we note that our global average LGM surface reservoir age of ~1132 ^{14}C years from runs VENT and VENTx is comparable to the ~1241 ^{14}C years obtained by Skinner et al. (2017) for the LGM. The model-based estimates of surface reservoir age from Butzin et al. (2017) indicate a much lower LGM value of ~780 ^{14}C years, and values ranging from 540 to 1250 ^{14}C years between 50 and 25 kyr BP. Note that these estimates are based on model-simulated values between 50°N and 50°S. If the polar regions are included in the calculation (see Fig. 8c), their surface reservoir age estimates become comparable to our glacial values (range of 911 to 1354 ^{14}C years), and between about 34 and 22 kyr BP can exceed them, including even those from model runs VENT and VENTx, unless atmospheric $\Delta^{14}C$ and CO_2 are prescribed (dashed colored lines in Fig. 8c). Interestingly, this is also roughly the time period where our deconvolutions of the IntCal13 and Hulu Cave $\Delta^{14}C$ records give production rate estimates that are about 17.5 percent higher than the reconstructions, which indicates at the very least this is an important piece of the puzzle of

the glacial-interglacial Δ^{14}C problem, given that the effect of upper ocean stratification and/or sea ice on air-sea gas exchange is particularly important for surface reservoir ages.

Comparison of our surface reservoir ages with estimates from Skinner et al. (2019) will have to await a future study. A clear picture of the spatiotemporal evolution of the global average surface reservoir age has yet to emerge, but the regionally distinct patterns as demonstrated by Skinner et al. (2019) have important implications for the calibration of marine radiocarbon samples. These results need to be scrutinized more carefully and investigated in more detail with models, and with experiments specifically designed with this question in mind.

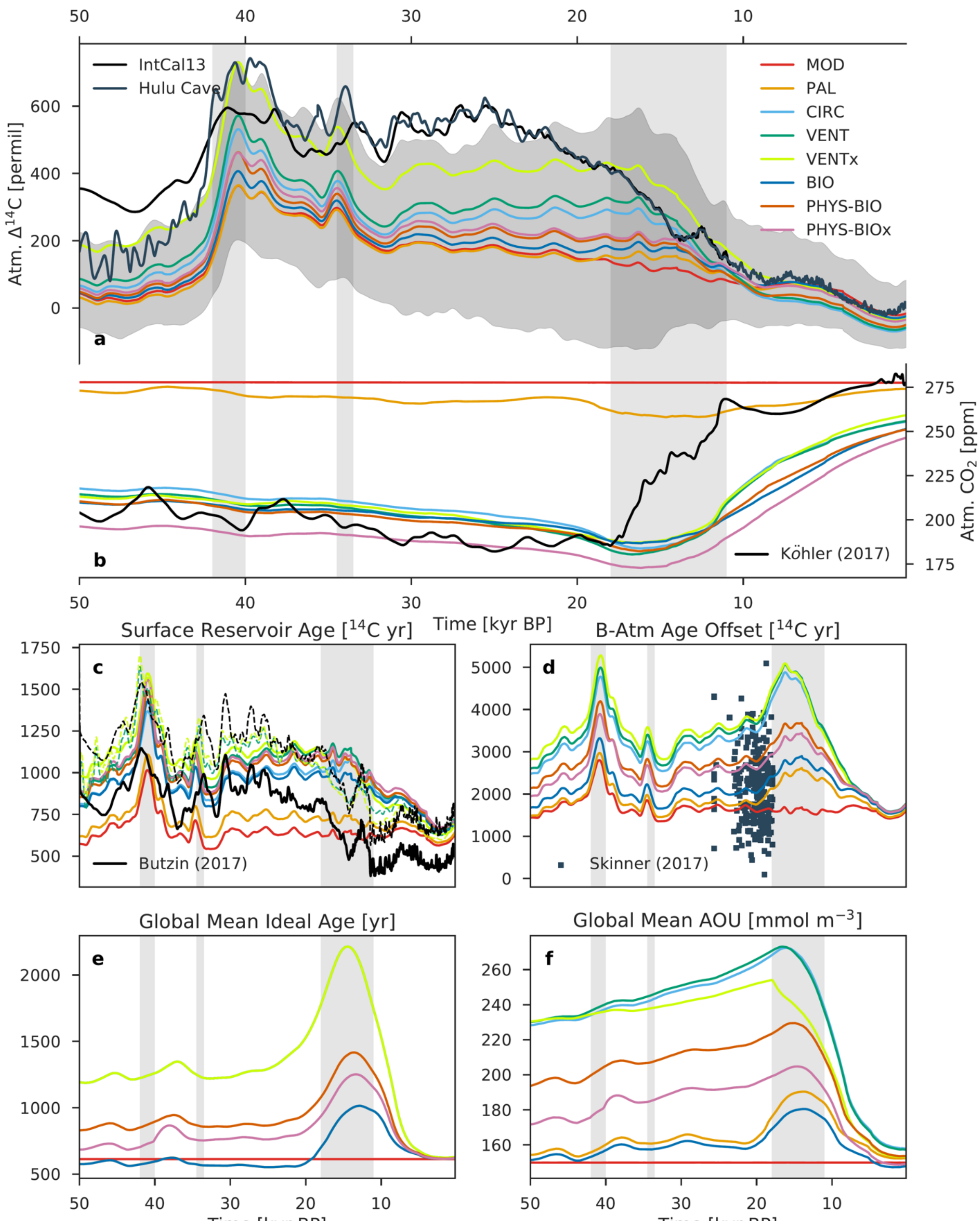

Fig. 8. Modelled records of atmospheric (a) $\Delta^{14}C$ and (b) CO_2, compared with their reconstructed histories (black and dark blue lines). Also shown are modelled records of the global average (c) surface reservoir age and (d) B-Atm ^{14}C age offset, compared with a recent compilation of LGM marine radiocarbon data (dark blue squares) by Skinner et al.

(2017) and model-based surface reservoir age estimates between 50°N and 50°S (solid black line) and across all latitudes (dashed black line) from Butzin et al. (2017), as well as (e) ideal age and (f) apparent oxygen utilization (AOU). Colored lines show the results of model runs using the mean paleointensity-based ^{14}C production rate and the eight different carbon cycle scenarios described in Sect. 2.4 and Table 1. The gray envelope in (a) shows the uncertainty (2σ) from all production rate reconstructions and carbon cycle scenarios, providing a bounded estimate of $\Delta^{14}C$ change. The dashed colored lines in (c) show the surface reservoir age results from VENT and VENTx where atmospheric $\Delta^{14}C$ and CO_2 are prescribed. Radiocarbon ventilation ages are expressed here as radiocarbon reservoir age offsets following Soulet et al. (2016) which are used extensively by the radiocarbon dating community.

We have added the observed and modelled records of Skinner et al. (2017) and Butzin et al. (2017), respectively, to Fig. 8d,c as well as added a paragraph to Sect. 3.3 that discusses the model-data comparison of B-Atm and surface R-age:

Driven by a reduction in ocean circulation, model run CIRC predicts a substantial increase in B-Atm during the last glacial, which is defined here as 40 to 18 kyr BP to avoid biasing global mean estimates toward Laschamp values. The global average glacial B-Atm predicted by CIRC is ~3225 ^{14}C years, representing an increase in B-Atm of ~1599 ^{14}C years relative to the preindustrial value of ~1626 ^{14}C years. Model run VENT predicts a slightly larger increase in glacial B-Atm due to the inhibition of air-sea gas exchange. The "oldest" glacial waters are found in model run VENTx where air-sea gas exchange is severely restricted, yielding an increase in B-Atm of ~1912 ^{14}C years (glacial B-Atm ~3538 ^{14}C years). The glacial B-Atm values given by runs CIRC, VENT, and VENTx, as well as the ~717 year increase in ideal age during the last glacial relative to preindustrial, suggest that the glacial deep ocean was about two times older than its preindustrial counterpart. Comparison of our LGM B-Atm estimates (range of 3682 to 3962 ^{14}C years) with the compiled LGM marine radiocarbon data of Skinner et al. (2017) demonstrate that the carbon cycle scenarios are extreme, although it should be noted that Skinner et al. consider a wider depth range (~500 to 5000 m) of the ocean than we do. Skinner et al. (2017) predict a global average LGM B-Atm value of ~2048 ^{14}C years, an increase of ~689 ^{14}C years relative to preindustrial. Turning our comparison to surface reservoir ages, we note that our global average LGM surface R-age of ~1132 ^{14}C years from runs VENT and VENTx is comparable to the ~1241 ^{14}C years obtained by Skinner et al. (2017) for the LGM. The model-based estimates of surface R-age from Butzin et al. (2017) indicate a much lower LGM value of ~780 ^{14}C years, and values ranging from 540 to 1250 ^{14}C years between 50 and 25 kyr BP. Note that these estimates are based on model-simulated values between 50°N and 50°S. If the polar regions are included in the calculation (see Fig. 8c), their surface R-age estimates become comparable to our glacial values (range of 911 to 1354 ^{14}C years), and between about 34 and 22 kyr BP can exceed them, including even those from model runs VENT and VENTx, unless $\Delta^{14}C_{atm}$ and CO_2 are prescribed (dashed colored lines in Fig. 8c) as in the simulation by Butzin et al. (2017).

9. Please state somewhere the absolute (PI) values of those parameters which are changed in your sensitivity experiments, maybe in Table 1?

We would like to direct the referee, and the reader, to the appendix of Roth et al. (2014) for the Bern3D model parameter set.

The following text has been added to the Table 1 caption:

See Roth et al. (2014) for the Bern3D model parameter set.

10. Table 2: 14C production rates is given in relative units, relative to what? Probably preindustrial state. I also do not remember if the 14C production rate in absolute numbers is once given in the manuscript for preindustrial state, please insert somewhere.

Our model-based records of the global production rate of ^{14}C are in units relative to the preindustrial value, as mentioned in lines 416-417. We will include the preindustrial steady-state absolute value of 443.9 mol ^{14}C per year (1.66 atoms cm^{-2} s^{-1}) in Sect. 2.2.

We have added the preindustrial steady-state absolute value of atmospheric ^{14}C production of 443.9 mol ^{14}C per year (or 1.66 atoms cm^{-2} s^{-1}) to Sect. 2.2.

11. Fig 4 captions does not need a description of the different colors of the lines, since a legend is given in the figures themselves.

Here we reference the colored lines in order to remind the reader that their labels refer to the model configurations representing different combinations of global carbon reservoirs, which is important when comparing the response of $\Delta^{14}C$ to the step changes.

Referee #2

1. Line 11: I feel that the term 'mystery interval' has become current without having a particularly clear meaning; it seems to be used to refer to a chronozone, for which there already is a name (Heinrich Stadial 1, etc…). Furthermore, the 'mysterious' part of the interval seems to be perceived differently by different people; is it the atmospheric radiocarbon decline, the proposed lack of marine radiocarbon activity increase, the entire 'mystery' of deglaciation? Not everyone shares the same notions regarding such 'mysteries', particularly regarding the marine radiocarbon inventory change, against which the term 'mystery interval' seems to have been directed. I would like to stick my neck out and suggest that this term has served its purpose in stimulating interest in a topic, and no longer serves a purpose for clear communication of a specific idea. I would therefore propose that the authors refer to other more clearly established chronozone designations, or even dates if these are trusted sufficiently.

We agree with the referee that using the term "mystery interval" to refer to the sharp drop in $\Delta^{14}C$ across Heinrich Stadial 1 ~17.5 to 14.5 kyr BP serves no purpose other than to stimulate interest. We will update the manuscript to be more precise, such that "mystery interval" is replaced by Heinrich Stadial 1.

We have replaced the term "mystery interval" with "Heinrich Stadial 1" throughout the revised manuscript.

2. Line 18: I think the word "more" can be dispensed with, here and elsewhere. One wonders: more than what?

Models allow us to investigate specific phenomena in more idealized settings compared to the "real world". However, we agree that, in this context, referring to such settings as "more idealized" rather than simply "idealized" is not very useful. The manuscript will be updated accordingly.

We have replaced the phrase "more idealized" with "idealized" throughout the revised manuscript.

3. Line 40: here and throughout the manuscript I was not sure whether "millennial-scale" was a helpful designation, as it made me think of variability associated with Dansgaard-Oeschger events. Perhaps the term, or another such as "short term" etc…, can be defined clearly when first used?

The primary focus of this work is on the specific mechanisms responsible for variations in atmospheric $\Delta^{14}C$ on millennial time scales (i.e., time scale of thousands of years). We do not attempt to resolve more abrupt climate perturbations such as Dansgaard-Oeschger warming events, which is noted in lines 637-641 of the original manuscript. To avoid confusion, we will add a note of caution in Sect. 2.4 when we introduce the carbon cycle scenarios considered in the model runs.

We have added a note of caution when introducing the model carbon cycle scenarios in Sect. 2.4:

A note of caution. Because millennial-scale $\Delta^{14}C_{atm}$ variations during the last glacial are what we are interested in, we do not attempt to reproduce abrupt climate perturbations such as Dansgaard-Oeschger warming events in the model runs.

4. Line 60: same thoughts as above regarding the term "mystery interval"; if it is coincident with HS1, then we should use that term instead I think. At the time of the Broecker and Barker (2007) study there was proposed to be a lack of evidence for a radiocarbon depleted ocean interior at the LGM, and a subsequent increase in its radiocarbon activity; however, this is arguably no longer the case.

This comment has already been addressed in our response to comment #1.

5. Line 67: probably best to be more specific, e.g. "…used only high accumulation sites, and square barrel gravity cores with minimal sediment disturbance.."

We agree with the referee that it would be valuable for the reader if we elaborated on the coring and sampling methods that minimize the influence of drilling disturbance. This will be done in a revised manuscript.

We have included additional details on the coring and sampling methods that minimize the influence of drilling disturbance:

Paleointensity-based reconstructions are sensitive to coring disturbances of poorly consolidated sediments. The last 50 kyr are represented by the relatively slushy uppermost few meters of recovered marine sediment cores (Channell et al., 2018). Channell et al. (2018) preferentially selected cores recovered using conventional piston and square barrel gravity coring methods, and from sites with high mean (> 15 cm kyr^{-1}) sedimentation rates, so as to minimize the influence of drilling disturbance, and reached very different production rates than, e.g., Laj et al. (2000).

6. Line 72, last sentence of the paragraph: I don't mean to suggest that ther is anyh I gotta incorrect about this sentence, but I found this to be an odd way of phrasing things. To me there is one question, "why was atmospheric radiocarbon activity so high during the last glacial (including well after the Laschamp excursion)", which entails a subsidiary question, "how much did production changes contribute to this elevated atmospheric radiocarbon activity".

We agree with the referee that it is unnecessary to make a distinction between the contribution of production changes to high glacial $\Delta^{14}C$ levels and their contribution to the deglacial $\Delta^{14}C$ decline. Our goal was to remind the reader that only if estimates of past changes in ^{14}C production are robust can one improve assessments of the relative importance of the two fundamental mechanisms responsible for glacial-interglacial $\Delta^{14}C$ changes (i.e., production and carbon cycle changes).

We have reframed what the interpretation problem caused by uncertainties in past estimates of ^{14}C production is:

The large uncertainties associated with the reconstruction of past changes in ^{14}C production hamper our ability to predict reliably the extent to which production changes contributed to high glacial $\Delta^{14}C_{atm}$ levels. Only if estimates of past changes in ^{14}C production are robust can one improve assessments of the relative importance of the two fundamental mechanisms responsible for glacial-interglacial $\Delta^{14}C$ changes: (1) production changes and (2) carbon cycle changes.

7. Line 95: I would say that the time required for ocean ventilation is not "up to", but rather "over" 1000yrs. Perhaps Primeau (2005) can be referenced for this. 8. Line 100: multi-millennial timescales?

While the ventilation time scale for the deep ocean is typically of order 1000 years, we note that the deep ocean ventilation time scale can exceed 1000 years, as demonstrated by the modelling study of Primeau (2005). This time scale depends on which Ocean General Circulation Model and tracer was used to predict the time scale of the penetration of water from the surface into the ocean interior.

We have qualified that the deep ocean ventilation time scale can exceed 1000 years per Primeau (2005).

9. Line 106: Andrey Ganopolski would disagree (see Ganopolski et al., CP, 2017). Perhaps this statement should be modified to say that it is currently not possible to do so without the use of any parameterisations of key processes, or something more specific?

While Ganopolski & Brovkin (2017) reproduce the overall trends and more general features of glacial–interglacial variability of climate, ice sheets, and atmospheric CO_2 concentration using only orbital forcing to drive the CLIMBER-2 model, the finer-scale temporal dynamics of the simulated CO_2 evolution do not match the reconstructions. In particular, the model fails to simulate the correct timing of the deglacial CO_2 rise. In addition, the model underestimates the magnitude of the deglacial decline in atmospheric $\Delta^{14}C$. Therefore, we think it is reasonable to conclude that models cannot yet reproduce climate and atmospheric CO_2 variations on the basis of orbital forcing alone.

10. Line 113: this sentence seems to suggest that the main proposals for explaining glacial-interglacial CO2 involve exchanges with the solid earth, but this is not really true. Arguably, as has been sketched out many times before, including in a recent review (Galbraith 2020), the "ingredients" for glacial-interglacial CO2 change are well accounted for, it is their 'calibration' and organisation within an orbital pacing framework that remains elusive.

We agree with the referee. The text will be modified to highlight the role of ocean-based physical and biological mechanisms in explaining the glacial-interglacial variations in atmospheric CO_2, and to clarify that what is missing is a single framework in which these mechanisms are linked to each other in a predictable manner under the influence of orbital forcing.

We have rephrased the discussion of the glacial-interglacial CO_2 problem:

A wide variety of mechanisms, both physical and biological, centered on or connected with the ocean, as well as exchange processes with the land biosphere, marine sediments, coral reefs, and the lithosphere, are thought to play a role in explaining the glacial-interglacial variations in atmospheric CO_2 (Archer et al., 2000; Fischer et al., 2010; Wallmann et al., 2016; Galbraith and Skinner, 2020), but how they interacted over time under the influence of orbital forcing remains elusive. We appear to still be missing a single framework in which these mechanisms are linked to each other in a predictable manner.

11. Line 118: in idealised settings..

This comment has already been addressed in our response to comment #2.

12. Line 122: here and throughout the manuscript it would be best to suffix D14Catm, so that we know what reservoir is referred to.

We agree this notation would be useful for the reader and will apply it in a revised manuscript.

We have replaced the term "$\Delta^{14}C$" with "$\Delta^{14}C_{atm}$", when appropriate, throughout the revised manuscript.

13. Line 125: is it not more accurate to state that the production rate is inferred from an atmospheric radiocarbon budget, combined with a range of hypothetical radiocarbon and carbon cycle scenarios?

We agree with the referee it would be more precise to state that our model-based 50,000-year reconstruction of the ^{14}C production rate is based on an atmospheric radiocarbon budget that is put together by forcing the Bern3D carbon cycle model with reconstructed changes in atmospheric $\Delta^{14}C$ and CO_2 as well as carbon cycle scenarios.

We have qualified that our new reconstruction of the ^{14}C production rate relies upon carbon cycle model simulations, i.e.:

"…a new 50,000-year record of the ^{14}C production rate, as inferred by deconvolving the reconstructed histories of $\Delta^{14}C_{atm}$ and CO_2 with a prognostic carbon cycle model and considering the uncertainties associated with the glacial-interglacial ocean carbon cycle."

14. Line 159: air-sea equilibration times are very different, which is potentially important…

The air-sea equilibration time scale for $\Delta^{14}C$ by gas exchange depends in part on the gas transfer velocity, which is investigated in the sensitivity experiments presented in Sect. 3.1.3. These simulations demonstrate a modest response of $\Delta^{14}C$ of approximately 4-8% to a 100% reduction of the gas transfer velocity at the north (> 60°N) and south (> 48°S) poles.

We have added the following text to line 165:

Air-sea gas exchange is parameterized using a modified version of the standard gas transfer formulation of OCMIP-2, with exchange rates that vary across time and space (see Appendix A for more details).

15. Line 169: perhaps Stuiver et al. 1978 should be referenced.

We cited Stuiver and Polach (1977) in lines 35-36 of the original manuscript, but we see no reason why we should not cite them again in Sect. 2.2 as suggested.

We have included a citation for Stuiver and Polach (1977) in Sect. 2.2.

16. Line 170: would it be clearer to state that DI14C is simulated, separately from DIC?

We agree with the referee. We will modify Sect. 2.1 and 2.2 to clarify that CO_2, $^{14}CO_2$, DIC, and DI^4C are all carried by the model, and are used to diagnose atmospheric and oceanic $\Delta^{14}C$.

We have revised the description in Sect. 2.2 so that it is more obvious that the ^{14}C and carbon tracers are carried independently:

In this model study, $\Delta^{14}C$ is treated as a diagnostic variable using the two-tracer approach of OCMIP-2. Rather than treating the $^{14}C/C$ ratio as a single tracer, fractionation-corrected ^{14}C is carried independently from the carbon tracer. The modelled ^{14}C concentration is normalized by the standard ratio of the preindustrial atmosphere ($^{14}r_{std}$ = 1.170 x 10^{-12}; Orr et al., 2017) in order to minimize the numerical error of carrying very small numbers. For comparison to observations, $\Delta^{14}C$ is calculated from the normalized and fractionation-corrected modelled ^{14}C concentration as follows:

$$\Delta^{14}C = 1000\left({}^{14}r' - 1\right) \quad (1)$$

where $^{14}r'$ is the ratio of $^{14}C/C$ in either atmospheric CO_2 or oceanic DIC divided by $^{14}r_{std}$, depending on the reservoir being considered. The approach taken to simulate atmospheric $^{14}CO_2$ is analogous to the approach used for CO_2, except that the equation includes the terms due to atmospheric production and radioactive decay. For simulations where the sediment model is active, the oceanic DIC tracer sees a constant input from terrestrial weathering, whereas there is no weathering input of $DI^{14}C$ to the ocean (see Appendix A for more details).

17. Line 189: I wonder if this is not a major part of the whole problem with simulating atmospheric radiocarbon in the past? If the modern (pre-industrial) state is in fact far from *equilibrium then this would mean that production rates are all miscalibrated. Why not explore the possibility that production rates are higher than required for equilibrium, e.g. due to ongoing equilibration of sedimentation following the deglaciation and early Holocene? It seems to me that the very conclusions of this study require that this be explored as a possibility. More specifically, and perhaps I am not getting this right.. we might expect that, following the expansion of the terrestrial biosphere during the Holocene (and the removal of carbon from the atmosphere-ocean system, causing a slow reduction of 'young' carbonate sediment output from the ocean), the radiocarbon inventory of the ocean and atmosphere should be on a slow disequilibrium downward trend, so that a higher radiocarbon production would be needed to get today's radiocarbon activity as an equilibrium state. Is that correct? Or is it the opposite? In any event, one has a sneaking suspicion that this sort of thing might be important here.*

This is a very interesting point, but our results suggest that such a disequilibrium effect is of relatively minor importance. Firstly, disequilibrium effects are fully accounted for in the model simulations where atmospheric CO_2 and $\Delta^{14}C$ are prescribed (see Sect. 2.5 and 3.4), given that the transient time evolution is modelled. Here, there is a major mismatch between the reconstructed production rates and those diagnosed from our simulations (see Fig. 10 and 11). Furthermore, as shown in Fig. 8a, the mismatch between reconstructed and modelled atmospheric $\Delta^{14}C$ at the preindustrial is on the order of a few percent and scaling the production records accordingly would not remove the mismatch in atmospheric $\Delta^{14}C$ during the last glacial period. We refrain from such a posteriori scaling as the mismatch in atmospheric $\Delta^{14}C$ at the preindustrial is likely related to the mismatch between observed and modelled atmospheric CO_2 (see Fig. 8b). What we will say here is that an incorrect preindustrial ^{14}C production rate would introduce a potential bias, leading to systematic underestimates (or overestimates) of atmospheric $\Delta^{14}C$ values over time. However, increasing (or decreasing) the base level of our production rate would not fix the glacial $\Delta^{14}C$ problem, i.e., the persistent elevation of $\Delta^{14}C$ after ~33 kyr BP. This can also be understood by Fig. 9.

The uncertainty in the preindustrial production rate is on the order of 15% due to the uncertainties in the preindustrial ocean radiocarbon inventory (see Roth and Joos, 2013, Sect. 3.2). This potential systematic bias was not considered by our model simulations, but it would not affect our analysis as we consider normalized production rate changes (see, e.g., Fig. 7, 10, and 11).

Finally, the preindustrial ^{14}C production rate Q of 1.66 atoms cm^{-2} s^{-1} that is diagnosed at the end of the preindustrial spin-up agrees reasonably well with independent estimates from production rate models, e.g., Masarik and Beer (1999, 2009) (Q = 2.05 atoms cm^{-2} s^{-1} for a solar modulation potential of 550 MeV) and Kovaltsov et al. (2012) (Q = 1.88 atoms cm^{-2} s^{-1} for the period 1750 to 1900 AD), and from Roth and Joos (2013) using an earlier Bern3D-LPX model version (Q = 1.75 atoms cm^{-2} s^{-1} for the period 1750 to 1900 AD).

We have added the following text after the second paragraph in the summary and conclusions section (line 715):

Atmospheric $\Delta^{14}C$ that is modelled at any point in time reflects ^{14}C production at that point, as well as the legacy of past production and carbon cycle changes. The question arises as to whether our conclusions are affected by unaccounted legacy effects, e.g., linked to the preindustrial spin-up simulation or model-diagnosed production rates. Transient simulations forced by reconstructed changes in ^{14}C production (Sect. 3.2 and 3.3) are initialized at 70 kyr BP, but their interpretation is restricted to the last 50,000 years of the integration to minimize legacy effects from model spin-up. Available reconstructions of the ^{14}C production rate in relative units (Sect. 2.5) are applied as a scale factor to the preindustrial steady-state absolute value, which is diagnosed by running the Bern3D model to equilibrium under preindustrial boundary conditions. This approach represents an approximation and equilibrium conditions do not fully apply. Indeed, there is a mismatch between reconstructed and modelled $\Delta^{14}C_{atm}$ at the preindustrial (see Fig. 8a). This mismatch is on the order of a few percent or less and adjusting the base level of production accordingly would not remove the large mismatch between reconstructed and modelled $\Delta^{14}C_{atm}$ during the last glacial. In addition, the uncertainty in the absolute value of the preindustrial production rate is on the order of 15%, primarily due to the uncertainties in the preindustrial ocean radiocarbon inventory (see Roth and Joos, 2013, Sect. 3.2). This potential systematic bias, however, does not affect our conclusions as we consider normalized production rate changes (see Fig. 7, 10, and 11).

We have also added the following text to the third paragraph in the summary and conclusions section:

Here, non-equilibrium effects are fully accounted for by transient simulations where $\Delta^{14}C_{atm}$ and CO_2 are prescribed (Sect. 3.4) following their reconstructed histories. Yet, these simulations indicate that the discrepancy between measurement- and model-based estimates of the ^{14}C production rate remains for the last glacial (Fig. 10b). This would suggest that unaccounted legacy effects do not significantly affect our conclusions.

18. Line 220: "…levels, given available 14C production scenarios."

We agree with the referee it would be more precise to state that what we are interested in investigating is the extent to which changes in the ocean carbon cycle could explain high glacial $\Delta^{14}C$ levels, given available reconstructions of past changes in ^{14}C production.

We have qualified this point in Sect. 2.4:

The goal is to investigate the extent to which changes in the ocean carbon cycle could explain high glacial $\Delta^{14}C_{atm}$ levels, given available reconstructions of past changes in ^{14}C production.

19. Line 244: Why was benthic d18O chosen? It is a smooth, slow function that lags behind most of the climatic processes that were important for the carbon cycle. Although it might seem circular, I don't think it is any more ad hoc to scale these parameters to atmospheric CO2 instead.. having rapid jumps in HS1 and the YD, and a faster change than benthic d18O, might help with getting the deglacial CO2 change 'right' (for parameterised reasons).

We agree with the referee that a different scaling approach would be preferential when addressing the last glacial termination as benthic $\delta^{18}O$ lags the rise in atmospheric CO_2 and temperature as shown by Shackelton (2000). However, as our primary focus is on the last glacial period, a different scaling, e.g., by CO_2, would not change our conclusions.

20. Line 254: the cited study is based entirely on the 'plateau tuning' approach, which may be questioned. Perhaps best to also cite Skinner et al. (2017) who showed that the LGM ocean was 'older' pretty conclusively with a range of other data.

We agree with the referee that Skinner et al. (2017) would be a good study to cite here.

We have added a citation for Skinner et al. (2017).

21. Line 283: It seems crucially important to me that the 10Be and 36Cl flux records from the ice cores are NOT consistent with the final age scale that they are all placed on. As far as I can tell from Adolphi et al. (2018), the ice core data were converted to fluxes based on each ice core's individual age scale, and then they were all placed on the GICC05 age-scale, whereas Channell et al. (2018) argued that this age scale implies very different fluxes. Surely the ice core cosmogenic nuclide data ALL need to be placed on the same age scale and THEN the fluxes should be calculated and 'stacked'. I think this is a really crucial thing, and I am really confused as to why the specialists working with these isotope records take a different approach that surely produces incorrect fluxes. A basic test I would propose is: are the individual ice core flux records consistent with the accumulation rates that are implied for each ice core by the GICC05 age scale? If not, they need to be corrected, surely. I suspect this will only make matters worse for reconciling everything, but it is still important to consider carefully.

We are afraid that there has been a misunderstanding. The referee is correct that all time scale revisions impact ice-core accumulation rates and hence fluxes. We want to point out, however, that, as described in Adolphi et al. (2018) (Sect. 3.1, first paragraph), all ice cores were first placed on the same time scale (GICC05) before fluxes were calculated. Channell et al. (2018), on the other hand, describe the differences that arise from using the old ss09sea time scale (where accumulation rates are based on an empirical relationship with $\delta^{18}O$) instead of GICC05 (where they are based on the annual layer count) – so this does not apply to the record by Adolphi et al. (2018). And yes, as demonstrated by our results, using the GICC05 accumulation rates does make it more difficult to reconcile ^{14}C and ^{10}Be as compared to the ss09sea accumulation rates. As mentioned in lines 70-72, ice-core

accumulation rates remain the largest source of systematic uncertainty in the ^{10}Be-based production rate estimates. However, the largest systematic uncertainty in the calculation of accumulation rates comes from the correction of layer thinning through ice flow modelling, which is a slowly varying function of depth, and hence is relatively insensitive to minor corrections of the time scales themselves.

We have added the following text to line 288:

All ice cores were first placed on the same time scale (GICC05) before ^{10}Be fluxes were calculated.

22. Line 355: note again that this conflicts with the premise that the modern state is at equilibrium!

This comment has already been addressed in our response to comment #17.

23. Line 448: my intuition tells me that air-sea has exchange may have a small effect, but depending on the circulation state. Is it not possible that changes in air-sea exchange might combine non-linearly with particular changes in the circulation geometry?

As noted in lines 448-449, air-sea gas exchange has only a small effect on atmospheric CO_2 as compared to ocean circulation, given that the time scale of deep ocean ventilation (of the order of several hundred years to 1000 years or more) is much longer than the time scale of air-sea equilibration for CO_2 by gas exchange (approximately one year). In other words, the rate limiting step that determines the kinetics of the oceanic uptake of CO_2 is ocean circulation, not air-sea gas exchange. We will clarify this point in the third and fourth paragraphs of Sect. 3.1.3.

In Sect. 3.1.3, we have included an explanation for why the increase in $\Delta^{14}C_{atm}$ induced by a change in the gas transfer velocity is not accompanied by a significant change in the atmospheric carbon inventory:

The air-sea equilibration time scale for CO_2 by gas exchange is about 1 year for a ~75-m thick surface mixed layer (Broecker and Peng, 1974), which is much smaller than the ventilation time scale for the deep ocean (on the order of several hundred years or more). One would therefore expect that the oceanic uptake of CO_2 demonstrates only a very small response to changes in k_w.

24. Line 460: Although I see why the authors try to wiggle free from resolving the deglacial CO2 problem, I think it is it entirely possible to set it aside, and I also think it is basically not true that the study deals only with the glacial portion of the record. It is the glacial versus interglacial amplitude of atmospheric D14C that is of concern, and therefore the change across the deglaciation is entirely relevant! In fact, as suggested below, I would propose *provocatively that this study shows that atmospheric radiocarbon can be explained reasonably well up until the deglaciation, and that it is the modern radiocarbon activity that defies explanation. I wonder what the authors think of this contention.*

What we have tried to demonstrate with this work, especially by the analysis shown in Fig. 9, is that although models are able to reproduce successfully the high glacial $\Delta^{14}C$ levels associated with the Laschamp (~41 kyr BP) event, it is very difficult to explain the persistence of relatively high $\Delta^{14}C$ values after ~33 kyr BP, given available reconstructions of past changes in ^{14}C production and extreme changes in the ocean carbon cycle. We think that this may be crucial for explaining the deglacial $\Delta^{14}C$ decline, as the model representation of the mechanisms responsible for high glacial $\Delta^{14}C$ levels will determine the carbon inventories of the different reservoirs prior to the deglacial $\Delta^{14}C$ decline. And yes, the model fails to simulate the correct magnitude and timing of the deglacial $\Delta^{14}C$ decline. But given that we did not attempt to reproduce accurately the observed glacial-interglacial variations in atmospheric CO_2 and $\Delta^{14}C$, this work seeks to highlight the persistent elevation of $\Delta^{14}C$ after ~33 kyr BP as a major outstanding problem in our understanding of the atmospheric $\Delta^{14}C$ record.

In other words, we can reach the amplitude of the Laschamp-related $\Delta^{14}C$ change, but we cannot sustain the high levels during the last glacial nor can we get down low enough or fast enough during the last deglaciation.

25. Line 537, the discussion of simulated B-Atm values: why do the authors not refer at all to published data for comparison? The compilation of Skinner et al. (2017) estimated, with the available data, that the global average ageing of the ocean at the LGM was 'only' ~689 14C years. This is relevant here, and indeed it would suggest that all of the model scenarios produce rather extreme outcomes as compared to available data.

We agree comparison with measurement- and model-based estimates of radiocarbon reservoir age offsets from, e.g., Skinner et al. (2017) and Butzin et al. (2017), is a missed opportunity. It was a sacrifice made to reduce the length of an already very lengthy manuscript. Nonetheless, some intriguing points can be made by such a comparison, so we will incorporate it into Sect. 3.3 and Fig. 8.

Comparison of our LGM B-Atm age offset estimates from runs CIRC, VENT, and VENTx (range of 3682 to 3962 ^{14}C years) with the compiled LGM marine radiocarbon data of Skinner et al. (2017) demonstrate that the carbon cycle scenarios are extreme, although it should be noted that they consider a wider depth range (~500 to 5000 m) of the ocean than we do. Skinner et al. (2017) predict a global average LGM B-Atm value of ~2048 ^{14}C years, an increase of ~689 ^{14}C years relative to preindustrial. Turning our comparison to surface reservoir ages, we note that our global average LGM surface reservoir age of ~1132 ^{14}C years from runs VENT and VENTx is comparable to the ~1241 ^{14}C years obtained by Skinner et al. (2017) for the LGM. The model-based estimates of surface reservoir age from Butzin et

al. (2017) indicate a much lower LGM value of ~780 ^{14}C years, and values ranging from 540 to 1250 ^{14}C years between 50 and 25 kyr BP. Note that these estimates are based on model-simulated values between 50°N and 50°S. If the polar regions are included in the calculation (see Fig. 8c), their surface reservoir age estimates become comparable to our glacial values (range of 911 to 1354 ^{14}C years), and between about 34 and 22 kyr BP can exceed them, including even those from model runs VENT and VENTx, unless atmospheric $\Delta^{14}C$ and CO_2 are prescribed (dashed colored lines in Fig. 8c). Interestingly, this is also roughly the time period where our deconvolutions of the IntCal13 and Hulu Cave $\Delta^{14}C$ records give production rate estimates that are about 17.5 percent higher than the reconstructions, which indicates at the very least this is an important piece of the puzzle of the glacial-interglacial $\Delta^{14}C$ problem, given that the effect of upper ocean stratification and/or sea ice on air-sea gas exchange is particularly important for surface reservoir ages.

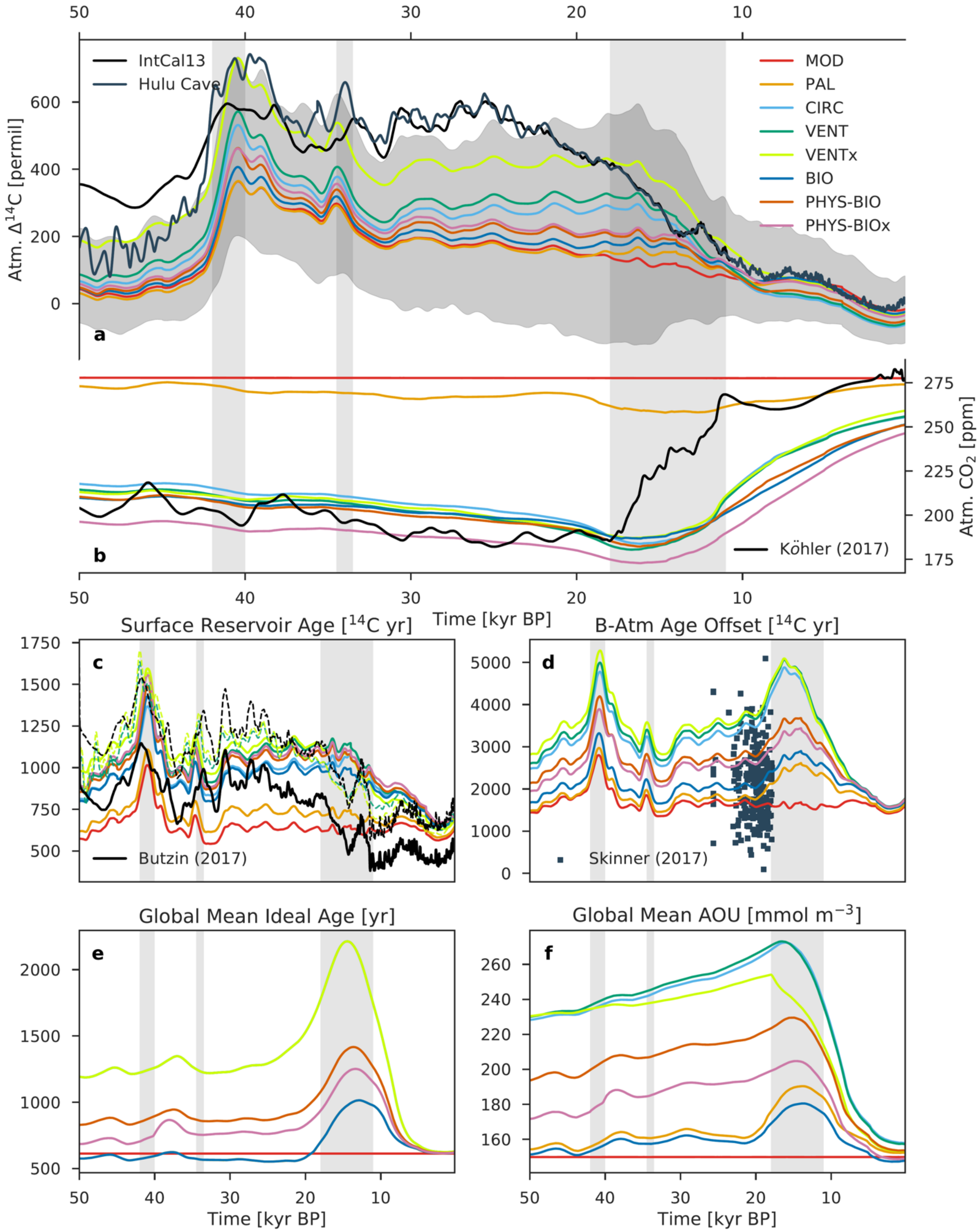

Fig. 8. Modelled records of atmospheric (a) $\Delta^{14}C$ and (b) CO_2, compared with their reconstructed histories (black and dark blue lines). Also shown are modelled records of the global average (c) surface reservoir age and (d) B-Atm ^{14}C age offset, compared with a recent compilation of LGM marine radiocarbon data (dark blue squares) by Skinner et al.

(2017) and model-based surface reservoir age estimates between 50°N and 50°S (solid black line) and across all latitudes (dashed black line) from Butzin et al. (2017), as well as (e) ideal age and (f) apparent oxygen utilization (AOU). Colored lines show the results of model runs using the mean paleointensity-based ^{14}C production rate and the eight different carbon cycle scenarios described in Sect. 2.4 and Table 1. The gray envelope in (a) shows the uncertainty (2σ) from all production rate reconstructions and carbon cycle scenarios, providing a bounded estimate of $\Delta^{14}C$ change. The dashed colored lines in (c) show the surface reservoir age results from VENT and VENTx where atmospheric $\Delta^{14}C$ and CO_2 are prescribed. Radiocarbon ventilation ages are expressed here as radiocarbon reservoir age offsets following Soulet et al. (2016) which are used extensively by the radiocarbon dating community.

We have added the observed and modelled records of Skinner et al. (2017) and Butzin et al. (2017), respectively, to Fig. 8d,c as well as added a paragraph to Sect. 3.3 that discusses the model-data comparison of B-Atm and surface R-age:

Driven by a reduction in ocean circulation, model run CIRC predicts a substantial increase in B-Atm during the last glacial, which is defined here as 40 to 18 kyr BP to avoid biasing global mean estimates toward Laschamp values. The global average glacial B-Atm predicted by CIRC is ~3225 ^{14}C years, representing an increase in B-Atm of ~1599 ^{14}C years relative to the preindustrial value of ~1626 ^{14}C years. Model run VENT predicts a slightly larger increase in glacial B-Atm due to the inhibition of air-sea gas exchange. The "oldest" glacial waters are found in model run VENTx where air-sea gas exchange is severely restricted, yielding an increase in B-Atm of ~1912 ^{14}C years (glacial B-Atm ~3538 ^{14}C years). The glacial B-Atm values given by runs CIRC, VENT, and VENTx, as well as the ~717 year increase in ideal age during the last glacial relative to preindustrial, suggest that the glacial deep ocean was about two times older than its preindustrial counterpart. Comparison of our LGM B-Atm estimates (range of 3682 to 3962 ^{14}C years) with the compiled LGM marine radiocarbon data of Skinner et al. (2017) demonstrate that the carbon cycle scenarios are extreme, although it should be noted that Skinner et al. consider a wider depth range (~500 to 5000 m) of the ocean than we do. Skinner et al. (2017) predict a global average LGM B-Atm value of ~2048 ^{14}C years, an increase of ~689 ^{14}C years relative to preindustrial. Turning our comparison to surface reservoir ages, we note that our global average LGM surface R-age of ~1132 ^{14}C years from runs VENT and VENTx is comparable to the ~1241 ^{14}C years obtained by Skinner et al. (2017) for the LGM. The model-based estimates of surface R-age from Butzin et al. (2017) indicate a much lower LGM value of ~780 ^{14}C years, and values ranging from 540 to 1250 ^{14}C years between 50 and 25 kyr BP. Note that these estimates are based on model-simulated values between 50°N and 50°S. If the polar regions are included in the calculation (see Fig. 8c), their surface R-age estimates become comparable to our glacial values (range of 911 to 1354 ^{14}C years), and between about 34 and 22 kyr BP can exceed them, including even those from model runs VENT and VENTx, unless $\Delta^{14}C_{atm}$ and CO_2 are prescribed (dashed colored lines in Fig. 8c) as in the simulation by Butzin et al. (2017).

26. Line 545: I think it is worth specifying in what ways these indirect methods are also potentially inaccurate, due to different processes affecting e.g. oxygen and radiocarbon.

A comparison of modelled apparent oxygen utilization (AOU) with the model ocean's deep-water reservoir age (B-Atm age offset) is not meant to be taken as a direct comparison. The goal of showing the parallel occurrence of depleted ocean interior oxygen levels (i.e., increased AOU) was to provide the reader with additional (indirect) evidence that deep water ageing is occurring in the model runs that consider reductions in ocean circulation and air-sea gas exchange (e.g., scenarios CIRC, VENT, and VENTx). A significant reduction in deep ocean ventilation permits the enhanced accumulation of remineralized carbon in the ocean interior, and therefore the progressive consumption of dissolved oxygen, as well as an increase in the radiocarbon disequilibrium between the deep ocean and the atmosphere, due to a decrease in the rate of transport and mixing of younger (higher $\Delta^{14}C$) waters. These observations (increased AOU and increased B-Atm age offset) taken together suggest that deep water ageing is occurring. We will clarify this point further in the third and fourth paragraphs of Sect. 3.3.

In Sect. 3.3, we have elaborated briefly on what the parallel occurrence of increased AOU and increased B-Atm indicates:

Indirect evidence for deep water ageing can be provided by the occurrence of depleted ocean interior oxygen levels, due to the progressive consumption of dissolved oxygen during organic matter remineralization in the water column. This situation is amplified by the slow escape of accumulating remineralized carbon in the ocean interior (see, e.g., Skinner et al., 2017), leading to higher values of apparent oxygen utilization ($AOU = O_{2,pre} - O_2$). These two concepts (increased AOU and increased B-Atm) taken together signal a significant reduction in deep ocean ventilation characterized by a decrease in the exchange rate between younger (higher $\Delta^{14}C$) surface waters and older (^{14}C-depleted), carbon-rich deep waters.

27. Line 567: ..is a dedicated 'control knob', in the model.

We agree with the referee it would be prudent to clarify that air-sea gas exchange is a principal "control knob" governing atmospheric $\Delta^{14}C$ in a model framework.

We have qualified this point in Sect. 3.3:

In contrast to a change in ocean circulation, air-sea gas exchange is a dedicated $\Delta^{14}C_{atm}$ "control knob" that can be invoked by models for a further increase of $\Delta^{14}C_{atm}$ without changing atmospheric CO_2.

28. Line 605: viewed as tentative, perhaps. The viewing is not tentative; the results are.

Agreed.

We have modified the text to read that the results must be "regarded as tentative".

29. Line 676: is it worth stating by how much this polar bias would have to be in order to reconcile everything? Is that magnitude reasonable?

Interesting point. However, we would rather not discuss the polar bias further as we do not think that it can really reconcile everything. Firstly, the geomagnetic field reconstructions do not suffer from a polar bias and yet, cannot explain atmospheric Δ^{14}C either. Secondly, as shown in Fig. 7c, the difference between reconstructed Δ^{14}C and modelled ^{10}Be (or RPI)-based Δ^{14}C is changing over time and the largest changes of this difference occur between ~35 and 30 kyr BP and then during the last deglaciation, not during the Laschamp event as one might expect if these mismatches were due to a polar bias. Instead, production rates (as inferred from ^{10}Be and RPI) were relatively stable across these two periods. Hence, it seems difficult to explain the mismatch by the presence of a polar bias alone.

The text on line 676 has been modified to read:

If a polar bias was present, it would lead to an underestimation of the geomagnetic modulation of the ice-core ^{10}Be flux, and therefore variations in the ^{10}Be-based ^{14}C production rate would also be underestimated. However, the mismatch of up to ~544 to 558 permil between reconstructed and modelled ^{10}Be-based Δ$^{14}C_{atm}$ during the last glacial (see Fig. 7c) appears to be much too large to be reconciled by considering uncertainties in the polar bias alone. Furthermore, this mismatch with reconstructed Δ$^{14}C_{atm}$ is qualitatively similar when using paleointensity-based ^{14}C production rates that do not suffer from a polar bias (Fig. 7c).

30. Line 703: in this paragraph the realism of the implied sea ice changes is discussed, but again no mention is made of what existing marine radiocarbon data imply. These are really important constraints to mention, surely.

This comment has already been addressed in our response to comment #25.

31. Line 726: I couldn't help but feel that the conclusion of the study might be more hard hitting if we had a more specific 'shopping list' of things that could help to resolve this puzzle. For example, constraining the global marine radiocarbon inventory change across the deglaciation, estimating any gradient in cosmogenic nuclide production across latitudes (i.e. polar bias, perhaps from tropical ice cores?), estimates of global carbonate/POC export rates (which already exist incidentally; Cartapanis et al., 2016; 2018), etc…

What may help to resolve the glacial radiocarbon problem is progress in several different areas. Additional records of glacial atmospheric Δ^{14}C would help to further refine the IntCal Δ^{14}C record. Cosmogenic isotope production records may be improved, e.g., by refining

estimates of ice accumulation, by developing a better understanding of ^{10}Be transport and deposition during the glacial, by recovering additional long and continuous records from Antarctic ice cores and including marine ^{10}Be records, and by obtaining additional geomagnetic data. An expanded spatiotemporal coverage of $\Delta^{14}C$ of DIC in the surface and deep ocean would allow one to narrow the time scales of surface-to-deep transport and air-sea equilibration of $\Delta^{14}C$, carbon and nutrients, and thereby guide model-based analyses. Models should be improved to better represent the glacial cycles of carbon and radiocarbon, by taking into account exchange with sediments and the lithosphere, by better representing coastal processes, and by representing a wide variety of paleo proxies such as $\delta^{13}C$, Nd isotopes, carbonate ion concentration, lysocline evolution, and biological productivity proxies in a 3-D dynamic context. What is also missing are methods to quantify how the global ocean carbon inventory, which co-determines the $^{14}C/C$ ratio and thus $\Delta^{14}C$ value in the ocean, has changed over the last 50,000 years.

We have added the following text to the last paragraph in the summary and conclusions section:

Progress in several different areas may help to resolve the glacial-interglacial radiocarbon problem. Additional records of glacial $\Delta^{14}C_{atm}$ would help refine the older portion of the IntCal $\Delta^{14}C$ record. Cosmogenic isotope production records may be improved, e.g., by refining estimates of ice accumulation, by developing a better understanding of ^{10}Be transport and deposition during the glacial, by recovering additional long and continuous records from Antarctic ice cores and including marine ^{10}Be records, and by obtaining additional geomagnetic field data. An expanded spatiotemporal observational coverage of $\Delta^{14}C$ of DIC in the surface and deep ocean would help narrow the time scales of surface-to-deep transport and air-sea equilibration of $\Delta^{14}C$, carbon and nutrients, and thereby guide model-based analyses. Models should become more sophisticated and detailed in order to reproduce successfully the glacial-interglacial changes in carbon and radiocarbon, by including exchange with sediments and the lithosphere and by better representing coastal processes, and by representing a wide variety of paleo proxies such as $\delta^{13}C$, Nd isotopes, carbonate ion concentration, lysocline evolution, and paleo-productivity proxies in a 3-D dynamic context for model evaluation. What is also missing are methods to quantify how the ocean carbon inventory, which co-determines the $^{14}C/C$ ratio and thus the $\Delta^{14}C$ values in the ocean and atmosphere, has changed over the last 50,000 years.

32. Table 1: it would be helpful to specify here which simulations have active sediments included. Incidentally, why was the rain ratio changed in one simulartion?

As mentioned in lines 209-210 of the original manuscript, all transient simulations are performed with Bern3D model configuration ALL, which is the atmosphere–ocean–land–sediment model configuration. Hence, transient simulations include the 10-layer sediment model of Heinze et al. (1999) and Gehlen et al. (2006). We will clarify this point in Table 1 caption.

As discussed in lines 267-276 and summarized in Table 1, the $CaCO_3$-to-POC export ratio was changed over time in model scenarios BIO, PHYS-BIO, and PHYS-BIOx in order to investigate the impact of biological carbon pump changes on atmospheric $\Delta^{14}C$. While changes in the $CaCO_3$-to-POC export ratio are important for achieving glacial atmospheric CO_2 drawdown, our model results demonstrate that biogeochemical changes alone (scenario BIO) do not lead to an improved simulation of high glacial $\Delta^{14}C$ levels as compared to model runs invoking only physical changes (i.e., changes in ocean circulation and/or air-sea gas exchange). This is clearly illustrated by Fig. 8 and 9.

We have modified the Table 1 caption so that it is clear that the Bern3D model configuration with sediments was used for the transient historical simulations:

In all scenarios, the fully coupled model configuration, including the major global carbon reservoirs (atmosphere, terrestrial biosphere, ocean, and sediments), is used.

33. Fig 3, caption: I think it is more mathematically correct to state <100m and >1500m, no?

Yes, this is a typo that will be corrected in a revised manuscript.

This typo has been corrected in the revised manuscript.

34. Fig 7, caption, line 1203: I think it would be helpful to state ". . .using the mean reconstructed palaeointensity.."

We agree it would be more precise to state that RPI-based $\Delta\Delta^{14}C$ is the difference between reconstructed $\Delta^{14}C$ and model-simulated $\Delta^{14}C$ based on the mean RPI-based ^{14}C production rate.

We have revised the Fig. 7c caption to:

Difference between reconstructed $\Delta^{14}C$ and model-simulated $\Delta^{14}C$ using averaged paleointensity data (RPI-based $\Delta\Delta^{14}C$; gray) and the ice-core ^{10}Be data of Adolphi et al. (2018) (^{10}Be-based $\Delta\Delta^{14}C$; purple), compared with the atmospheric CO_2 record (red).

35. Fig 8: shouldn't all the simulated D14Catm traces start at the same value and end at different values? Although this might look nasty, it suggests a different outlook in my view. Incidentally, the outputs in plots c and d are obvious candidates for comparison with existing data (e.g. Skinner et al., 2019, 20176), perhaps for a future study if not this one.

Since different carbon cycle scenarios (and therefore processes) were used to force the model into a glacial state over a 50,000-year integration, during which the glacial drawdown of atmospheric CO_2 was achieved, the model runs start from different global

$^{14}C/C$ distributions, and therefore different values of atmospheric $\Delta^{14}C$, at 70 kyr BP. The analysis presented in Fig. 9 effectively normalizes the various $\Delta^{14}C$ records so that they are comparable, using two different "corrections".

We have now added the observed data of Skinner et al. (2017) and model results of Butzin et al. (2017), respectively, to Fig. 8d,c.

36. Fig 9: this is a fascinating figure, though I find it slightly problematic. First, what is the rationale for normalizing to the average D14Catm value 0-50ka? I think that plots a and b should be replaced with normalization to the final 'modern' value, and that plots c and d should be extended up to the present. The latter is surely important, as it shows how we (well, you!) can do a pretty good job at simulating the amplitude of D14Catm change in the glacial when tweaking all the model's knobs, but that we can't subsequently get the deglacial change to the modern value, just as we can't quite get the deglacial change in CO2. I feel this must be significant… I wonder what the authors think.

The reason for subtracting the mean value from the $\Delta^{14}C$ records shown in Fig. 9a,b was to remove the offset/trend and emphasize the fluctuations in the $\Delta^{14}C$ data about the overall trend. This is effectively an offset correction normalization. Here, we can see that none of the model runs are able to sustain the high $\Delta^{14}C$ levels after the Mono Lake excursion or capture the sharp decline in $\Delta^{14}C$ during the last deglaciation. We agree with the referee that the $\Delta^{14}C$ records shown in Fig. 9c,d should be extended up to 0 kyr BP.

We do not think that showing $\Delta^{14}C$ anomalies relative to the last millennium $\Delta^{14}C$ value would provide much new information compared to the existing Fig. 7 and 8. Simulated modern $\Delta^{14}C$ values shown in Fig. 7 and 8 are relatively close to observed last millennium values and the remaining discrepancy is small compared to the model-data mismatch during the last glacial period.

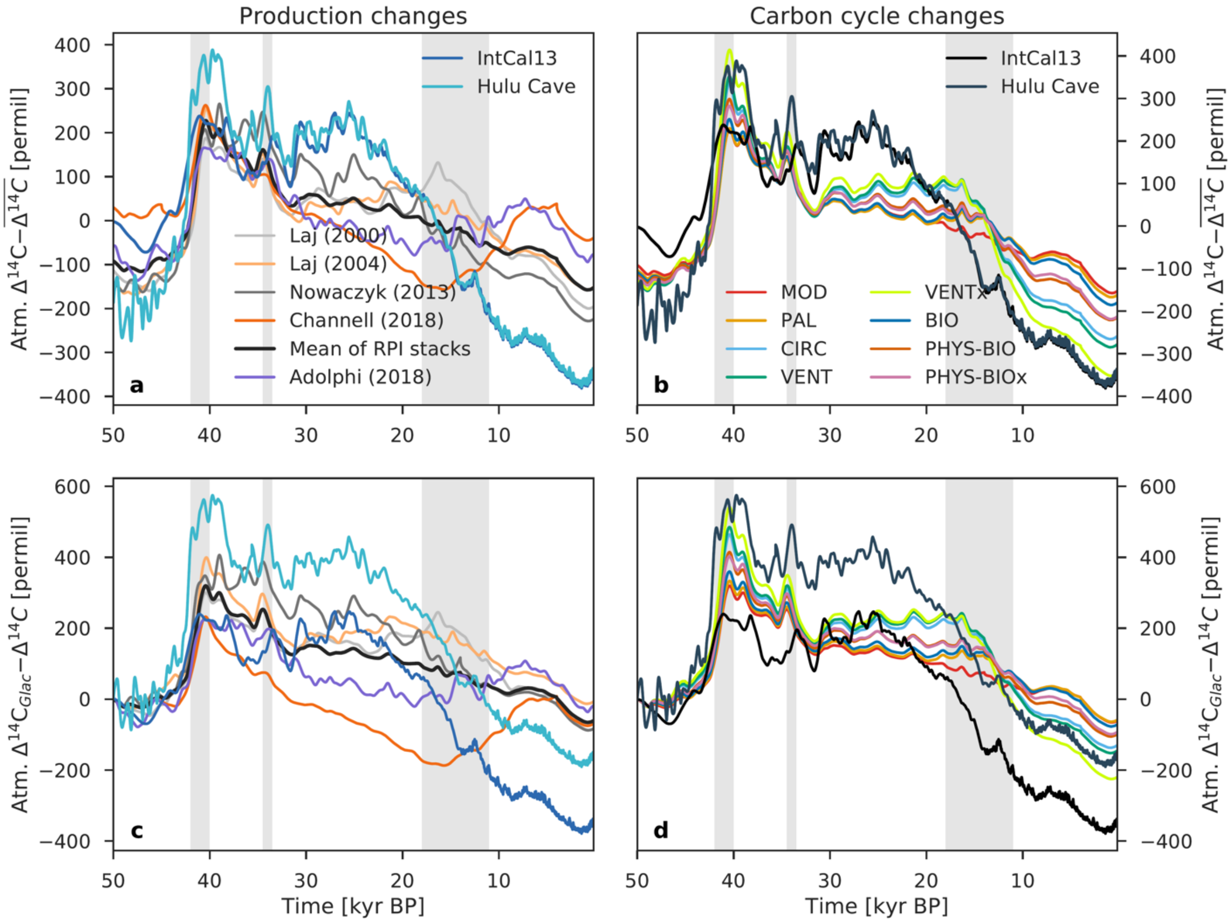

Fig. 9. Comparison of atmospheric Δ^{14}C variability caused by changes in the ocean carbon cycle (b, d) with production-driven changes in atmospheric Δ^{14}C using scenario MOD (a, c). For the analysis of carbon cycle changes, only the results of model runs using the mean paleointensity-based ^{14}C production rate are shown. The Δ^{14}C records in the upper panel (a, b) have been detrended by removing the mean, whereas the lower panel (c, d) shows Δ^{14}C anomalies expressed as differences relative to the Δ^{14}C value at 50 kyr BP. Three vertical light gray bars indicate the Laschamp (~41 kyr BP) and Mono Lake (~34 kyr BP) geomagnetic excursions, and the last glacial termination (~18 to 11 kyr BP).

We have extended the time axis of Fig. 9c,d to 0 kyr BP.

37. Figure 10 and 11: I would suggest including a narrow plot at the base of each of these showing the offsets between simulated and observed values over time.

This is a difficult comparison to make as there is no one true (correct) target value. Nonetheless, we agree that such a comparison would allow the reader to more easily visualize the time periods where disagreement between the deconvolution- and measurement-based production rate estimates is highest, i.e., between 32 and 22 kyr BP.

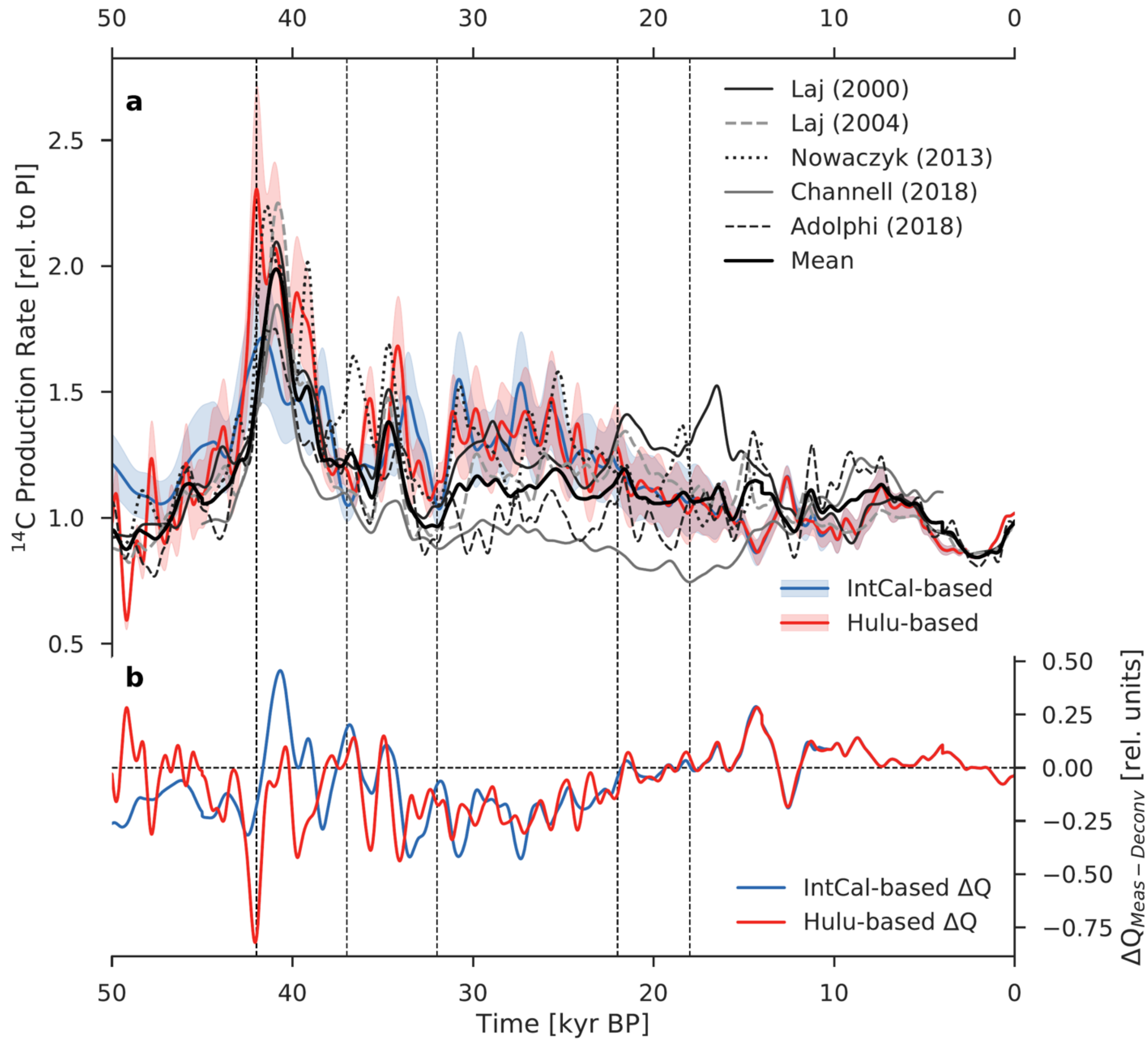

Fig. 10. Comparison of ^{14}C production rate estimates inferred from a deconvolution of the atmospheric Δ^{14}C record and from paleointensity and ice-core ^{10}Be data. (a) ^{14}C production rate calculated as the sum of the modelled air-sea and atmosphere-land $^{14}CO_2$ fluxes and the reconstructed change in the atmospheric ^{14}C inventory and loss of ^{14}C due to radioactive decay (see Eq. [2]). Model-based $^{14}CO_2$ fluxes were obtained by forcing the Bern3D carbon cycle model with reconstructed variations in atmospheric Δ^{14}C and CO_2 as well as seven different carbon cycle scenarios. Results of model runs using the IntCal13 calibration curve are shown in the light blue envelope (2σ), whereas the light red envelope (2σ) shows the results from simulations using the composite Hulu Cave (10.6 to 50 kyr BP) and IntCal13 (0 to 10.6 kyr BP) Δ^{14}C record. The heavy black line is the mean of five available production rate reconstructions: Laj et al. (2000), Laj et al. (2004), Nowaczyk et al. (2013), Channell et al. (2018), and Adolphi et al. (2018). (b) Difference between the mean of the measurement-based production rate estimates (heavy black line) and estimates based on the

deconvolution of the IntCal13 (IntCal-based ΔQ; blue) and Hulu Cave (Hulu-based ΔQ; red) $\Delta^{14}C$ data.

We have added a subplot to Fig. 10 showing the difference between the mean measurement-based ^{14}C production rate and our new estimates based on the deconvolution of the IntCal13 and Hulu Cave $\Delta^{14}C$ records, and updated its caption to better describe the model-based deconvolution approach.

Mysteriously high $\Delta^{14}C$ of the glacial atmosphere: Influence of ^{14}C production and carbon cycle changes

Ashley Dinauer[1,*], Florian Adolphi[1,2], Fortunat Joos[1]

[1]Climate and Environmental Physics, Physics Institute and Oeschger Centre for Climate Change Research, University of Bern, Sidlerstrasse 5, 3012 Bern, Switzerland

[2]Quaternary Sciences, Department of Geology, Lund University, Sölvegatan 12, 22362 Lund, Sweden

*To whom correspondence should be addressed. Email: ashley.dinauer@climate.unibe.ch

Abstract. Despite intense focus on the ~190 permil drop in atmospheric $\Delta^{14}C$ during Heinrich Stadial 1 ~17.4 to 14.6 kyr BP, the specific mechanisms responsible for the apparent $\Delta^{14}C$ excess in the glacial atmosphere have received considerably less attention. The computationally efficient Bern3D earth system model of intermediate complexity, designed for long-term climate simulations, allows us to address a very fundamental but still elusive question concerning the atmospheric $\Delta^{14}C$ record: How can we explain the persistence of relatively high $\Delta^{14}C$ values during the millennia after the Laschamp event? Large uncertainties in the pre-Holocene ^{14}C production rate, as well as in the older portion of the $\Delta^{14}C$ record, complicate our qualitative and quantitative interpretation of the glacial $\Delta^{14}C$ elevation. Here we begin with sensitivity experiments that investigate the controls on atmospheric $\Delta^{14}C$ in idealized settings. We show that the interaction with the ocean sediments may be much more important to the simulation of $\Delta^{14}C$ than had been previously thought. In order to provide a bounded estimate of glacial $\Delta^{14}C$ change, the Bern3D model was integrated with five available estimates of the ^{14}C production rate as well as reconstructed and hypothetical paleoclimate forcing. Model results demonstrate that none of the available reconstructions of past changes in ^{14}C production can reproduce the elevated $\Delta^{14}C$ levels during the last glacial. In order to increase atmospheric $\Delta^{14}C$ to glacial levels, a drastic reduction of air-sea exchange efficiency in the polar regions must be assumed, though discrepancies remain for the portion of the record younger than ~33 kyr BP. We end with an illustration of how the ^{14}C production rate would have had to evolve to be consistent with the $\Delta^{14}C$ record, by combining an atmospheric radiocarbon budget with the Bern3D model. The overall conclusion is that the remaining discrepancies with respect to glacial $\Delta^{14}C$ may be linked to an underestimation of ^{14}C production and/or a biased-high reconstruction of $\Delta^{14}C$ over the time period of interest. Alternatively, we appear to still be missing an important carbon cycle process for atmospheric $\Delta^{14}C$.

Deleted: across the deglacial "mystery interval"

Deleted: more

Deleted: long-term process of sedimentation

Deleted: sized

1 Introduction

The cosmogenic radionuclide radiocarbon (^{14}C) is a powerful tracer for the study of several ocean processes including deep ocean circulation and ventilation. Past changes in atmospheric $^{14}C/C$ (i.e., $\Delta^{14}C_{atm}$, in permil; corresponding to Δ from Stuiver and Polach, 1977), as recorded in absolutely dated tree rings, plant macrofossils, speleothems, corals, and foraminifera, have been interpreted as possibly reflecting real changes in the ocean's large-scale overturning circulation (Siegenthaler et al., 1980). The extended 54,000-year record of $\Delta^{14}C_{atm}$ from the latest IntCal compilation (i.e., IntCal13; Reimer et al., 2013) and from two Hulu Cave stalagmites (Cheng et al., 2018) suggests that large millennial-scale variations in $\Delta^{14}C_{atm}$ have occurred during the last glacial, compared to the relatively small (~30 ppm) change in atmospheric CO_2 over the same time period (Fig. 1). When interpreting the implications of such changes, it is important to note that $\Delta^{14}C_{atm}$ is controlled not only by global carbon cycle processes but also by variations in the atmospheric ^{14}C production rate. Therefore, the use of $\Delta^{14}C_{atm}$ as an indicator of past oceanic conditions, particularly those associated with air-sea exchange efficiency and deep ocean ventilation rates, requires reliable estimates of the ^{14}C production rate over time.

The vast majority of all ^{14}C production changes are the result of either solar or geomagnetic modulation of the cosmic ray flux reaching the Earth (Masarik and Beer, 1999; Poluianov et al., 2016). Fig. 1 shows several different proxy records of the global production rate of ^{14}C in relative units covering the full range of the ^{14}C dating method, based on geomagnetic field data from marine sediments (Laj et al., 2000; Laj et al., 2004; Nowaczyk et al., 2013; Channell et al., 2018) and on ^{10}Be and ^{36}Cl measurements in polar ice cores (Adolphi et al., 2018). A fundamental difference between these reconstruction methods is that paleointensity-based estimates of the ^{14}C production rate, by definition, do not reflect changes in the solar modulation of the cosmic radiation, whereas ice-core ^{10}Be-based estimates give the combined influence of solar and geomagnetic modulation on radionuclide production. Of note is the striking coherence in all three records $\Delta^{14}C_{atm}$, paleointensity-based production, and ice-core ^{10}Be-based production) of the Laschamp excursion (~41 kyr BP), when the Earth's geomagnetic dipole field briefly reversed and its intensity was close to zero (Nowaczyk et al., 2012; Laj et al., 2014). According to reconstructions and production rate models, this large geomagnetic event caused a doubling of the ^{14}C production rate, leading to the highest $\Delta^{14}C_{atm}$ values over the last 54 kyr. Relatively high $\Delta^{14}C_{atm}$ values continued until ~25 kyr BP, then gradually diminished to preindustrial levels, interrupted by a sharp drop in $\Delta^{14}C_{atm}$ during Heinrich Stadial 1 (HS1), ~17.4 to 14.6 kyr BP (sometimes called the "mystery interval"; Broecker and Barker, 2007). While the Laschamp geomagnetic excursion appears to be responsible for the $\Delta^{14}C_{atm}$ peak at ~41 kyr BP, the production rate estimates during much of the pre-Holocene period are subject to considerable uncertainty.

Paleointensity-based reconstructions are sensitive to coring disturbances of poorly consolidated sediments. The last 50 kyr are represented by the relatively slushy uppermost few meters of recovered marine sediment cores (Channell et al., 2018). Channell et al. (2018) preferentially selected cores recovered using conventional piston and square barrel gravity coring methods, and from sites with high mean (> 15 cm kyr^{-1}) sedimentation rates, so as to minimize the influence of drilling disturbance, and reached very different production rates than, e.g., Laj et al. (2000). On the other hand, ice-core ^{10}Be records are affected by changes in the transport and deposition of atmospheric ^{10}Be, which may overprint the production rate changes (e.g., Heikkilä et al., 2013). Furthermore, in order to calculate the ice-core ^{10}Be deposition fluxes, snow accumulation rates must be known for each specific ice core, which themselves have uncertainties on the order of 10 to 20 percent that propagate into the ice-core ^{10}Be fluxes (Gkinis et al., 2014;

Deleted: atmospheric $\Delta^{14}C$

Deleted: $\Delta^{14}C$

Deleted: Fig. 1

Deleted: atmospheric $\Delta^{14}C$

Deleted: atmospheric $\Delta^{14}C$

Deleted: Figure 1

Deleted: ($\Delta^{14}C$

Deleted: $\Delta^{14}C$

Deleted: $\Delta^{14}C$

Deleted: $\Delta^{14}C$

Deleted: the

Deleted: so-called "mystery interval"

Deleted: 5

Deleted: 5

Deleted: coincident with Heinrich Stadial 1 [HS1]

Deleted: $\Delta^{14}C$

Deleted: unconsolidated

Deleted: uppermost,

Deleted: centi

Deleted: used

Deleted: only highly accumulating sites and different coring equipment

Deleted: avoid

Deleted: some of these problems

Deleted: conclusions

Deleted: Similarly

Rasmussen et al., 2013). The large uncertainties associated with the reconstruction of past changes in ^{14}C production hamper our ability to predict reliably the extent to which production changes contributed to high glacial $\Delta^{14}C_{atm}$ levels. Only if estimates of past changes in ^{14}C production are robust can one improve assessments of the relative importance of the two fundamental mechanisms responsible for glacial-interglacial $\Delta^{14}C$ changes: (1) production changes and (2) carbon cycle changes.

Earlier model studies have focused heavily on the ~190 permil drop in $\Delta^{14}C_{atm}$ during HSI and on the deglacial trends in $\Delta^{14}C_{atm}$ after HS1 (Muscheler et al., 2004; Broecker and Barker, 2007; Skinner et al., 2010; Mariotti et al., 2016; Delaygue et al., 2003; Marchal et al., 2001; Huiskamp and Meissner, 2012; Hain et al., 2014). Historically, the younger portion of the $\Delta^{14}C_{atm}$ record has received more attention than the glacial section because of the early emphasis on the general climatic trends of the North Atlantic stadials (HS1 and the Younger Dryas [YD]) and the Bølling-Allerød (BA) warm period, and on the important role of an exceptionally aged (^{14}C-depleted) deep-water mass in the pulsed rise of atmospheric CO_2 during the last glacial termination (e.g., Skinner et al., 2017). Less research over the last few decades has studied the specific mechanisms responsible for high glacial $\Delta^{14}C_{atm}$ levels. The model studies that are available point out the difficulties in simulating the correct glacial $\Delta^{14}C_{atm}$ levels (Hughen et al., 2004; Köhler et al., 2006). These studies demonstrate with box models that glacial levels of $\Delta^{14}C_{atm}$ cannot be attained without invoking significant changes in ocean circulation, air-sea gas exchange, and carbonate sedimentation. However, the box models were not able to reproduce $\Delta^{14}C_{atm}$ values higher than 700 permil, and these results still need to be scrutinized with models of higher complexity. To our knowledge, no three-dimensional ocean biogeochemical model has yet simulated the 50,000-year record of $\Delta^{14}C_{atm}$. Many questions remain unanswered, in particular: What mechanism can account for the persistence of relatively high $\Delta^{14}C_{atm}$ values during the millennia after the Laschamp excursion?

The expected time scale for sustaining elevated levels of $\Delta^{14}C_{atm}$ after a production peak is on the order of thousands of years, a time scale tied to the mean lifetime of ^{14}C (~8223 years; Audi et al., 2003; Bé et al., 2013) and the time required for deep ocean ventilation (on the order of 1000 years or more; Primeau, 2005). Specifically, Muscheler et al. (2004) demonstrate that the characteristic time constant for equilibration of $\Delta^{14}C_{atm}$ after a perturbation in atmospheric production is 5000 years. By this analysis, the Laschamp event, which lasted only about 1500 to 2000 years (Laj et al., 2000), was insufficient to sustain the high $\Delta^{14}C_{atm}$ values observed over the next ~15,000 years. The lack of significant changes (only ~10 percent) in atmospheric CO_2 during the time period of interest raises the question of what causes variations in $\Delta^{14}C_{atm}$, but not CO_2, on millennial time scales? The obvious answers are: cosmic ray modulation and air-sea gas exchange. Ultimately, no explanation for high glacial $\Delta^{14}C_{atm}$ levels can be complete in the absence of more robust estimates of the pre-Holocene ^{14}C production rate, as well as a good understanding of the ocean carbon cycle under glacial climate conditions.

One of the major challenges associated with modelling glacial-interglacial climate cycles is that it is currently not possible to reproduce climate and atmospheric CO_2 variations on the basis of orbital forcing alone. Problems

Deleted: lead to two distinct interpretation problems with respect to the atmospheric $\Delta^{14}C$ record: (1) the specific mechanisms responsible for high glacial

Deleted: $\Delta^{14}C$ levels, and (2) the extent to which production changes contributed to the deglacial $\Delta^{14}C$ decline.

Deleted: atmospheric $\Delta^{14}C$

Deleted: across the mystery interval

Deleted: $\Delta^{14}C$

Deleted: $\Delta^{14}C$

Deleted: $\Delta^{14}C$

Deleted: $\Delta^{14}C$

Deleted: $\Delta^{14}C$

Deleted: $\Delta^{14}C$

Deleted: $\Delta^{14}C$

Deleted: $\Delta^{14}C$

Deleted: atmospheric $\Delta^{14}C$

Deleted: up to about 1000 years

Deleted: $\Delta^{14}C$

Deleted: $\Delta^{14}C$

Deleted: atmospheric $\Delta^{14}C$

Deleted: $\Delta^{14}C$

include the complexity of the Earth system, making it difficult to represent all the relevant processes in models, and the long time scales involved, making simulations covering tens of thousands of years costly in computation time. Glacial-interglacial simulations with dynamic ocean and land models of intermediate complexity have begun to emerge, but these models are not yet able to reproduce the reconstructed variations in important proxy data or the timing of CO_2 variations during the last glacial termination (Brovkin et al., 2012; Ganopolski and Brovkin, 2017; Menviel et al., 2012). A wide variety of mechanisms, both physical and biological, centered on or connected with the ocean, as well as exchange processes with the land biosphere, marine sediments, coral reefs, and the lithosphere, are thought to play a role in explaining the glacial-interglacial variations in atmospheric CO_2 (Archer et al., 2000; Fischer et al., 2010; Wallmann et al., 2016; Galbraith and Skinner, 2020), but how they interacted over time under the influence of orbital forcing remains elusive. We appear to still be missing a single framework in which these mechanisms are linked to each other in a predictable manner. As long as there are still large gaps in our understanding of the glacial climate and associated ocean carbon cycle, a convenient way to examine the impact of the possible mechanisms on atmospheric CO_2 levels, and here on $\Delta^{14}C_{atm}$ is to perform sensitivity experiments and scenario-based simulations with models. This allows us to investigate specific phenomena in idealized settings, permitting us to investigate in detail which parameters and processes are most important in controlling $\Delta^{14}C_{atm}$ levels.

In this paper we extend previous modelling efforts concerning the record of $\Delta^{14}C_{atm}$ with respect to three issues: (1) the sensitivity of the $\Delta^{14}C_{atm}$ response to carbon cycle changes and the potential importance of marine sediments, (2) the simulation of $\Delta^{14}C_{atm}$ covering the time range of the IntCal13 radiocarbon calibration curve (50,000 years), the primary focus being the explanation of high glacial $\Delta^{14}C_{atm}$ levels, and (3) a new 50,000-year record of the ^{14}C production rate, as inferred by deconvolving the reconstructed histories of $\Delta^{14}C_{atm}$ and CO_2 with a prognostic carbon cycle model and considering the uncertainties associated with the glacial-interglacial ocean carbon cycle. In the following sections we first introduce the Bern3D earth system model of intermediate complexity and describe the carbon cycle scenarios for forcing it. We then use step changes in the ^{14}C production rate and in selected parameters of the ocean carbon cycle model to gain insight into the transient and equilibrium response of $\Delta^{14}C_{atm}$. After these sensitivity experiments we present the results of paleoclimate simulations forced by available reconstructions of past changes in ^{14}C production together with reconstructed and hypothetical carbon cycle changes accompanying glacial-interglacial climate cycles. Finally, we present results for a first attempt to reconstruct the glacial history of the ^{14}C production rate using the Bern3D model forced with reconstructed variations in $\Delta^{14}C_{atm}$ and CO_2 as well as a wide range of carbon cycle scenarios. We end with a comparison of three fundamentally different (model-based, paleointensity-based, and ice-core ^{10}Be-based) reconstructions of atmospheric ^{14}C production.

2 Materials and methods

2.1 Brief description of the Bern3D model

Deleted: related to the ocean and land carbon cycles including…
Deleted: have been proposed to
Deleted: the causes
Deleted: $\Delta^{14}C$
Deleted: more
Deleted: atmospheric $\Delta^{14}C$
Deleted: atmospheric $\Delta^{14}C$
Deleted: $\Delta^{14}C$
Deleted: $\Delta^{14}C$
Deleted: $\Delta^{14}C$
Deleted: model-based
Deleted: reconstruction
Deleted: for the last 50 kyr as inferred from
Deleted: an atmospheric radiocarbon budget
Deleted: atmospheric $\Delta^{14}C$
Deleted: well-known
Deleted: sized
Deleted: atmospheric $\Delta^{14}C$
Deleted: .

Simulations are performed with the computationally efficient Bern3D earth system model of intermediate complexity (version 2.0), which is designed for long-term climate simulations over several tens of thousands of years. The Bern3D couples a frictional geostrophic 3-D ocean general circulation model (Edwards et al., 1998; Edwards and Marsh, 2005; Müller et al., 2006), a 2-D energy-moisture balance atmosphere model (Ritz et al., 2011), an ocean carbon cycle model (Müller et al., 2008; Tschumi et al., 2008; Parekh et al., 2008), a chemically active 10-layer ocean sediment model (Heinze et al., 1999; Tschumi et al., 2011; Roth et al., 2014; Jeltsch-Thömmes et al., 2019), and a four-box model representing carbon stocks in the terrestrial biosphere (Siegenthaler and Oeschger, 1987). The coarse-resolution ocean model is implemented on a 41 x 40 horizontal grid, with 32 logarithmically spaced layers in the vertical. The seasonal cycle is resolved with 96 time steps per year. The tracers carried in the ocean model include temperature, salinity, dissolved inorganic carbon (DIC), dissolved organic carbon (DOC), carbon isotopes (^{14}C and ^{13}C) of DIC and DOC, alkalinity (Alk), phosphate, silicate, iron, dissolved oxygen (O_2), preformed dissolved oxygen ($O_{2,pre}$), and an "ideal age" tracer. The ideal age is set to zero in the surface layer, increased by Δt in all interior grid cells at each time step of duration Δt, and transported by advection, diffusion, and convection. Atmospheric CO_2, $^{14}CO_2$, and $^{13}CO_2$ are also carried as tracers in the atmosphere model. For a more complete description of the Bern3D model, the reader is referred to Appendix A.

2.2 Implementation of the ^{14}C tracer

Natural radiocarbon (^{14}C) is a cosmogenic radionuclide produced in the atmosphere by cosmic radiation. Once oxidized to $^{14}CO_2$, it participates in the global carbon cycle. Atmospheric $^{14}CO_2$ invades the ocean by air-sea gas exchange, where it is subject to the same physical and biogeochemical processes that affect DIC. The only difference is that ^{14}C is lost by radioactive decay (half-life of 5700 $\pm$ 30 years; Audi et al., 2003; Bé et al., 2013). The governing natural processes, namely, atmospheric ^{14}C production, air-sea gas exchange, physical transport and mixing in the water column, biological production and export of particulate and dissolved matter from the surface ocean, particle flux through the water column, particle deposition on the sea floor, remineralization and dissolution in the water column and the sediment pore waters, and vertical sediment advection and sediment accumulation, are explicitly represented in the Bern3D model (see Fig. 2). Air-sea gas exchange is parameterized using a modified version of the standard gas transfer formulation of OCMIP-2, with exchange rates that vary across time and space (see Appendix A for more details).

Radiocarbon measurements are generally reported as $\Delta^{14}C$, i.e., the ratio of ^{14}C to total carbon C relative to that of the AD 1950 atmosphere, with a correction applied for fractionation effects, e.g., due to gas exchange and photosynthesis (see Stuiver and Polach, 1977). In this model study, $\Delta^{14}C$ is treated as a diagnostic variable using the two-tracer approach of OCMIP-2. Rather than treating the ^{14}C/C ratio as a single tracer, fractionation-corrected ^{14}C is carried independently from the carbon tracer. The modelled ^{14}C concentration is normalized by the standard ratio of the preindustrial atmosphere ($^{14}r_{std}$ = 1.170 x 10^{-12}; Orr et al., 2017) in order to minimize the numerical error of

Deleted: this model study

Deleted: 3

Deleted: 4

Deleted: ALK

Formatted: Font colour: Text 1

Deleted: Fig. 2

Deleted: Modelled ^{14}C is often expressed relative to carbon, which is convenient for comparison to

Deleted: r

Deleted: which

Deleted: . The purpose of $\Delta^{14}C$

Deleted: fractionation-corrected

Deleted: /

Deleted: is to isolate the effect of radioactive decay

Deleted: modelling only

Deleted: the

Deleted: tracer

Formatted: Superscript

Deleted: It

carrying very small numbers. For comparison to observations, $\Delta^{14}C$ is calculated from the normalized and fractionation-corrected modelled ^{14}C concentration as follows:

$$\Delta^{14}C = 1000\left({}^{14}r' - 1\right) \qquad (1)$$

where ${}^{14}r'$ is the ratio of $^{14}C/C$ in either atmospheric CO_2 or oceanic DIC divided by ${}^{14}r_{std}$, depending on the reservoir being considered. The approach taken to simulate atmospheric $^{14}CO_2$ is analogous to the approach used for CO_2, except that the equation includes the terms due to atmospheric production and radioactive decay. For simulations where the sediment model is active, the oceanic DIC tracer sees a constant input from terrestrial weathering, whereas there is no weathering input of $DI^{14}C$ to the ocean (see Appendix A for more details).

In the preindustrial spin-up simulation needed to initialize the Bern3D model, atmospheric CO_2 is held constant at 278.05 ppm and $\Delta^{14}C_{atm}$ at 0 permil. During this integration time the ocean inventories of carbon and ^{14}C adjust to the forcing fields. The resulting changes after >50,000 years of integration are negligibly small. Fig. 3 shows the steady-state $\Delta^{14}C$ distribution in the surface (< 100 m) and deep (> 1500 m) ocean for the preindustrial control run. The large-scale distribution of modelled oceanic $\Delta^{14}C$ broadly resembles the observed pattern in the Global Ocean Data Analysis Project (GLODAP; Key et al., 2004). That final state (i.e., the end of the preindustrial spin-up) is used to diagnose the ^{14}C production rate for the preindustrial atmosphere, such that the rate of ^{14}C production is balanced by radioactive decay and the net fluxes out of the atmosphere. For transient simulations, an adjustable scale factor is applied to the preindustrial steady-state value of 443.9 mol ^{14}C per year (1.66 atoms cm^{-2} s^{-1}) in order to account for production changes induced by solar and/or geomagnetic modulation. These production changes are derived from, e.g., available reconstructions of the ^{14}C production rate in relative units, as detailed in Sect. 2.5. Note the preindustrial spin-up results in steady-state values for weathering-derived inputs of DIC, Alk, P, and Si of 0.46 Gt C per year, 34.37 Tmol HCO_3^- per year, 0.17 Tmol P per year, and 6.67 Tmol Si per year, respectively. These terrestrial weathering rates were chosen to balance the sedimentation rates on the sea floor and are held fixed and constant throughout the simulations.

2.3 Model configurations

We focus in this paper on the response of $\Delta^{14}C_{atm}$ to changes in ^{14}C production and the ocean carbon cycle. For a deeper mechanistic understanding of the driving processes, step response experiments are first performed (see Sect. 3.1). These simulations include perturbations of the steady-state $^{14}C/C$ distribution under preindustrial conditions. We investigate the impact of step changes in (1) the ^{14}C production rate ("higher production" scenario), (2) wind stress and vertical diffusivity ("reduced deep ocean ventilation" scenario), and (3) the gas transfer velocity ("enhanced permanent sea ice cover" scenario). After a step change at time 0, the simulations are run to near-equilibrium over a 50,000-year integration. The following model configurations and therefore exchanging carbon reservoirs are

Deleted: . It is also fractionation corrected
Deleted: is
Deleted:
Formatted: Not Superscript/ Subscript
Deleted: .
Deleted: source-minus-sink equation for
Deleted: the atmospheric carbon tracer (i.e., gaseous
Deleted:)
Deleted: that
Deleted: 14
Deleted: omits
Deleted: source–sink
Deleted: With respect to the ocean carbon cycle model, the
Deleted: oceanic carbon tracer
Deleted: of DIC
Deleted: on land
Deleted: supply
Deleted: from terrestrial weathering
Deleted: .
Deleted: atmospheric $\Delta^{14}C$
Formatted: Font colour: Text 1
Deleted: Figure 3
Deleted: The former is
Deleted: atmospheric $\Delta^{14}C$

considered: atmosphere–ocean (OCN), atmosphere–ocean–land (OCN-LND), atmosphere–ocean–sediment (OCN-SED), and atmosphere–ocean–land–sediment (ALL).

Next we examine the influence of changes that are transient in nature. We simulate $\Delta^{14}C_{atm}$ over the full range of the ^{14}C dating method (i.e., 50 to 0 kyr BP) (see Sect. 3.2 and 3.3). These transient simulations are initialized at 70 kyr BP using model configuration ALL, and forced by reconstructed changes in ^{14}C production (see Sect. 2.5) over a 70,000-year integration. The first 20,000 years of the integration are considered a spin-up. Although the full record is simulated, we focus our analysis on the millennial-scale variation in $\Delta^{14}C_{atm}$ before incipient deglaciation at ~18 kyr BP. Eight model runs are carried out for each production rate reconstruction, using different combinations of forcing fields and parameter values as described next.

Deleted: atmospheric $\Delta^{14}C$

Deleted: atmospheric $\Delta^{14}C$

2.4 Carbon cycle scenarios

In our transient simulations with the Bern3D model, eight scenarios based on different assumptions about the global carbon cycle are considered, the details of which are summarized in Table 1. The goal is to investigate the extent to which changes in the ocean carbon cycle could explain high glacial $\Delta^{14}C_{atm}$ levels, given available reconstructions of past changes in ^{14}C production. We therefore consider a wide range of carbon cycle scenarios, including some extreme cases. A note of caution. Because millennial-scale $\Delta^{14}C_{atm}$ variations during the last glacial are what we are interested in, we do not attempt to reproduce abrupt climate perturbations such as Dansgaard-Oeschger warming events in the model runs.

Deleted: $\Delta^{14}C$

Formatted: Superscript

In the first scenario (MOD), the model is run with fixed preindustrial boundary conditions for the Earth's orbital parameters, radiative forcing due to well-mixed greenhouse gases, and ice sheet extent. As a consequence, atmospheric CO_2 remains approximately constant at the preindustrial level of 278.05 ppm over the simulation. The second scenario (PAL) considers reasonably well-known climate forcing over the last glacial-interglacial cycle. Simulations under this scenario are initialized with output from a previous spin-up simulation forced by glacial boundary conditions with respect to orbital parameters (Berger, 1978), greenhouse gas radiative forcing based on reconstructed atmospheric greenhouse gases (Köhler et al., 2017; Enting, 1987), and ice sheet extent. In simulations under PAL, the model is integrated until 0 kyr BP following the reconstructed histories of the former. Ice sheets for the preindustrial and Last Glacial Maximum (LGM) states are taken from Peltier (1994) and linearly scaled using the global benthic $\delta^{18}O$ stack of Lisiecki and Stern (2016), which is a global ice volume proxy. Changes in the albedo, salinity and latent heat flux associated with the ice sheet buildup or melting are also taken into account (Ritz et al., 2011). Note that, although the radiative forcing for CO_2 is prescribed, the atmospheric CO_2 concentration is allowed to evolve freely, except in the simulations described in Sect. 2.5.

Model scenario PAL appears to still be missing an important process or feedback for atmospheric CO_2, as it cannot reproduce the observed low glacial CO_2 level without invoking additional changes (see, e.g., Tschumi et al., 2011; Menviel et al., 2012; Roth and Joos, 2013; Jeltsch-Thömmes et al., 2019). Variations in atmospheric CO_2 govern how fast $\Delta^{14}C$ signatures are passed between the atmosphere and ocean. Gross fluxes of ^{14}C between the atmosphere and ocean, and vice versa, scale with atmospheric pCO_2 and its $^{14}C/C$ ratio. It is therefore important to reproduce low glacial atmospheric CO_2 concentrations in at least some of the model scenarios, thereby capturing the influence of temporal changes in CO_2 on the air-sea exchange of ^{14}C. In this study, we consider six scenarios that invoke additional changes to force the model toward the observed low glacial CO_2 concentration. In addition to the PAL forcing, a time-varying scale factor $F(t)$ is applied to some combination of tunable model parameters: wind stress scale factor τ, vertical diffusivity K_V, gas transfer velocity k_w, $CaCO_3$-to-particulate organic carbon (POC) export ratio rr, and POC remineralization length scale ℓ_{POC}. For the preindustrial period, the value of $F(t)$ is fixed at 1, whereas the theoretical LGM value was chosen in order to achieve an atmospheric CO_2 concentration close to the LGM level of ~190 ppm (see Table 1), as determined by sensitivity experiments. Note that the same values of $F(t)$ apply to any of the model parameters considered in a given scenario. To obtain intermediate values, $F(t)$ is linearly scaled using the global benthic $\delta^{18}O$ stack (see Fig. 1). For the spin-up needed to initialize these simulations, the glacial spin-up simulation of PAL was integrated for 50,000 model years, with tunable parameters adjusted to their appropriate glacial values. Atmospheric CO_2 drawdown of up to ~100 ppm is achieved over this 50,000-year integration. From that final spun-up state, the model is run forward in time until 0 kyr BP with PAL and $F(t)$ forcing.

The first of these scenarios (CIRC) allows us to test the sensitivity of the model results with respect to changes in ocean circulation. Tunable model parameters τ and K_V were reduced to 40 percent of their preindustrial values throughout the global ocean during the LGM (i.e., $F_{\tau,K_V} = 0.4$). Such a drastic change in the wind stress field is not realistic. Rather, these changes should be viewed as "tuning knobs" that force the ocean model into a poorly ventilated state with an "older" ideal age and ^{14}C-depleted deep waters, as suggested for the glacial ocean (e.g., Sarnthein et al., 2013; Skinner et al., 2017). In the model's implementation, a change in wind stress does not affect the gas transfer velocity k_w, unlike in the real ocean where changes in wind stress and wind speed act together. The influence of a change in air-sea exchange efficiency on the model results was investigated in a second scenario (VENT) where k_w is reduced in the model's north (> 60°N) and south (> 48°S) polar areas in addition to global reductions of τ and K_V ($F_{\tau,K_V,k_w} = 0.4$). A 60 percent reduction of k_w is unlikely to be correct but is a straightforward way to reduce the model's gas exchange efficiency. In the third scenario (VENTx), reduction of polar k_w to 0 percent of its preindustrial value was tested ($F_{\tau,K_V} = 0.4$; $F_{k_w} = 0.0$). Here, k_w remains fixed at 0 percent during the last glacial and is adjusted to its preindustrial value via a linear ramp across the last glacial termination (~18 to 11 kyr BP). In this scenario, sea ice would permanently cover 100 percent of the Southern Ocean during the last glacial, which is not supported by the sea ice reconstructions of Gersonde et al. (2005) and Allen et al. (2011), and also the high-latitude (> 60°N) North Atlantic and Arctic Ocean, for which there is some evidence (Müller and Stein, 2014; Hoff et al., 2016).

We end by investigating the sensitivity of the model results to changes in the parameters controlling the export production of $CaCO_3$ and the water column remineralization of POC. Model scenario BIO considers changes of the $CaCO_3$-to-POC export ratio (and thus also the $CaCO_3$-to-POC rain ratio; Archer and Maier-Reimer, 1994)

Deleted: ¶
¶

Deleted: Fig. 1

Deleted:

(F_{rr} = 0.8) and POC remineralization length scale (Roth et al., 2014) ($F_{\ell_{POC}}$ = 1.2). These changes impact the global carbon cycle by influencing the vertical gradients of DIC, Alk, and nutrients in the water column. A change in the fluxes of POC and $CaCO_3$ to the sea floor drives a change in the magnitude of their removal by sedimentation on the sea floor. A modest reduction in the export ratio during the last glacial is compatible with reconstructed variations in carbonate ion concentrations (Jeltsch-Thömmes et al., 2019). How the depth of POC remineralization changed over time is still unknown. The last two scenarios consider the combined effect of physical and biogeochemical changes: PHYS-BIO ($F_{\tau,K_V,k_w,rr}$ = 0.7) and PHYS-BIOx ($F_{\tau,K_V,k_w,rr}$ = 0.8; $F_{\ell_{POC}}$ = 1.2).

Deleted: ALK

Deleted: POC and $CaCO_3$ burial in the sediments

2.5 Measurement- and model-based reconstruction of ^{14}C production

Deleted: Field

Our ability to attribute past changes in $\Delta^{14}C_{atm}$ to climate-related changes in the ocean carbon cycle is limited by our ability to reconstruct a precise and accurate history of the ^{14}C production rate. Past changes in ^{14}C production can be estimated from geomagnetic field reconstructions and from ^{10}Be measurements in polar ice cores. For ice-core ^{10}Be-based estimates, we use the ice-core radionuclide stack of Adolphi et al. (2018), which is based on ^{36}Cl data from the GRIP ice core (Baumgartner et al., 1998), and on ^{10}Be data from the GRIP (Yiou et al., 1997; Baumgartner et al., 1997; Wagner et al., 2001; Muscheler et al., 2004; Adolphi et al., 2014) and GISP2 (Finkel and Nishiizumi, 1997) ice cores. It also includes ^{10}Be data from the NGRIP, EDML, EDC, and Vostok ice cores around the Laschamp geomagnetic excursion (Raisbeck et al., 2017). It has been extended to the present using the ^{10}Be stack of Muscheler et al. (2016). All ice cores were first placed on the same time scale (GICC05) before ^{10}Be fluxes were calculated. This 70,000-year ^{10}Be stack provides relative changes of ^{14}C production rates under the assumption that ^{14}C and ^{10}Be production rates are directly proportional, as indicated by the most recent production rate models (e.g., Herbst et al., 2017).

Deleted: atmospheric $\Delta^{14}C$

For paleointensity-based estimates, we employ (1) the North Atlantic Paleointensity Stack, or NAPIS, by Laj et al. (2000) as extended by Laj et al. (2002), (2) the Global Paleointensity Stack, or GLOPIS, by Laj et al. (2004), (3) a high-resolution paleointensity stack from the Black Sea (Nowaczyk et al., 2013), and (4) a paleointensity stack from Iberian Margin sediments (Channell et al., 2018). In principle, stacks of widely distributed cores (NAPIS/GLOPIS) are expected to yield a better representation of the global geomagnetic dipole moment, whereas the paleointensity stacks from the Black Sea and the Iberian Margin avoid some of the problems associated with coring disturbances. The four different paleointensity stacks were converted to ^{14}C production rates using the production rate model of Herbst et al. (2017), the local interstellar spectrum of Potgieter et al. (2014), and assuming a constant solar modulation potential of 630 MeV.

An alternative approach to estimating the ^{14}C production rate is to combine an atmospheric radiocarbon budget with a prognostic carbon cycle model. Here simulations are performed with the Bern3D model and forced by reconstructed changes in $\Delta^{14}C_{atm}$ and CO_2, as well as reconstructed and hypothetical carbon cycle changes, over the last 50 kyr. Both the IntCal13 calibration curve (Reimer et al., 2013) and the recent Hulu Cave $\Delta^{14}C_{atm}$ dataset (Cheng

Deleted: atmospheric $\Delta^{14}C$

Deleted: $\Delta^{14}C$

et al., 2018) are used. Note that although the forthcoming IntCal20 calibration curve (Reimer et al., in press) will be the new standard atmospheric radiocarbon record for the last 55,000 years, essentially all data underlying IntCal20 before 13.9 kyr BP are tied to the Hulu Cave dataset, either via time scales (Lake Suigetsu plant macrofossil data) or marine reservoir corrections (marine records). Hence, the IntCal20 and Hulu Cave $\Delta^{14}C_{atm}$ records are very similar and using IntCal20 would not impact our conclusions.

The ^{14}C production rate Q is calculated, each model year, from the air-sea $^{14}CO_2$ flux (F_{as}), the atmosphere-land $^{14}CO_2$ flux (F_{ab}), the loss of ^{14}C due to radioactive decay, and the change ($\dot{I}_a$) in the atmospheric ^{14}C inventory (I_a):

$$Q = F_{as} + F_{ab} + \lambda I_a + \dot{I}_a \tag{2}$$

where λ is the radioactive decay constant for ^{14}C, i.e., $\lambda = \ln 2 / 5700 \text{ years} = 1.2160 \times 10^{-4} \text{ yr}^{-1}$. The radioactive decay term λI_a and the change in inventory $\dot{I}_a$ follow the reconstructed $\Delta^{14}C_{atm}$ and CO_2 records, whereas F_{as} and F_{ab} are explicitly computed by the model. The F_{as} term depends strongly on the carbon cycle scenario under consideration (see Sect. 2.4 and Table 1). For comparison with other reconstructions, Q is converted into a relative value by normalizing it by the preindustrial value.

3 Results and discussion

3.1 Atmospheric $\Delta^{14}C$ response to step changes

We use step changes in the ^{14}C production rate, and in selected carbon cycle parameters, to gain insight into the characteristic magnitude and time scale of the corresponding $\Delta^{14}C_{atm}$ changes (Fig. 4). Besides variations of the production rate, changes in ocean circulation and air-sea gas exchange are considered the most important factors affecting $\Delta^{14}C_{atm}$. Their effect on $\Delta^{14}C_{atm}$ can be understood in terms of their effect on the reservoir sizes involved in the global carbon cycle and on the exchange rates between the reservoirs. We investigate the relative importance of the major global carbon reservoirs (atmosphere, terrestrial biosphere, ocean, and sediments) by considering four different model configurations (see Sect. 2.3), with particular emphasis on the role of marine sediments.

In model studies, the process of sedimentation (defined here as the difference between deposition and remineralization/dissolution of material on the sea floor) is often neglected because it is a relatively minor flux. In the Bern3D model, sedimentation removes only about 0.46 Gt C and 45.31 mol ^{14}C per year in the preindustrial steady state. Indeed, the interaction with the ocean sediments has little influence on the global mean value of oceanic $\Delta^{14}C$ and therefore $\Delta^{14}C_{atm}$ as long as the total oceanic amount of carbon remains approximately constant (Siegenthaler et al., 1980); however, this is not always true, particularly in the case of millennial-scale climate perturbations. This is demonstrated by the differences between the model runs with and without sediments (i.e., ALL versus OCN-LND,

Deleted: $\Delta^{14}C$

Deleted: $\Delta^{14}C$

Deleted: Fig. 4

Deleted: atmospheric $\Delta^{14}C$

Deleted: $\Delta^{14}C$

Deleted: here used specifically to refer to

Deleted: balance

Deleted: at the sediment-water interface

Deleted: ,

Deleted: atmospheric $\Delta^{14}C$

Deleted: T

Deleted:

Deleted: two sets of model runs shown in Fig. 4

and OCN-SED versus OCN) as shown in Fig. 4. The response of $\Delta^{14}C_{atm}$ to various perturbations depends on the magnitude of the change in the ocean carbon inventory, with a larger change achieved by considering the interaction with the ocean sediments and the imbalance between weathering and sedimentation (see Fig. 5e,f). In order to facilitate our discussion, we will make only direct comparisons between model runs ALL and OCN-LND, which both include the four-box terrestrial biosphere model. We note that the ^{14}C exchange rate between the atmosphere and the terrestrial biosphere is only of minor importance for long time scales of millennia and more.

Deleted: are due to
Deleted: sedimentation-driven
Deleted: s
Deleted: only

3.1.1 Change of ^{14}C production

At steady state, the relative change of $\Delta^{14}C_{atm}$ is equal to the relative change of the ^{14}C production rate, irrespective of the individual reservoirs considered. Fig. 4 shows that $\Delta^{14}C_{atm}$ increases by about 100 permil (or 10 percent) when the production rate is increased by 10 percent. In model run ALL, $\Delta^{14}C_{atm}$ increases approximately exponentially to its new steady-state value with a characteristic time constant T of about 6170 years (i.e., $1 - 1/e \approx 63$ percent of the total change in $\Delta^{14}C_{atm}$ occurs within 6170 years). This e-folding time scale is close to the mean lifetime of ^{14}C (~8223 years), which is modulated by the time required for $\Delta^{14}C$ to equilibrate between the atmosphere and the ocean (i.e., the time scale for deep ocean ventilation, of the order of hundreds of years to 1000 years or more). In the next section, we will investigate the effect of ocean carbon cycle processes on $\Delta^{14}C_{atm}$.

Deleted: atmospheric $\Delta^{14}C$
Deleted: Figure 4
Deleted: atmospheric $\Delta^{14}C$
Deleted: $\Delta^{14}C$
Deleted: $\Delta^{14}C$
Deleted: equilibration
Deleted: atmospheric $\Delta^{14}C$

Note that for simplicity, we investigated only step changes in atmospheric production, although, in reality, ^{14}C production varies continuously over time due to changes in the solar and/or geomagnetic modulation of the cosmic radiation. This results in a non-steady state value of $\Delta^{14}C_{atm}$.

Deleted: atmospheric $\Delta^{14}C$

3.1.2 Change of ocean circulation

The exchange rate between the surface and deep ocean is mainly determined by physical transport and mixing processes. The overall effect of these processes is to transport ^{14}C-enriched surface waters to the thermocline and deep ocean, where waters are typically ^{14}C-depleted. In addition, the nutrient supply by transport and mixing plays an important role in determining the production and export of biogenic material from the surface ocean, constituting a second pathway for transporting ^{14}C to the deep ocean.

In the Bern3D model, the tunable model parameters affecting the ventilation of the deep ocean include a scale factor τ for the wind stress field and vertical diffusivity K_V. Fig. 4 shows the $\Delta^{14}C_{atm}$ response after a sudden decrease of τ and K_V by 50 percent. Although a halving of τ and K_V does not represent a realistic change, the resulting state of the ocean's large-scale overturning circulation can be interpreted in terms of the "ideal age" of water, which represents the average time since a water mass last made surface boundary contact. The new steady-state ideal age after a halving of τ and K_V is almost three times greater than the preindustrial steady-state value (i.e., ~1664 years versus ~613 years). This "ageing" of the ocean is achieved through a weakening and shoaling of the global meridional

Deleted: Figure 4
Deleted: atmospheric $\Delta^{14}C$

overturning circulation as evident from a moderate reduction in the meridional overturning stream function for the Indo-Pacific Ocean from about 14 to 9.5 Sv (1 Sv = 10^6 m^3 s^{-1}), and a very strong reduction from about 18 to 8 Sv in the Atlantic meridional overturning stream function, consistent with evidence for the glacial ocean. Here, as expected, the overall effect of deep water ageing is a stronger vertical $\Delta^{14}C$ gradient in the water column and a subsequent increase in $\Delta^{14}C_{atm}$. The exact nature of the $\Delta^{14}C_{atm}$ response, however, depends on the carbon reservoirs considered.

If the ocean sediment reservoir is neglected, the time required for $\Delta^{14}C_{atm}$ to adjust to step changes in τ and K_V is relatively short. $\Delta^{14}C_{atm}$ increases rapidly to its new steady-state value of ~159 permil, with a time constant T of about 600 years. This increase of $\Delta^{14}C_{atm}$ can be explained by the fact that, owing to a weaker and shallower overturning circulation, a comparatively large amount of carbon is moved from the atmosphere to the ocean. More specifically, the atmospheric carbon inventory decreases by 14.6 percent, whereas the atmospheric ^{14}C inventory decreases by only 1.1 percent (Fig. 5c). The ^{14}C being produced in the atmosphere is therefore diluted by a smaller carbon inventory, increasing the atmospheric $^{14}C/C$ ratio; this asymmetry in the drawdown of CO_2 and $^{14}CO_2$ is what permits the increase of $\Delta^{14}C_{atm}$. Since the ocean carbon inventory changes by only +0.2 percent, the mean $\Delta^{14}C$ value for the global ocean is nearly unaffected, a decrease of only ~11 permil in the new steady state (Fig. 6g).

In the model run where the sediment model is active, there are two distinct time constants. A rapid increase of $\Delta^{14}C_{atm}$ occurs, ~143 permil in the first few hundred years, then $\Delta^{14}C_{atm}$ gradually decreases to its final value of ~91 permil after tens of thousands of years. Reduced deep ocean ventilation is again responsible for the rapid $\Delta^{14}C_{atm}$ change and the respective time constant (T = ~480 years). The second time constant of ~23,390 years is due to the relatively long time required for the ocean carbon inventory to adjust to the ocean circulation-driven imbalance between weathering and sedimentation.

The process of ocean circulation interacts with the efficiency of the ocean's biological carbon pump, via its impact on export production, ocean interior oxygen levels, and seawater carbonate chemistry/equilibria. This has important implications for the sedimentation of biogenic material on the sea floor and, on a time scale of tens of thousands of years, the total oceanic amount of carbon. Through this coupling of ocean circulation and sea floor sedimentation via the biological carbon pump, a halving of τ and K_V leads to a 9.8 percent increase of the ocean carbon inventory in the new steady state (Fig. 5e). Qualitatively, a reduction in the ocean's overturning circulation leads to a lower surface nutrient supply, which limits the production and export of biogenic material from the surface ocean. This, in turn, decreases the fluxes of POC and $CaCO_3$ to the sea floor, with major consequences for the magnitude of their removal by sedimentation. At the same time, a constant input of DIC, Alk, and nutrients is added to the ocean from terrestrial weathering which is no longer balanced by sedimentation on the sea floor (this is what permits a larger ocean carbon inventory). The overall effect is a gradual reduction of oceanic $\Delta^{14}C$ by ~76 permil (Fig. 6g), which dilutes the initial $\Delta^{14}C_{atm}$ peak by 52 permil.

3.1.3 Change of gas transfer velocity

Deleted: atmospheric $\Delta^{14}C$

Deleted: $\Delta^{14}C$

Deleted: sedimentation

Deleted: $\Delta^{14}C$

Deleted: Atmospheric $\Delta^{14}C$

Deleted: $\Delta^{14}C$

Deleted: Fig. 5

Deleted: atmospheric $\Delta^{14}C$

Deleted: Fig. 6

Deleted: with sedimentation

Deleted: atmospheric $\Delta^{14}C$

Deleted: $\Delta^{14}C$

Deleted: $\Delta^{14}C$

Deleted: adjustment of

Deleted: changes in sedimentation

Deleted: at

Deleted: Fig. 5

Deleted: their

Deleted: amount

Deleted: ALK

Deleted: the

Deleted: flux

Deleted: global-ocean

Deleted: Fig. 6

Deleted: atmospheric $\Delta^{14}C$

It takes about a decade for the isotopic ratios of carbon to equilibrate between the atmosphere and a ~75-m thick surface mixed layer by air-sea gas exchange (Broecker and Peng, 1974). A consequence of this is that the surface ocean is undersaturated with respect to $\Delta^{14}C_{atm}$ (see Fig. 3). The choice of gas transfer velocity k_w as a function of wind speed is critical for the efficiency of air-sea gas exchange. A reduction of k_w corresponds to a higher resistance for gas transfer across the air-sea interface, which means that the ^{14}C produced in the atmosphere escapes into the surface ocean at a slower rate. The effect of a lower k_w is a larger air-sea gradient of $\Delta^{14}C$ and higher $\Delta^{14}C_{atm}$ values. In contrast, the $\Delta^{14}C$ value for the surface ocean is nearly unaffected so long as the ocean carbon inventory remains approximately constant, since the vertical gradient of $\Delta^{14}C$ in the ocean is dominated by physical transport and mixing processes. Although the exact nature of the gas transfer velocity under glacial climate conditions remains unclear, k_w represents a straightforward way to reduce the model's air-sea exchange efficiency due to theoretical changes in wind stress, sea ice, etc.

Fig. 4 shows how $\Delta^{14}C_{atm}$ responds to a perturbation in the gas transfer velocity. In the model run without sediments, reduction of k_w to 0 percent of its preindustrial value, in the model's north (> 60°N) and south (> 48°S) polar areas, leads to a moderate increase of $\Delta^{14}C_{atm}$ in the new steady state. The amplitude of $\Delta^{14}C_{atm}$ change is ~42 permil, which is achieved with an e-folding time scale T of about 180 years. This relatively short time constant can be explained by the multidecadal time scale required for $\Delta^{14}C$ to equilibrate between the model's atmosphere, upper ocean, and terrestrial biosphere. As shown in Fig. 6, the mean $\Delta^{14}C$ values for the surface, deep, and global ocean in the new steady state are only slightly different from the preindustrial steady-state values, as expected from the fact that the ocean carbon inventory remains relatively stable.

Interestingly, if sediments are included in the model, the final value of $\Delta^{14}C_{atm}$ is much higher (~91 permil). In this case, a perturbation in k_w leads to a very rapid initial increase of $\Delta^{14}C_{atm}$ (~42 permil), and a much slower subsequent increase of $\Delta^{14}C_{atm}$ (~49 permil). The latter has an e-folding time scale T of about 14,200 years. This slow doubling of the initial $\Delta^{14}C_{atm}$ increase is unexpected, but can be explained by the fact that a reduction of k_w involves also a reduction of air-sea O_2 gas exchange in the deep water formation regions, decreasing the oceanic oxygen that is available for transport to the deep ocean. This, in turn, implies lower oxygen concentrations in the water column and the sediment pore waters, decreasing the rate of POC remineralization in the sediments. Reducing this has the overall effect of enhancing POC sedimentation on the sea floor, causing the ocean carbon inventory to decrease. As shown in Fig. 5f, the total oceanic amount of carbon decreases by 5.9 percent in the new steady state, resulting in elevated $\Delta^{14}C$ values for the surface (+56 permil), deep (+30 permil), and global (+37 permil) ocean as well as for the atmosphere (+91 permil) (see Fig. 6). Note that the increase in $\Delta^{14}C_{atm}$ is not accompanied by a significant change in the atmospheric carbon inventory, which decreases by only 2.2 to 3.3 percent. The air-sea equilibration time scale for CO_2 by gas exchange is about 1 year for a ~75-m thick surface mixed layer (Broecker and Peng, 1974), which is much smaller than the ventilation time scale for the deep ocean (on the order of several hundred years or more). One would therefore expect that the oceanic uptake of CO_2 demonstrates only a very small response to changes in k_w.

Deleted: alone
Deleted: atmospheric $\Delta^{14}C$
Deleted: Fig. 3
Deleted: k_w
Formatted: Font colour: Text 1
Deleted: atmospheric $\Delta^{14}C$
Deleted: Figure 4
Deleted: atmospheric $\Delta^{14}C$
Deleted: ation
Deleted: atmospheric $\Delta^{14}C$
Deleted: $\Delta^{14}C$
Deleted: Fig. 6
Deleted: global mean
Deleted: sedimentation is
Deleted: atmospheric $\Delta^{14}C$
Deleted: $\Delta^{14}C$
Deleted: $\Delta^{14}C$
Deleted: $\Delta^{14}C$
Deleted: strengthening
Deleted: at
Deleted: Fig. 5
Deleted: Fig. 6
Deleted: atmospheric $\Delta^{14}C$
Deleted: (CO_2)
Deleted: (i.e., it
Deleted:)
Formatted: Subscript
Formatted

Overall, findings from these sensitivity experiments demonstrate that (1) the response of $\Delta^{14}C_{atm}$ to changes in the internal parameters of the ocean carbon cycle, in contrast to ^{14}C production changes, depends strongly on whether or not the balance between terrestrial weathering and sedimentation on the sea floor is simulated, (2) the e-folding time scale for the initial adjustment of $\Delta^{14}C_{atm}$ to ocean carbon cycle changes, i.e., changes in ocean circulation and gas exchange, is shorter than that for production changes (i.e., ~600 years and ~180 years versus ~6170 years), (3) air-sea gas exchange, in contrast to ocean circulation, has only a small effect on atmospheric CO_2, given that gas exchange is not the rate-limiting step for oceanic CO_2 uptake, and (4) on time scales of tens of thousands of years changes in the balance between weathering and sedimentation can potentially diminish (or elevate) the $\Delta^{14}C_{atm}$ value. This is new, important information for future paleoclimate simulations and suggests that changes in $\Delta^{14}C_{atm}$ may be overestimated (or underestimated) in models that do not simulate the interaction between sea floor sediments and the overlying water column.

Deleted: atmospheric $\Delta^{14}C$

Deleted: sedimentation at the sea floor

Deleted: atmospheric $\Delta^{14}C$

Deleted: the sedimentation of biogenic material

Deleted: atmospheric $\Delta^{14}C$

Deleted: , indicating

Deleted: $\Delta^{14}C$

3.2 Role of ^{14}C production in past atmospheric $\Delta^{14}C$ variability

We now consider the component of past $\Delta^{14}C_{atm}$ variability caused by production changes alone. Fig. 7 shows the results of model runs using different reconstructions of the ^{14}C production rate, as inferred from paleointensity data and from ice-core ^{10}Be fluxes. The global carbon cycle is assumed to be constant and under preindustrial conditions for these simulations (i.e., scenario MOD is used). Our analysis is restricted to the glacial portion of the record (50 to 18 kyr BP), in part because this is the time period which experiences the largest production changes, and in part because we did not attempt to reproduce the ~80 ppm change in atmospheric CO_2 that occurred during the last glacial termination. As we have already noted, much research over the last decades has attempted to explain the observed glacial-interglacial variations in $\Delta^{14}C_{atm}$ and CO_2, and this was not the goal of this study.

Deleted: atmospheric $\Delta^{14}C$

Deleted: Figure 7

Deleted: atmospheric $\Delta^{14}C$

At first glance, the millennial-scale structure of model-simulated $\Delta^{14}C_{atm}$ is comparable to that of the reconstructions. These similarities appear to be highest for the oldest portion of the record, roughly before 30 kyr BP. The model reproduces major features of the reconstructed $\Delta^{14}C_{atm}$ variability such as the large changes associated with the Laschamp (~41 kyr BP) and Mono Lake (~34 kyr BP) geomagnetic excursions. These two events are clearly expressed as distinct maxima in all model-simulated records. A more detailed comparison reveals a high correlation between the modelled and reconstructed $\Delta^{14}C_{atm}$ values between 50 and 33 kyr BP. Of note is the better agreement with the new Hulu Cave $\Delta^{14}C_{atm}$ dataset as compared to the IntCal13 calibration curve (i.e., Pearson correlation coefficient r of 0.96 versus 0.91). This is likely due to the fact that the Laschamp excursion is smoothed/smeared out during the stacking process of the IntCal13 $\Delta^{14}C_{atm}$ datasets (Adolphi et al., 2018). The correlation between modelled and reconstructed $\Delta^{14}C_{atm}$ is much weaker during the millennia after the Mono Lake excursion (33 to 18 kyr BP; r = 0.52 to 0.64). While it is clear that much of the millennial-scale variation in $\Delta^{14}C_{atm}$ is driven by past changes in ^{14}C production, the model fails to reproduce the glacial level of $\Delta^{14}C_{atm}$ and also does not capture the ~15,000-year persistent elevation of $\Delta^{14}C_{atm}$ or the subsequent decrease of $\Delta^{14}C_{atm}$ after ~25 kyr BP.

Deleted: $\Delta^{14}C$

Deleted: $\Delta^{14}C$

Deleted: $\Delta^{14}C$

Deleted: $\Delta^{14}C$

Deleted: $\Delta^{14}C$

Deleted: $\Delta^{14}C$

Deleted: $\Delta^{14}C$

Deleted: $\Delta^{14}C$

Deleted: $\Delta^{14}C$

Deleted: $\Delta^{14}C$

The reconstructions suggest that the highest values of $\Delta^{14}C_{atm}$ occurred during the Laschamp excursion, with a maximum value of ~595 permil at 41.1 kyr BP found in the IntCal13 record. The Hulu Cave record indicates even higher values for the Laschamp event $\Delta^{14}C_{atm}$ = ~742 permil, at 39.7 kyr BP). In contrast, the model is able to simulate maximum $\Delta^{14}C_{atm}$ values of only ~364 permil at 40.4 kyr BP, and ~236 permil at 40.5 kyr BP, as predicted by the paleointensity-based and ice-core ^{10}Be-based production rate estimates, respectively. Although the model is unable to reproduce the reconstructed values of $\Delta^{14}C_{atm}$, the modelled amplitude of the variation in $\Delta^{14}C_{atm}$ in response to the Laschamp event shows a reasonable agreement with the reconstructed amplitude of $\Delta^{14}C_{atm}$ change found in the IntCal13 record (~240 permil). The $\Delta^{14}C_{atm}$ change predicted by paleointensity data has a maximal amplitude of about 320 permil, whereas the ice-core ^{10}Be data indicate a smaller amplitude (~224 permil). Note that the IntCal13 and model-simulated amplitudes of the Laschamp-related $\Delta^{14}C_{atm}$ change are about two times smaller than that observed in the Hulu Cave record (~575 permil), which is more likely to be correct.

Moving onto the full glacial record (50 to 18 kyr BP), there are considerable discrepancies between reconstructed and modelled $\Delta^{14}C_{atm}$ ($\Delta\Delta^{14}$C; see Fig. 7). The use of ice-core ^{10}Be data to predict past changes in $\Delta^{14}C_{atm}$ results in the largest $\Delta\Delta^{14}$C, with offsets between the records as high as ~544 to 558 permil (root-mean-square error $RMSE$ = 404 to 408 permil). Model-simulated $\Delta^{14}C_{atm}$ given by paleointensity data varies widely between the four available reconstructions, yielding $\Delta\Delta^{14}$C values of ~325 to 639 permil ($RMSE$ = 206 to 455 permil). Note that the upper limit of the paleointensity-based $\Delta\Delta^{14}$C overlaps with the ice-core ^{10}Be-based $\Delta\Delta^{14}$C. Given the uncertainties associated with the reconstruction of past changes in ^{14}C production, accurate predictions of its contribution to past changes in $\Delta^{14}C_{atm}$ are challenging. Nonetheless, the substantial systematic offsets between the reconstructed and model-simulated $\Delta^{14}C_{atm}$ records after ~33 kyr BP point toward insufficiently high ^{14}C production rates over this period of time. The question arises as to whether another factor besides geomagnetic modulation of the cosmic ray intensity was responsible for elevated glacial $\Delta^{14}C_{atm}$ levels. The effect of ocean carbon cycle changes on the evolution of $\Delta^{14}C_{atm}$ is considered next.

3.3 Carbon cycle contribution to high glacial atmospheric Δ^{14}C levels

Here we investigate the magnitude and timing of the maximum possible $\Delta^{14}C_{atm}$ change during the last glacial period, obtained by running the Bern3D model with eight different carbon cycle scenarios (see Table 1). For the sake of clarity, we will discuss only the results of model runs using the mean paleointensity-based ^{14}C production rate, though all available reconstructions were used. We emphasize that this is not a best-guess estimate of paleointensity-based ^{14}C production. One should focus on the relative changes of $\Delta^{14}C_{atm}$ between model scenarios, and how specific carbon cycle processes affect the glacial level of $\Delta^{14}C_{atm}$.

Modelled 50,000-year records of $\Delta^{14}C_{atm}$ and CO_2 as well as their reconstructed histories are shown in Fig. 8. In order to provide a basis for comparison of modelling efforts, the results of model run MOD (which assumes a

Deleted: Δ^{14}C
Deleted: (Δ^{14}C
Deleted: Δ^{14}C
Deleted: Δ^{14}C
Deleted: Δ^{14}C
Deleted: Δ^{14}C
Deleted: Δ^{14}C
Deleted: Δ^{14}C
Deleted: Δ^{14}C
Deleted: Fig. 7
Deleted: Δ^{14}C
Deleted: Δ^{14}C
Deleted: Δ^{14}C
Deleted: model-simulated
Deleted: reconstructed
Deleted: Δ^{14}C
Deleted: Δ^{14}C
Deleted: atmospheric Δ^{14}C
Deleted: Δ^{14}C
Deleted: Δ^{14}C
Deleted: Δ^{14}C
Deleted: atmospheric Δ^{14}C
Deleted: plus corresponding
Deleted: Fig. 8

constant preindustrial carbon cycle) are presented. The influence of ocean carbon cycle changes on $\Delta^{14}C_{atm}$ was tested in the other model runs. Interestingly, the forcing fields for model run PAL (orbital parameters, greenhouse gas radiative forcing, and ice sheet extent) have only a minimal impact on $\Delta^{14}C_{atm}$. The PAL forcing fields also do not achieve sufficiently low glacial CO_2 concentrations. Only a slight reduction of atmospheric CO_2 by ~20 ppm could be achieved, which unrealistically occurs during the last glacial termination (CO_2 = 258.07 ppm, at 14.6 kyr BP). With hypothetical carbon cycle changes, the agreement between observed and modelled CO_2 during the last glacial period is good (as by design), but the deglacial CO_2 rise is lagged and ~60 ppm too small at 11 kyr BP. Since this study focuses on glacial $\Delta^{14}C_{atm}$ levels before incipient deglaciation at ~18 kyr BP, we will not discuss the lag any further.

Model simulation of high glacial $\Delta^{14}C_{atm}$ levels can be significantly improved by considering hypothetical carbon cycle changes in conjunction with PAL forcing. The amplitude of $\Delta^{14}C_{atm}$ change is highest for runs CIRC, VENT, and VENTx. This behavior is due to the fact that, owing to a reduction of τ, K_V, and k_w, strong vertical $\Delta^{14}C$ gradients in the ocean, as well as a large air-sea $\Delta^{14}C$ gradient, are established. As shown in Fig. 8, a more sluggish ventilation of deep waters is clearly expressed as an increase in the model ocean's global average ideal age and surface- and deep-water reservoir ages, where the latter two are calculated for the surface ocean and bottom water grid cells, respectively. These are equivalent to radiocarbon reservoir age offsets following Soulet et al. (2016). The deep-water reservoir age (i.e., B-Atm ^{14}C age offset, or B-Atm) provides a measure of the radiocarbon disequilibrium between the deep ocean and the atmosphere, which arises due to the combined effect of air-sea gas exchange efficiency and the deep ocean ventilation rate, whereas the effect of upper ocean stratification and/or sea ice on air-sea gas exchange is particularly important for surface reservoir ages (i.e., surface R-age) (Skinner et al., 2019).

Driven by a reduction in ocean circulation, model run CIRC predicts a substantial increase in B-Atm during the last glacial, which is defined here as 40 to 18 kyr BP to avoid biasing global mean estimates toward Laschamp values. The global average glacial B-Atm predicted by CIRC is ~3225 ^{14}C years, representing an increase in B-Atm of ~1599 ^{14}C years relative to the preindustrial value of ~1626 ^{14}C years. Model run VENT predicts a slightly larger increase in glacial B-Atm due to the inhibition of air-sea gas exchange. The "oldest" glacial waters are found in model run VENTx where air-sea gas exchange is severely restricted, yielding an increase in B-Atm of ~1912 ^{14}C years (glacial B-Atm ~3538 ^{14}C years). The glacial B-Atm values given by runs CIRC, VENT, and VENTx, as well as the ~717 year increase in ideal age during the last glacial relative to preindustrial, suggest that the glacial deep ocean was about two times older than its preindustrial counterpart. Comparison of our LGM B-Atm estimates (range of 3682 to 3962 ^{14}C years) with the compiled LGM marine radiocarbon data of Skinner et al. (2017) demonstrate that the carbon cycle scenarios are extreme, although it should be noted that Skinner et al. consider a wider depth range (~500 to 5000 m) of the ocean than we do. Skinner et al. (2017) predict a global average LGM B-Atm value of ~2048 ^{14}C years, an increase of ~689 ^{14}C years relative to preindustrial. Turning our comparison to surface reservoir ages, we note that our global average LGM surface R-age of ~1132 ^{14}C years from runs VENT and VENTx is comparable to the ~1241 ^{14}C years obtained by Skinner et al. (2017) for the LGM. The model-based estimates of surface R-age from Butzin et al. (2017) indicate a much lower LGM value of ~780 ^{14}C years, and values ranging from 540 to 1250 ^{14}C years between

Deleted: atmospheric $\Delta^{14}C$…was tested in the other model runs. Interestingly, the forcing fields for model run PAL (orbital parameters, greenhouse gas radiative forcing, and ice sheet extent) have only a minimal impact on $\Delta^{14}C_{atm}\Delta^{14}C$... [1]

Deleted: sized…carbon cycle changes, the agreement between observed and modelled CO_2 during the last glacial period is good (as by design), but the deglacial CO_2 rise is lagged and ~60 ppm too small at 11 kyr BP. Since this study focuses on glacial $\Delta^{14}C_{atm}\Delta^{14}C$ ... [2]

Deleted: Running the model with…additional …ypothetical carbon cycle changes leads to an improvement of modelled $\Delta^{14}C$…as compared to model ru…n conjunction withn…PAL forcing. The amplitude of $\Delta^{14}C_{atm}$atmospheric $\Delta^{14}C$ ... [3]

Deleted: Fig. 8…, the reduction in ocean ventilation… more sluggish ventilation of deep waters is clearly expressed in the observed…s an increase inof…the model ocean's global average ideal age as well as…nd surface- and deep-water reservoir ages, where the latter two are calculated for the surface ocean and bottom water grid cells, respectively. These being …re equivalent to radiocarbon reservoir age offsets following Soulet et al. (2016). …The deep-water reservoir age (i.e., B-Atm ^{14}C age offset, or B-Atm) provides a measure of the radiocarbon disequilibrium between the deep ocean and the atmosphere, which arises due to the combined effect of air-sea gas exchange efficiency and the strength of the ocean's overturning circulation (i.e., …he deep ocean ventilation rate)… whereas the effect of upper ocean stratification and/or sea ice on air-sea gas exchange is particularly important for surface reservoir ages (i.e., surface R-age) (Skinner et al., 2019).. ... [4]

Deleted: …riven by aAs a consequence of the…reduction in the meridional overturning…cean circulation, model run CIRC predicts a substantial increase in B-Atm for the glacial ocean…uring the last glacial, which is defined here as 40 to 18 kyr BP to avoid biasing global mean estimates toward Laschamp values.,…The global average …lacial B-Atm with values…redicted by CIRC reaching …sas high as…~32253236…^{14}C years, representing an increase in B-Atm of ~1599 ^{14}C years relative to the preindustrial value of nearly double the preindustrial value of …1626 ^{14}C years. Model run VENT predicts a slightly larger increase (+166 ^{14}C years) …n the …lacial ocean's…B-Atm , …ue to the inhibition of air-sea gas exchange. The "oldest" glacial waters are found in model run VENTx where air-sea gas exchange is severely restricted, giving …ielding an increase in glacial …-Atm value of ~3576…f ~1912 ^{14}C years (. …lacial B-Atm ~3538 ^{14}C years). The glacial B-Atm values given by runs CIRC, VENT, and VENTx, as well as the ~717 year increase in ideal age during the last glacial relative to preindustrial, suggest that theThis…would imply that the model's …lacial deep ocean was more …bout than ... [5]

50 and 25 kyr BP. Note that these estimates are based on model-simulated values between 50°N and 50°S. If the polar regions are included in the calculation (see Fig. 8c), their surface R-age estimates become comparable to our glacial values (range of 911 to 1354 ^{14}C years), and between about 34 and 22 kyr BP can exceed them, including even those from model runs VENT and VENTx, unless $\Delta^{14}C_{atm}$ and CO_2 are prescribed (dashed colored lines in Fig. 8c) as in the simulation by Butzin et al. (2017).

Indirect evidence for deep water ageing can be provided by the occurrence of depleted ocean interior oxygen levels, due to the progressive consumption of dissolved oxygen during organic matter remineralization in the water column. This situation is amplified by the slow escape of accumulating remineralized carbon in the ocean interior (see, e.g., Skinner et al., 2017), leading to higher values of apparent oxygen utilization (AOU = $O_{2,pre} - O_2$). These two concepts (increased AOU and increased B-Atm) taken together signal a significant reduction in deep ocean ventilation characterized by a decrease in the exchange rate between younger (higher $\Delta^{14}C$) surface waters and older (^{14}C-depleted), carbon-rich deep waters. Model runs CIRC, VENT, and VENTx do indeed indicate a large increase in AOU of about 95 mmol m^{-3} from its preindustrial value of ~150 mmol m^{-3}. The reason for this AOU increase is that a reduction of deep ocean ventilation permits enhanced accumulation of remineralized carbon in the ocean interior and therefore a more efficient biological carbon pump. Model runs BIO, PHYS-BIO, and PHYS-BIOx allow us to investigate the impact of other biological carbon pump changes on $\Delta^{14}C_{atm}$ and CO_2 (i.e., changes in the $CaCO_3$-to-POC export ratio and POC remineralization length scale). While these changes lead to an effective atmospheric CO_2 drawdown mechanism, model results confirm that their effect on $\Delta^{14}C_{atm}$ is much less important (see Fig. 8).

Model run VENTx gives the best results with respect to glacial levels of $\Delta^{14}C_{atm}$, with a maximum underestimation of ~202 to 229 permil ($RMSE$ = 103 to 110 permil) and a relatively good correlation (r = 0.79 to 0.91). Only one model parameter was changed for run VENTx as compared to runs CIRC and VENT, namely, the polar gas transfer velocity k_w was reduced to 0 percent of its preindustrial value during the last glacial. In this extreme scenario, we assume that sea ice cover extended in the northern hemisphere as far south as 60°N and in the southern hemisphere as far north as 48°S, which is not supported by the reconstructions (Gersonde et al., 2005; Allen et al., 2011). Nonetheless, considering extreme assumptions about polar air-sea exchange efficiency under glacial climate conditions is interesting for two reasons: (1) a change in gas exchange hardly affects the atmospheric CO_2 concentration, and (2) an additional change of $\Delta^{14}C_{atm}$ could possibly be achieved on a time scale of tens of thousands of years by changing the balance between weathering and sedimentation (see Sect. 3.1.3). This behavior has important implications for the glacial atmosphere, which is characterized by high $\Delta^{14}C$ levels in conjunction with low but relatively stable CO_2 concentrations. In contrast to a change in ocean circulation, air-sea gas exchange is a dedicated $\Delta^{14}C_{atm}$ "control knob" that can be invoked by models for a further increase of $\Delta^{14}C_{atm}$ without changing atmospheric CO_2. Here, an additional increase in $\Delta^{14}C_{atm}$ of ~130 permil relative to CIRC and VENT is achieved if gas exchange is reduced permanently to 0 percent in the polar regions.

Deleted: Further support comes from the model-simulated ideal age, which indicates that the ventilation time scale for the glacial ocean was about two times longer than for the preindustrial ocean (i.e., ~1297 years versus ~613 years).

Formatted: Indent: First line: 0 cm

Deleted: POC

Deleted: would signal

Deleted: –

Deleted: –

Deleted: atmospheric $\Delta^{14}C$

Deleted: atmospheric $\Delta^{14}C$

Deleted: Fig. 8

Deleted: $\Delta^{14}C$

Deleted: atmospheric $\Delta^{14}C$

Deleted: through a

Deleted: e

Deleted: in

Deleted: at the sea floor

Deleted: $\Delta^{14}C$

Deleted: atmospheric $\Delta^{14}C$

Deleted: of

Deleted: $\Delta^{14}C$

Deleted: by

Deleted: , as compared to

Deleted: runs

Deleted: ,

While the modelled $\Delta^{14}C_{atm}$ values obtained by VENTx show rather good agreement with the reconstructions between 50 and 33 kyr BP (r = 0.92 to 0.96; $RMSE$ = 74 to 102 permil), considerable discrepancies remain for the younger portion of the record. The analysis shown in Fig. 9 illustrates that even with extreme changes in the ocean carbon cycle it is very difficult to reproduce the reconstructed $\Delta^{14}C_{atm}$ values after ~33 kyr BP. During this period of time, VENTx underestimates $\Delta^{14}C_{atm}$ by up to ~203 permil ($RMSE$ = 118 to 128 permil), and is very poorly (r = 0.1) correlated with the reconstructions, confirming that there are still considerable gaps in our understanding. Although it may be possible that permanent North Atlantic-Arctic and Antarctic sea ice cover extended to lower and higher latitudes than previously reconstructed, we conclude from our model study that even extreme assumptions about sea ice cover are insufficient to explain the elevated $\Delta^{14}C_{atm}$ levels after ~33 kyr BP. It appears instead that the glacial ^{14}C production rate was higher than previously estimated and/or the reconstruction of glacial $\Delta^{14}C_{atm}$ levels is biased high. The older portion of the $\Delta^{14}C_{atm}$ record is based on data from archives other than tree rings (i.e., plant macrofossils, speleothems, corals, and foraminifera) (Reimer et al., 2013), providing, except for the Lake Suigetsu plant macrofossil data (Bronk Ramsey et al., 2012), only indirect measurements of $\Delta^{14}C_{atm}$. Note that these data show uncertainty in calendar age that propagate into the estimation of past $\Delta^{14}C_{atm}$ levels.

Large uncertainties in the pre-Holocene ^{14}C production rate also hamper our qualitative and quantitative interpretation of the $\Delta^{14}C_{atm}$ record. There is considerable disagreement between the available reconstructions of past changes in ^{14}C production (Fig. 1). Paleointensity-based estimates typically predict higher ^{14}C production rates than ice-core ^{10}Be-based ones. An exception is the paleointensity stack from Channell et al. (2018), which predicts lower production rates. But, irrespective of the scatter, it is clear that all of the ^{14}C production rate estimates are insufficiently high to explain the elevated $\Delta^{14}C_{atm}$ levels during the last glacial. Given the uncertainties in these estimates, it is very difficult to quantitatively describe the role of the ocean carbon cycle in determining the $\Delta^{14}C$ and CO_2 levels in the glacial atmosphere.

3.4 Reconstructing the ^{14}C production rate by deconvolving the atmospheric $\Delta^{14}C$ record

The unresolved discrepancy between reconstructed and model-simulated $\Delta^{14}C_{atm}$ raises the question how the ^{14}C production rate would have had to evolve to be consistent with the IntCal13 calibration curve or the new Hulu Cave $\Delta^{14}C_{atm}$ dataset. This question is addressed by deconvolving the $\Delta^{14}C_{atm}$ reconstruction over the last 50 kyr, using the Bern3D carbon cycle model forced with reconstructed histories of $\Delta^{14}C_{atm}$ and CO_2 (see Eq. [2]). The carbon cycle scenarios described in Table 1, with the exception of MOD, are used in order to provide an estimate of the uncertainty associated with the model's glacial ocean carbon cycle. We note that the carbon cycle scenarios are not designed to capture the specific features of the last glacial termination, and therefore the results of the deconvolution over this time period must be considered very preliminary (and regarded as tentative). A detailed analysis of the Holocene ^{14}C production rate is available in the literature (Roth and Joos, 2013). Finally, we consider the uncertainties associated with the older portion of the $\Delta^{14}C_{atm}$ record by deconvolving both the IntCal13 and Hulu Cave $\Delta^{14}C_{atm}$ records. Hulu Cave data overlap with IntCal13 between ~10.6 and 33.3 kyr BP (Cheng et al., 2018), as expected from the fact that

Deleted: $\Delta^{14}C$
Deleted: for run
Deleted: Fig. 9
Deleted: $\Delta^{14}C$
Deleted: model run
Deleted: $\Delta^{14}C$
Deleted: $\Delta^{14}C$
Deleted: atmospheric $\Delta^{14}C$
Deleted: $\Delta^{14}C$
Deleted: atmospheric $\Delta^{14}C$
Deleted: atmospheric $\Delta^{14}C$
Deleted: atmospheric $\Delta^{14}C$
Deleted: Fig. 1
Deleted: $\Delta^{14}C$
Deleted: $\Delta^{14}C$
Deleted: $\Delta^{14}C$
Deleted: atmospheric $\Delta^{14}C$
Deleted: atmospheric
Deleted: $\Delta^{14}C$
Deleted: viewed tentatively
Deleted: $\Delta^{14}C$
Deleted: $\Delta^{14}C$

IntCal13 between 10.6 and 26.8 kyr BP is based in part on Hulu Cave stalagmite H82 (Southon et al., 2012), whereas there are substantial offsets before ~30 kyr BP.

Fig. 10 shows the new, model-based reconstruction of past changes in ^{14}C production compared with available measurement-based reconstructions. Before the onset of the Laschamp excursion at ~42 kyr BP, production rates as inferred from the Hulu Cave record are near modern levels, whereas those obtained from the IntCal13 record are somewhat higher than modern. As expected, peak production occurs during the Laschamp event (~42 to 40 kyr BP), with the Hulu Cave dataset yielding the largest amplitude (factor of ~2 greater than modern). The IntCal13 record predicts a smaller amplitude of ~1.6 times the modern value. Both $\Delta^{14}C_{atm}$ records predict production minima at ~37 kyr BP (~7 percent higher than modern) and ~32 kyr BP (~5 percent higher than modern), interrupted by a prominent peak (factors of ~1.5 and ~1.4, respectively) during the Mono Lake geomagnetic excursion (~34 kyr BP), though the details of the timing and structure differ between the two records. Between 32 and 22 kyr BP, model-based estimates of the ^{14}C production rate are ~1.3 times the modern value, which then decrease to around modern levels by HS1 (~18 kyr BP).

Model-based estimates of ^{14}C production during the last glacial are typically higher than paleointensity-based and ice-core ^{10}Be-based ones, as expected from Sect. 3.2. Between 32 and 22 kyr BP, the deconvolutions of the IntCal13 and Hulu Cave $\Delta^{14}C_{atm}$ records give estimates that are about 17.5 percent higher than the reconstructions. It is important to note that the differences between the reconstructions based on proxy data (i.e., paleointensity data and ice-core ^{10}Be fluxes) are as large as the differences between our deconvolution results and the reconstructions (see Table 2). As shown in Fig. 11, it is extremely difficult to reconcile the discrepancies between measurement- and model-based ^{14}C production on the basis of carbon cycle changes alone. Nonetheless, the fact remains that two independent estimates of the ^{14}C production rate (i.e., estimates inferred from paleointensity data and from ice-core ^{10}Be fluxes) show systematically lower rates than those obtained by our model-based deconvolution of $\Delta^{14}C_{atm}$ in particular between 32 and 22 kyr BP. The differences between the production rate results shown in Fig. 10 and Fig. 11 and Table 2 stem from various uncertainties that are discussed next.

Uncertainties associated with the glacial ocean carbon cycle (Fig. 10, colored shading; Fig. 11, colored lines) are systematic in our approach. The deconvolutions, e.g., of the Hulu Cave $\Delta^{14}C_{atm}$ record, under different model scenarios are offset against one another, whereas the millennial-scale variability is maintained (see Fig. 11). We do not attempt to resolve uncertainties associated with Dansgaard-Oeschger warming events and related Antarctic and tropical climatic excursions in the model runs. Such climatic events may have influenced the atmospheric radiocarbon budget, but their influence on long-term variations in $\Delta^{14}C_{atm}$, and therefore inferred production rates, is presumably limited. As may be expected, the lowest production rates (the lowest F_{as} values) are found in VENTx and the highest in scenarios PAL and BIO, mirroring the high and low glacial $\Delta^{14}C_{atm}$ levels achieved by these model scenarios as discussed in Sect. 3.3. Note that there is a large uncertainty in the model-based ^{14}C production rate stemming from

Deleted: Figure 10
Deleted: $\Delta^{14}C$
Deleted: the analysis in
Deleted: $\Delta^{14}C$
Deleted: production rate estimates inferred from
Deleted: the
Deleted: Fig. 11
Deleted: reconstructed
Deleted: atmospheric $\Delta^{14}C$
Deleted: .
Deleted: Fig. 10
Deleted: 11
Deleted: Fig. 10
Deleted: Fig. 11
Deleted: $\Delta^{14}C$
Deleted: Fig. 11
Deleted: atmospheric $\Delta^{14}C$
Deleted: extreme scenario
Deleted: $\Delta^{14}C$

uncertainties associated with the reconstruction of past changes in $\Delta^{14}C_{atm}$, in particular the older portion of the $\Delta^{14}C_{atm}$ record.

A shortcoming of paleointensity-based reconstructions of the ^{14}C production rate is that they neglect changes in the solar modulation of the cosmic radiation. The solar modulation potential, which describes the impact of the solar magnetic field on isotope production, varied between 100 and 1200 MeV during the Holocene on decadal to centennial time scales, with a median value of approximately 565 MeV (Roth and Joos, 2013). A halving of the solar modulation potential (e.g., from 600 to 300 MeV) increases the ^{14}C production rate by about 25 percent for the modern geomagnetic field strength (Roth and Joos, 2013; see their Fig. 13). This sensitivity remains similar when changes in the strength of the geomagnetic field are limited as during the last ~35 kyr (Muscheler and Heikkilä, 2011). A shift to lower solar modulation potential could have materialized if the sun spent on average more time in the postulated “Grand Minimum” mode (Usoskin et al., 2014) during the last glacial than during the Holocene. The sensitivity of isotope production to variations in solar modulation potential becomes large during the Laschamp event when the intensity of the geomagnetic field was close to zero and changes in the solar modulation of the cosmic ray flux may have a discernible impact on the high $\Delta^{14}C_{atm}$ levels found over this period. A reduction of the solar modulation potential from 600 to 0 MeV would double ^{14}C production during times of zero geomagnetic field strength (Masarik and Beer, 2009). However, it is likely that changes in the solar modulation potential were insufficient to explain the discrepancy between paleointensity-based production rate estimates and the results of our deconvolution, in particular for the post-Laschamp period and for the reconstruction by Channell et al. (2018). Uncertainties associated with the paleointensity-based reconstructions stem also from uncertainties in estimating the age-scales of the marine sediments and the geomagnetic field data.

The ice-core ^{10}Be-based reconstruction of past changes in ^{14}C production reflects, by definition, the combined influence of changes in the solar and geomagnetic modulation of the cosmic ray flux reaching the Earth. This method, therefore, avoids a fundamental shortcoming of reconstructions based on geomagnetic field data. The assumption is that the ^{10}Be and ^{36}Cl deposited on polar ice and measured in ice cores scales with the amount of cosmogenic isotopes in the atmosphere. A difficulty is to extrapolate measurements from a single or a few locations to the global atmosphere. Changes in climate influence atmospheric transport and deposition of ^{10}Be as well as the snow accumulation rate, which affect the ice-core ^{10}Be concentration (Elsässer et al., 2015). Furthermore, the sensitivity of ^{10}Be in polar ice versus the sensitivity of total production to magnetic field variations, or “polar bias”, is a point of debate, but atmospheric transport models (Heikkilae et al., 2009; Field et al., 2006) and data analyses (Bard et al., 1997; Adolphi and Muscheler, 2016; Adolphi et al., 2018) reach different conclusions about its existence and magnitude. If a polar bias was present, it would lead to an underestimation of the geomagnetic modulation of the ice-core ^{10}Be flux, and therefore variations in the ^{10}Be-based ^{14}C production rate would also be underestimated. However, the mismatch of up to ~544 to 558 permil between reconstructed and modelled ^{10}Be-based $\Delta^{14}C_{atm}$ during the last glacial (see Fig. 7c) appears to be much too large to be reconciled by considering uncertainties in the polar bias alone.

Deleted: atmospheric $\Delta^{14}C$

Deleted: $\Delta^{14}C$

Deleted: $\Delta^{14}C$

Deleted:

Formatted: Superscript

Furthermore, this mismatch with reconstructed $\Delta^{14}C_{atm}$ is qualitatively similar when using paleointensity-based ^{14}C production rates that do not suffer from a polar bias (Fig. 7c).

Given the uncertainties associated with the proxy records, it may not be surprising that estimates of the ^{14}C production rate for the last 50 kyr, as obtained by three fundamentally different methods (geomagnetic field data from marine sediments, ^{10}Be and ^{36}Cl measurements in polar ice cores, and model-based deconvolution of $\Delta^{14}C_{atm}$), disagree with one another, typically by order 10 percent and sometimes by up to 100 percent. At the same time, it is intriguing that two independent estimates of the ^{14}C production rate (i.e., estimates inferred from paleointensity and ice-core ^{10}Be data) give values that are systematically lower than what is required to match the $\Delta^{14}C_{atm}$ reconstruction.

4 Summary and conclusions

It is generally assumed that $\Delta^{14}C_{atm}$ is controlled by abiotic processes such as atmospheric ^{14}C production, air-sea gas exchange, and ocean circulation and mixing. Here, results from sensitivity experiments with the Bern3D earth system model of intermediate complexity suggest that $\Delta^{14}C_{atm}$ is potentially quite sensitive to the interaction with the ocean sediments on multimillennial time scales. This rather surprising result is due to the coupling of ocean circulation and the sedimentation of biogenic material on the sea floor via the biological carbon pump, which has important implications for the ocean carbon inventory. If the model's ocean carbon cycle is sufficiently perturbed, e.g., by changing the inputs or parameters controlling ocean circulation and/or gas exchange, the imbalance between weathering and sedimentation has a significant impact on the total oceanic amount of carbon. On time scales of tens of thousands of years this slow change in the ocean carbon inventory influences the partitioning of $^{14}C/C$ between the ocean and atmosphere, and thus also oceanic $\Delta^{14}C$ and $\Delta^{14}C_{atm}$. This is important information for long-term climate studies and paleoclimate modelling efforts concerning $\Delta^{14}C_{atm}$. Note that the representation of terrestrial weathering and sea floor sedimentation in the Bern3D is necessarily simplified compared to reality. Nonetheless, a change in the ocean carbon inventory linked with the weathering/sedimentation balance should be discussed as one of the potentially important factors affecting $\Delta^{14}C_{atm}$ during the last glacial period.

The reason for the high $\Delta^{14}C$ values exhibited by the glacial atmosphere is still not clear. In order to investigate potential mechanisms governing glacial $\Delta^{14}C_{atm}$ levels, the Bern3D model is again used as a tool. Results of model simulations forced only by production changes point out that none of the available reconstructions of the ^{14}C production rate can explain the full amplitude of $\Delta^{14}C_{atm}$ change during the last glacial. In order to test the sensitivity of the model results with respect to the ocean carbon cycle state, various model parameters, i.e., different sets of physical and biogeochemical parameters, were "tuned" to match the glacial CO_2 level. From this, we find that $\Delta^{14}C_{atm}$ is most sensitive to changes in physical model parameters, in particular those controlling ocean circulation and gas exchange. In order to achieve an $\Delta^{14}C_{atm}$ value close to the glacial level, the gas transfer velocity in the polar regions had to be reduced by 100 percent. If interpreted as being due to a greater extent of permanent sea ice cover, a reduction in polar air-sea exchange efficiency is a possible explanation for high glacial $\Delta^{14}C_{atm}$ levels. Although this hypothesis

Formatted: Superscript
Deleted: and therefore the ^{14}C production rate
Formatted
Deleted: atmospheric $\Delta^{14}C$
Deleted: $\Delta^{14}C$
Deleted: atmospheric $\Delta^{14}C$
Deleted: atmospheric $\Delta^{14}C$
Deleted: between sediments and the water column
Deleted: biogenic particle sedimentation
Deleted: resulting shift in sedimentation
Deleted: and therefore the average $\Delta^{14}C$ value of the ocean
Formatted: Not Highlight
Deleted: the impact of these changes on
Deleted: atmospheric $\Delta^{14}C$ is significant because of the long time scale associated with changes in the sedimentation of biogenic material
Deleted: $\Delta^{14}C$
Deleted: ocean-sedimen
Deleted: t interactions
Deleted: changing sedimentation
Deleted: atmospheric $\Delta^{14}C$
Deleted: $\Delta^{14}C$
Deleted: $\Delta^{14}C$
Deleted: atmospheric $\Delta^{14}C$
Deleted: atmospheric $\Delta^{14}C$
Deleted: $\Delta^{14}C$

is compelling, such a scenario is not supported by the proxy records of Antarctic sea ice cover (Gersonde et al., 2005; Allen et al., 2011) and the $^{13}C/^{12}C$ ratio of atmospheric CO_2 (Eggleston et al., 2016).

Atmospheric $\Delta^{14}C$ that is modelled at any point in time reflects ^{14}C production at that point, as well as the legacy of past production and carbon cycle changes. The question arises as to whether our conclusions are affected by unaccounted legacy effects, e.g., linked to the preindustrial spin-up simulation or model-diagnosed production rates. Transient simulations forced by reconstructed changes in ^{14}C production (Sect. 3.2 and 3.3) are initialized at 70 kyr BP, but their interpretation is restricted to the last 50,000 years of the integration to minimize legacy effects from model spin-up. Available reconstructions of the ^{14}C production rate in relative units (Sect. 2.5) are applied as a scale factor to the preindustrial steady-state absolute value, which is diagnosed by running the Bern3D model to equilibrium under preindustrial boundary conditions. This approach represents an approximation and equilibrium conditions do not fully apply. Indeed, there is a mismatch between reconstructed and modelled $\Delta^{14}C_{atm}$ at the preindustrial (see Fig. 8a). This mismatch is on the order of a few percent or less and adjusting the base level of production accordingly would not remove the large mismatch between reconstructed and modelled $\Delta^{14}C_{atm}$ during the last glacial. In addition, the uncertainty in the absolute value of the preindustrial production rate is on the order of 15%, primarily due to the uncertainties in the preindustrial ocean radiocarbon inventory (see Roth and Joos, 2013, Sect. 3.2). This potential systematic bias, however, does not affect our conclusions as we consider normalized production rate changes (see Fig. 7, 10, and 11).

Before model-simulated $\Delta^{14}C_{atm}$ can be taken seriously, it must be demonstrated that the reconstruction of past changes in ^{14}C production is reliable. There is, however, a substantial amount of scatter in the paleointensity-based and ice-core ^{10}Be-based estimates of ^{14}C production. Here we adopt an alternative approach to estimating the ^{14}C production rate, which would indeed benefit from further constraints and lines of supporting evidence. Our deconvolution-based approach assumes that the ^{14}C production rate can be derived from an atmospheric radiocarbon budget, constructed using a prognostic carbon cycle model combined with the $\Delta^{14}C_{atm}$ record. Here, non-equilibrium effects are fully accounted for by transient simulations where $\Delta^{14}C_{atm}$ and CO_2 are prescribed following their reconstructed histories (Sect. 3.4). Yet, these simulations indicate that the discrepancy between measurement- and model-based estimates of the ^{14}C production rate remains for the last glacial (Fig. 10b). This would suggest that unaccounted legacy effects do not significantly affect our conclusions. Our model results imply that the glacial ^{14}C production rate as inferred from paleointensity data and ice-core ^{10}Be fluxes may be underestimated by about 15 percent between 32 and 22 kyr BP, a time interval which appears to be an important piece of the glacial-interglacial $\Delta^{14}C_{atm}$ puzzle. Note that our model-based estimates are associated with uncertainties arising from the reconstruction of the older portion of the $\Delta^{14}C_{atm}$ record and from the model simulation of the glacial ocean carbon cycle (e.g., uncertainties in the glacial ocean circulation and air-sea CO_2 fluxes). An improved understanding of the role of ^{14}C production in past changes of $\Delta^{14}C_{atm}$ would open up the possibility of attributing model deficiencies to real changes in the ocean carbon cycle, but there is as yet no emerging single record of the ^{14}C production rate.

Formatted: Not Highlight

Formatted: Highlight

Formatted: Indent: First line: 1.27 cm

Deleted: $\Delta^{14}C$

Deleted: atmospheric $\Delta^{14}C$

Deleted: suggest

Deleted: $\Delta^{14}C$

Deleted: a too high

Deleted: Future improvements in the

Deleted: reconstruction of past changes in

Deleted: and

Deleted: atmospheric $\Delta^{14}C$

Deleted: .

Progress in several different areas may help to resolve the glacial-interglacial radiocarbon problem. Additional records of glacial $\Delta^{14}C_{atm}$ would help refine the older portion of the IntCal $\Delta^{14}C$ record. Cosmogenic isotope production records may be improved, e.g., by refining estimates of ice accumulation, by developing a better understanding of ^{10}Be transport and deposition during the glacial, by recovering additional long and continuous records from Antarctic ice cores and including marine ^{10}Be records, and by obtaining additional geomagnetic field data. An expanded spatiotemporal observational coverage of $\Delta^{14}C$ of DIC in the surface and deep ocean would help narrow the time scales of surface-to-deep transport and air-sea equilibration of $\Delta^{14}C$, carbon and nutrients, and thereby guide model-based analyses. Models should become more sophisticated and detailed in order to reproduce successfully the glacial-interglacial changes in carbon and radiocarbon, by including exchange with sediments and the lithosphere and by better representing coastal processes, and by representing a wide variety of paleo proxies such as $\delta^{13}C$, Nd isotopes, carbonate ion concentration, lysocline evolution, and paleo-productivity proxies in a 3-D dynamic context for model evaluation. What is also missing are methods to quantify how the ocean carbon inventory, which co-determines the $^{14}C/C$ ratio and thus the $\Delta^{14}C$ values in the ocean and atmosphere, has changed over the last 50,000 years. Ultimately, an improved knowledge of ^{14}C production during the last glacial, as well as more robust constraints on the prevailing climate conditions (e.g., ocean circulation, sea ice cover, and wind speed), are necessary to elucidate the processes permitting mysteriously high $\Delta^{14}C$ levels in the glacial atmosphere.

Deleted:

Formatted: Font colour: Auto

Appendix A: Description of the Bern3D model

Deleted: Complete d

The physical core of the Bern3D model is based on the 3-D rigid-lid ocean model of Edwards et al. (1998) as updated by Edwards and Marsh (2005). The forcing fields for the model integration are monthly mean wind stress data taken from NCEP/NCAR (Kalnay et al., 1996). Diapycnal mixing is parameterized with a uniform vertical diffusivity K_V of 2 x 10^{-5} m s^{-1}. The parameterization of eddy-induced transport is separated from that of isopycnal mixing, using the Gent-McWilliams skew flux (Griffies, 1998). Running at the same temporal and horizontal resolution, the one-layer energy-moisture balance atmosphere model performs an analysis of the energy budget of the Earth by involving solar radiation, infrared fluxes, evaporation and precipitation, and sensible and latent heat. The zonally averaged surface albedo climatology is taken from Kukla and Robinson (1980). Transport of moisture is performed by diffusion and advection and heat by eddy diffusion.

The Bern3D ocean carbon cycle model is based on the Ocean Carbon-Cycle Model Intercomparison Project (OCMIP-2) protocols. Air-sea gas exchange is parameterized using the standard gas transfer formulation adopted for OCMIP-2, except that the gas transfer velocity k_w parameterization is a linear function of wind speed (Krakauer et al., 2006) to which we have added a scale factor of 0.81 to match the observed global ocean inventory of bomb ^{14}C (Müller et al., 2008). It is assumed that CO_2 and O_2 are well-mixed in the atmosphere. Surface boundary conditions also include a virtual-flux term for biogeochemical tracers (e.g., DIC and Alk) to account for their dilution or concentration due to implicit freshwater fluxes. Following OCMIP-2 biotic protocol, new production is partitioned into particulate and dissolved organic matter. Modifications from the original OCMIP-2 biotic protocol include the

Deleted: ALK

prognostic formulation of new/export production as a function of light, temperature, and limiting nutrient concentrations, where the nutrient uptake follows Michaelis-Menten kinetics. The production of biogenic $CaCO_3$ and opal is computed on the basis of the modelled particulate organic carbon (POC) production and availability of silicate, with a maximum possible fraction of $CaCO_3$ material that can be produced. This threshold value is represented by the $CaCO_3$-to-POC export ratio. In the preindustrial control run, the global mean export ratio rr is 0.082.

Biogenic particles that have been produced in the 75-m production zone are redistributed over the water column in order to parameterize the downward particle flux through the water column. A power-law model referred to as the Martin curve is used to describe the vertical POC flux profile, whereas both $CaCO_3$ and opal export are redistributed over the water column with an exponential curve. POC is remineralized instantaneously back to dissolved form according to Redfield stoichiometry and with a 250–m length scale l_{POC} (i.e., in 250 m, the POC flux declines by $1 - 1/e \approx 63$ percent). Likewise, $CaCO_3$ and opal are dissolved within one time step, with e-folding depths of 5066 and 10,000 m, respectively. Biogenic particles reaching the model's sea floor form the upper boundary condition of the 10-layer sediment model after Heinze et al. (1999) and Gehlen et al. (2006). The sediment model includes four solid sediment components (POC, $CaCO_3$, opal, and clay) and is based on the sediment advection and accumulation scheme as in the work of Archer et al. (1993). The rate of POC remineralization in the sediments is primarily determined by the pore water concentration of oxygen, whereas the mineral dissolution rate is governed by the saturation state of sediment pore waters with respect to $CaCO_3$ or opal. Weathering (dissolution) of carbonate and silicate rocks on land, phosphorous release by chemical weathering of rocks, and volcanic outgassing of CO_2 are simulated as constant inputs of DIC, Alk (as bicarbonate ion, HCO_3^-), phosphate (P), and silicate (Si) to the ocean at rates intended to balance their removal from the ocean by sedimentation on the sea floor. These weathering inputs are added as a constant increment to each surface ocean grid cell along the coastlines. The preindustrial steady state of the model is used to diagnose the weathering rates that are held fixed and constant throughout the simulations. Note that the preindustrial spin-up results in steady-state values for weathering-derived inputs of DIC, Alk, P, and Si of 0.46 Gt C per year, 34.37 Tmol HCO_3^- per year, 0.17 Tmol P per year, and 6.67 Tmol Si per year, respectively. These values are within the range of observational estimates (see, e.g., Jeltsch-Thömmes et al., 2019). Additional details concerning the sediment model are provided in Tschumi et al. (2011), while the appendix of Jeltsch-Thömmes et al. (2019) gives a detailed description of the atmosphere–ocean–sediment spin-up.

The exchange of any isotopic perturbation between the atmosphere and the terrestrial biosphere is simulated by use of the four-box model of Siegenthaler and Oeschger (1987). The terrestrial biosphere is represented by four well-mixed compartments (ground vegetation plus leaves, wood, detritus, and soils), with a fixed total carbon inventory of 2220 Gt C. Net primary production is balanced by respiration of detritus and soils, and is set to 60 Gt C per year.

Deleted: material

Deleted: s

Deleted: is

Deleted: material

Deleted: s

Deleted: sediment

Formatted: Subscript

Formatted: Subscript

Formatted: Superscript

Deleted: The weathering input of DIC, ALK, and nutrients into the ocean is added as a constant increment to each wet grid cell along the coastlines. Any material input from terrestrial weathering is considered "radiocarbon dead". The values for these fluxes were chosen so that at the end of the preindustrial spin-up, input (weathering) and output (sedimentation) are balanced.

Deleted: and

Data availability. Model-simulated atmospheric $\Delta^{14}C$ presented in Fig. 7b and 8a, and model-based ^{14}C production rates shown in Fig. 10a, are included in the Supplement. Other data generated or analyzed during this study can be made available upon request to the corresponding author (A.D.).

Author contribution. This study was designed by F.J. and A.D. with input from F.A. A.D. developed and performed the model simulations. F.A. provided production data. A.D. wrote the manuscript with contributions from the co-authors.

Competing interests. The authors declare that they have no conflict of interest.

Acknowledgements. This work was made possible by the Swiss National Science Foundation (#200020_172476) and by the UniBE international 2021 fellowship program of the U. Bern. F.A. was supported by the Swedish Research Council (Vetenskaprådet DNR: 2016-00218).

References

Adolphi, F., and Muscheler, R.: Synchronizing the Greenland ice core and radiocarbon timescales over the Holocene – Bayesian wiggle-matching of cosmogenic radionuclide records, Climate of the Past, 12, 15–30, 2016.

Adolphi, F., Muscheler, R., Svensson, A., Aldahan, A., Possnert, G., Beer, J., . . . Thiéblemont, R.: Persistent link between solar activity and Greenland climate during the Last Glacial Maximum, Nature Geoscience, 7, 662–666, 2014.

Adolphi, F., Ramsey, C. B., Erhardt, T., Edwards, R. L., Cheng, H., Turney, C. S., . . . Muscheler, R.: Connecting the Greenland ice-core and U/Th timescales via cosmogenic radionuclides: testing the synchroneity of Dansgaard–Oeschger events, Climate of the Past, 14, 1755–1781, 2018.

Allen, C. S., Pike, J., and Pudsey, C. J.: Last glacial–interglacial sea-ice cover in the SW Atlantic and its potential role in global deglaciation, Quaternary Science Reviews, 30, 2446–2458, 2011.

Archer, D., and Maier-Reimer, E.: Effect of deep-sea sedimentary calcite preservation on atmospheric CO_2 concentration, Nature, 367, 260–263, 1994.

Archer, D., Lyle, M., Rodgers, K., and Froelich, P.: What controls opal preservation in tropical deep-sea sediments?, Paleoceanography, 8, 7–21, 1993.

Archer, D., Winguth, A., Lea, D., and Mahowald, N.: What caused the glacial/interglacial atmospheric pCO_2 cycles?, Reviews of Geophysics, 38, 159–189, 2000.

Audi, G., Bersillon, O., Blachot, J., and Wapstra, A. H.: The Nubase evaluation of nuclear and decay properties, Nuclear Physics A, 729, 3–128, 2003.

Bard, E., Raisbeck, G. M., Yiou, F., and Jouzel, J.: Solar modulation of cosmogenic nuclide production over the last millennium: comparison between ^{14}C and ^{10}Be records, Earth and Planetary Science Letters, 150, 453–462, 1997.

Deleted: A

Deleted: ll

Formatted: Font: Not Bold

Baumgartner, S., Beer, J., Wagner, G., Kubik, P., Suter, M., Raisbeck, G. M., and Yiou, F.: ^{10}Be and dust, Nuclear Instruments and Methods in Physics Research Section B: Beam Interactions with Materials and Atoms, 123, 296–301, 1997.

Baumgartner, S., Beer, J., Masarik, J., Wagner, G., Meynadier, L., and Synal, H.-A.: Geomagnetic Modulation of the ^{36}Cl Flux in the GRIP Ice Core, Greenland, Science, 279, 1330–1332, 1998.

Bé, M.-M., Chisté, V., Dulieu, C., Mougeot, X., Chechev, V., Kondev, F., . . . Wang, B.: Table of Radionuclides (Comments on evaluations), Monographie BIPM-5, 7, 2013.

Berger, A. L.: Long-term variations of daily insolation and Quaternary climatic changes, Journal of the Atmospheric Sciences, 35, 2362–2367, 1978.

Broecker, W., and Barker, S.: A 190‰ drop in atmosphere's Δ^{14}C during the "Mystery Interval" (17.5 to 14.5 kyr), Earth and Planetary Science Letters, 256, 90–99, 2007.

Broecker, W. S., and Peng, T.-H.: Gas exchange rates between air and sea, Tellus, 26, 21–35, 1974.

Bronk Ramsey, C., Staff, R. A., Bryant, C. L., Brock, F., Kitagawa, H., van der Plicht, J., Schlolaut, G., Marshall, M. H., Brauer, A., Lamb, H. F., Payne, R. L., Tarasov, P. E., Haraguchi, T., Gotanda, K., Yonenobu, H., Yokoyama, Y., Tada, R., and Nakagawa, T.: A complete terrestrial radiocarbon record for 11.2 to 52.8 kyr B.P., Science, 338, 370–374, 2012.

Brovkin, V., Ganopolski, A., Archer, D., and Munhoven, G.: Glacial CO_2 cycle as a succession of key physical and biogeochemical processes, Climate of the Past, 8, 251–264, 2012.

Butzin, M., Köhler, P., and Lohmann, G.: Marine radiocarbon reservoir age simulations for the past 50,000 years, Geophysical Research Letters, 44, 8473–8480, 2017.

Channell, J. E., Hodell, D. A., Crowhurst, S. J., Skinner, L. C., and Muscheler, R.: Relative paleointensity (RPI) in the latest Pleistocene (10-45 ka) and implications for deglacial atmospheric radiocarbon, Quaternary Science Reviews, 191, 57–72, 2018.

Cheng, H., Edwards, R. L., Southon, J., Matsumoto, K., Feinberg, J. M., Sinha, A., . . . Ning, Y.: Atmospheric ^{14}C/^{12}C changes during the last glacial period from Hulu Cave, Science, 362, 1293–1297, 2018.

Delaygue, G., Stocker, T. F., Joos, F., and Plattner, G.-K.: Simulation of atmospheric radiocarbon during abrupt oceanic circulation changes: trying to reconcile models and reconstructions, Quaternary Science Reviews, 22, 1647–1658, 2003.

Edwards, N. R., and Marsh, R.: Uncertainties due to transport-parameter sensitivity in an efficient 3-D ocean-climate model, Climate Dynamics, 24, 415–433, 2005.

Edwards, N. R., Willmott, A. J., and Killworth, P. D.: On the Role of Topography and Wind Stress on the Stability of the Thermohaline Circulation, Journal of Physical Oceanography, 28, 756–778, 1998.

Eggleston, S., Schmitt, J., Bereiter, B., Schneider, R., and Fischer, H.: Evolution of the stable carbon isotope composition of atmospheric CO_2 over the last glacial cycle, Paleoceanography, 31, 434–452, 2016.

Elsässer, C., Wagenbach, D., Levin, I., Stanzick, A., Christl, M., Wallner, A., . . . Dibb, J.: Simulating ice core ^{10}Be on the glacial–interglacial timescale, Climate of the Past, 11, 115–133, 2015.

Enting, I. G.: On the use of smoothing splines to filter CO_2 data, Journal of Geophysical Research, 92, 10,977–10,984, 1987.

Field, C. V., Schmidt, G. A., Koch, D., and Salyk, C.: Modeling production and climate-related impacts on ^{10}Be concentration in ice cores, Journal of Geophysical Research: Atmospheres, 111, https://doi.org/10.1029/2005JD006410, 2006.

Finkel, R. C., and Nishiizumi, K.: Beryllium 10 concentrations in the Greenland Ice Sheet Project 2 ice core from 3-40 ka, Journal of Geophysical Research: Oceans, 102, 26699–26706, 1997.

Fischer, H., Schmitt, J., Lüthi, D., Stocker, T. F., Tschumi, T., Parekh, P., . . . Wolff, E.: The role of Southern Ocean processes in orbital and millennial CO_2 variations – A synthesis, Quaternary Science Reviews, 29, 193–205, 2010.

Galbraith, E. D., and Skinner, L. C.: The Biological Pump During the Last Glacial Maximum, Annual Review of Marine Science, 12, 559–586, 2020.

Ganopolski, A., and Brovkin, V.: Simulation of climate, ice sheets and CO_2 evolution during the last four glacial cycles with an Earth system model of intermediate complexity, Climate of the Past, 13, 1695–1716, 2017.

Gehlen, M., Bopp, L. E., Aumont, O., Heinze, C., and Ragueneau, O.: Reconciling surface ocean productivity, export fluxes and sediment composition in a global biogeochemical ocean model, Biogeosciences, 3, 521–537, 2006.

Gersonde, R., Crosta, X., Abelmann, A., and Armand, L.: Sea-surface temperature and sea ice distribution of the Southern Ocean at the EPILOG Last Glacial Maximum—a circum-Antarctic view based on siliceous microfossil records, Quaternary Science Reviews, 24, 869–896, 2005.

Gkinis, V., Simonsen, S. B., Buchardt, S. L., White, J. W., and Vinther, B. M.: Water isotope diffusion rates from the NorthGRIP ice core for the last 16,000 years – Glaciological and paleoclimatic implications, Earth and Planetary Science Letters, 405, 132–141, 2014.

Griffies, S. M.: The Gent-McWilliams Skew Flux, Journal of Physical Oceanography, 28, 831–841, 1998.

Hain, M. P., Sigman, D. M., and Haug, G. H.: Distinct roles of the Southern Ocean and North Atlantic in the deglacial atmospheric radiocarbon decline, Earth and Planetary Science Letters, 394, 198–208, 2014.

Heikkilä, U., Beer, J., and Feichter, J.: Meridional transport and deposition of atmospheric ^{10}Be, Atmospheric Chemistry and Physics, 9, 515–527, 2009.

Heikkilä, U., Phipps, S. J., and Smith, A. M.: ^{10}Be in late deglacial climate simulated by ECHAM5-HAM – Part 1: Climatological influences on ^{10}Be deposition, Climate of the Past, 9, 2641–2649, 2013.

Heinze, C., Maier-Reimer, E., Winguth, A. M., and Archer, D.: A global oceanic sediment model for long-term climate studies, Global Biogeochemical Cycles, 13, 221–250, 1999.

Herbst, K., Muscheler, R., and Heber, B.: The new local interstellar spectra and their influence on the production rates of the cosmogenic radionuclides ^{10}Be and ^{14}C, Journal of Geophysical Research: Space Physics, 122, 23–34, 2017.

Hoff, U., Rasmussen, T. L., Stein, R., Ezat, M. M., and Fahl, K.: Sea ice and millennial-scale climate variability in the Nordic seas 90 kyr ago to present, Nature Communications, 7, doi:10.1038/ncomms12247, 2016.

Formatted: Subscript

Formatted: German (Switzerland)

Hughen, K., Lehman, S., Southon, J., Overpeck, J., Marchal, O., Herring, C., and Turnbull, J.: ^{14}C Activity and Global Carbon Cycle Changes over the Past 50,000 Years, Science, 303, 202–207, 2004.

Huiskamp, W. N., and Meissner, K. J.: Oceanic carbon and water masses during the Mystery Interval: A model-data comparison study, Paleoceanography and Paleoclimatology, 27, https://doi.org/10.1029/2012PA002368, 2012.

Jeltsch-Thömmes, A., Battaglia, G., Cartapanis, O., Jaccard, S. L., and Joos, F.: Low terrestrial carbon storage at the Last Glacial Maximum: constraints from multi-proxy data, Climate of the Past, 15, 849–879, 2019.

Köhler, P., Muscheler, R., and Fischer, H.: A model-based interpretation of low-frequency changes in the carbon cycle during the last 120,000 years and its implications for the reconstruction of atmospheric $\Delta^{14}C$, Geochemistry Geophysics Geosystems, 7, 1–22, 2006.

Köhler, P., Nehrbass-Ahles, C., Schmitt, J., Stocker, T. F., and Fischer, H.: A 156 kyr smoothed history of the atmospheric greenhouse gases CO_2, CH_4, and N_2O and their radiative forcing, Earth System Science Data, 9, 363–387, 2017.

Kalnay, E., Kanamitsu, M., Kistler, R., Collins, W., Deaven, D., Gandin, L., . . . Joseph, D.: The NCEP/NCAR 40-Year Reanalysis Project, Bulletin of the American Meteorological Society, 77, 437–471, 1996.

Key, R. M., Kozyr, A., Sabine, C. L., Lee, K., Wanninkhof, R., Bullister, J. L., . . . Peng, T.-H.: A global ocean carbon climatology: Results from Global Data Analysis Project (GLODAP), Global Biogeochemical Cycles, 18, https://doi.org/10.1029/2004GB002247, 2004.

Kovaltsov, G. A., and Usoskin, I. G.: A new 3D numerical model of cosmogenic nuclide ^{10}Be production in the atmosphere, Earth and Planetary Science Letters, 291, 182–188, 2010.

Krakauer, N. Y., Randerson, J. T., Primeau, F. W., Gruber, N., and Menemenlis, D.: Carbon isotope evidence for the latitudinal distribution and wind speed dependence of the air-sea gas transfer velocity, Tellus B: Chemical and Physical Meteorology, 58, 390–417, 2006.

Kukla, G., and Robinson, D.: Annual Cycle of Surface Albedo, Monthly Weather Review, 108, 56–68, 1980.

Laj, C., Kissel, C., Mazaud, A., Channell, J. E., and Beer, J.: North Atlantic palaeointensity stack since 75ka (NAPIS-75) and the duration of the Laschamp event, Philosophical Transactions of the Royal Society of London. Series A: Mathematical, Physical and Engineering Sciences, 358, 1009–1025, 2000.

Laj, C., Kissel, C., Mazaud, A., Michel, E., Muscheler, R., and Beer, J.: Geomagnetic field intensity, North Atlantic Deep Water circulation and atmospheric $\Delta^{14}C$ during the last 50 kyr, Earth and Planetary Science Letters, 200, 177-190, 2002.

Laj, C., Kissel, C., and Beer, J.: High resolution global paleointensity stack since 75 kyr (GLOPIS-75) calibrated to absolute values, Timescales of the Paleomagnetic Field, 145, 255–265, 2004.

Laj, C., Guillou, H., and Kissel, C.: Dynamics of the earth magnetic field in the 10-75 kyr period comprising the Laschamp and Mono Lake excursions: New results from the French Chaîne des Puys in a global perspective, Earth and Planetary Science Letters, 387, 184–197, 2014.

Lisiecki, L. E., and Stern, J. V.: Regional and global benthic δ18O stacks for the last glacial cycle, Paleoceanography, 31, 1368–1394, 2016.

Formatted: German (Switzerland)

Müller, J., and Stein, R.: High-resolution record of late glacial and deglacial sea ice changes in Fram Strait corroborates ice–ocean interactions during abrupt climate shifts, Earth and Planetary Science Letters, 403, 446–455, 2014.

Müller, S. A., Joos, F., Edwards, N. R., and Stocker, T. F.: Water Mass Distribution and Ventilation Time Scales in a Cost-Efficient, Three-Dimensional Ocean Model, Journal of Climate, 19, 5479–5499, 2006.

Müller, S. A., Joos, F., Plattner, G.-K., Edwards, N. R., and Stocker, T. F.: Modeled natural and excess radiocarbon: Sensitivities to the gas exchange formulation and ocean transport strength, Global Biogeochemical Cycles, 22, https://doi.org/10.1029/2007GB003065, 2008.

Marchal, O., Stocker, T. F., and Muscheler, R.: Atmospheric radiocarbon during the Younger Dryas: production, ventilation, or both?, Earth and Planetary Science Letters, 185, 383–395, 2001.

Mariotti, V., Paillard, D., Bopp, L., Roche, D. M., and Bouttes, N.: A coupled model for carbon and radiocarbon evolution during the last deglaciation, Geophysical Research Letters, 43, 1306–1313, 2016.

Masarik, J., and Beer, J.: Simulation of particle fluxes and cosmogenic nuclide production in the Earth's atmosphere, Journal of Geophysical Research: Atmospheres, 104, 12099–12111, 1999.

Masarik, J., and Beer, J.: An updated simulation of particle fluxes and cosmogenic nuclide production in the Earth's atmosphere, Journal of Geophysical Research: Atmospheres, 114, https://doi.org/10.1029/2008JD010557, 2009.

Menviel, L., Joos, F., and Ritz, S. P.: Simulating atmospheric CO_2, ^{13}C and the marine carbon cycle during the Last Glacial–Interglacial cycle: possible role for a deepening of the mean remineralization depth and an increase in the oceanic nutrient inventory, Quaternary Science Reviews, 56, 46–68, 2012.

Muscheler, R., and Heikkilä, U.: Constraints on long-term changes in solar activity from the range of variability of cosmogenic radionuclide records, Astrophysics and Space Sciences Transactions, 7, 355–364, 2011.

Muscheler, R., Beer, J., Wagner, G., Laj, C., Kissel, C., Raisbeck, G. M., . . . Kubike, P. W.: Changes in the carbon cycle during the last deglaciation as indicated by the comparison of ^{10}Be and ^{14}C records, Earth and Planetary Science Letters, 219, 325–340, 2004.

Muscheler, R., Adolphi, F., Herbst, K., and Nilsson, A.: The Revised Sunspot Record in Comparison to Cosmogenic Radionuclide-Based Solar Activity Reconstructions, Solar Physics, 291, 3025–3043, 2016.

Nowaczyk, N. R., Arz, H. W., Frank, U., Kind, J., and Plessen, B.: Dynamics of the Laschamp geomagnetic excursion from Black Sea sediments, Earth and Planetary Science Letters, 351-352, 54–69, 2012.

Nowaczyk, N. R., Frank, U., Kind, J., and Arz, H. W.: A high-resolution paleointensity stack of the past 14 to 68 ka from Black Sea sediments, Earth and Planetary Science Letters, 384, 1–16, 2013.

Orr, J. C., Najjar, R. G., Aumont, O., Bopp, L., Bullister, J. L., Danabasoglu, G., . . . Yool, A.: Biogeochemical protocols and diagnostics for the CMIP6 Ocean Model Intercomparison Project (OMIP), Geoscientific Model Development, 10, 2169–2199, 2017.

Parekh, P., Joos, F., and Müller, S. A.: A modeling assessment of the interplay between aeolian iron fluxes and iron-binding ligands in controlling carbon dioxide fluctuations during Antarctic warm events, Paleoceanography and Paleoclimatology, 23, https://doi.org/10.1029/2007PA001531, 2008.

Formatted: German (Switzerland)

Formatted: German (Switzerland)

Peltier, W. R.: Ice Age Paleotopography, Science, 265, 195–201, 1994.

Poluianov, S. V., Kovaltsov, G. A., Mishev, A. L., and Usoskin, I. G.: Production of cosmogenic isotopes ^{7}Be, ^{10}Be, ^{14}C, ^{22}Na, and ^{36}Cl in the atmosphere: Altitudinal profiles of yield functions, Journal of Geophysical Research: Atmospheres, 121, 8125–8136, 2016.

Potgieter, M. S., Vos, E. E., Boezio, M., De Simone, N., Di Felice, V., and Formato, V.: Modulation of Galactic Protons in the Heliosphere During the Unusual Solar Minimum of 2006 to 2009, Solar Physics, 289, 391–406, 2014.

Primeau, F.: Characterizing Transport between the Surface Mixed Layer and the Ocean Interior with a Forward and Adjoint Global Ocean Transport Model, Journal of Physical Oceanography, 35, 545–564, 2005.

Raisbeck, G. M., Cauquoin, A., Jouzel, J., Landais, A., Petit, J.-R., Lipenkov, V. Y., . . . Yiou, F.: An improved north-south synchronization of ice core records around the 41 kyr ^{10}Be peak, Climate of the Past, 13, 217–229, 2017.

Rasmussen, S. O., Abbott, P. M., Blunier, T., Bourne, A. J., Brook, E. J., Buchardt, S. L., . . . Winstrup, M.: A first chronology for the North Greenland Eemian Ice Drilling (NEEM) ice core, Climate of the Past, 9, 2713–2730, 2013.

Reimer, P., Bard, E., Bayliss, A., Beck, J., Blackwell, P., Ramsey, C., . . . Van der Plicht, J.: IntCal13 and Marine13 Radiocarbon Age Calibration Curves 0-50,000 Years cal BP, Radiocarbon, 55, 1869–1887, 2013.

Reimer, P., Austin, W.E.N., Bard, E., Bayliss, A., Blackwell, P. G., Ramsey, C. B., . . . Talamo, S.: The IntCal20 Northern Hemisphere radiocarbon age calibration curve (0-55 kcal BP), Radiocarbon, in press.

Ritz, S. P., Stocker, T. F., and Joos, F.: A Coupled Dynamical Ocean–Energy Balance Atmosphere Model for Paleoclimate Studies, Journal of Climate, 24, 349–375, 2011.

Roth, R., and Joos, F.: A reconstruction of radiocarbon production and total solar irradiance from the Holocene ^{14}C and CO_2 records: implications of data and model uncertainties, Climate of the Past, 9, 1879–1909, 2013.

Roth, R., Ritz, S. P., and Joos, F.: Burial-nutrient feedbacks amplify the sensitivity of atmospheric carbon dioxide to changes in organic matter remineralisation, Earth System Dynamics, 5, 321–343, 2014.

Sarnthein, M., Schneider, B., and Grootes, P. M.: Peak glacial ^{14}C ventilation ages suggest major draw-down of carbon into the abyssal ocean, Climate of the Past, 9, 2595–2614, 2013.

Siegenthaler, U., and Oeschger, H.: Biospheric CO_2 emissions during the past 200 years reconstructed by deconvolution of ice core data, Tellus, 39B, 140–154, 1987.

Siegenthaler, U., Heimann, M., and Oeschger, H.: ^{14}C Variations Caused by Changes in the Global Carbon Cycle, Radiocarbon, 22, 177–191, 1980.

Skinner, L. C., Fallon, S., Waelbroeck, C., Michel, E., and Barker, S.: Ventilation of the Deep Southern Ocean and Deglacial CO_2 Rise, Science, 328, 1147–1151, 2010.

Skinner, L. C., Primeau, F., Freeman, E., de la Fuente, M., Goodwin, P. A., Gottschalk, J., . . . Scrivner, A. E.: Radiocarbon constraints on the glacial ocean circulation and its impact on atmospheric CO_2, Nature Communications, 8, doi:10.1038/ncomms16010, 2017.

Formatted: German (Switzerland)

Deleted: 16010

Skinner, L. C., Muschitiello, F., and Scrivner, A. E.: Marine Reservoir Age Variability Over the Last Deglaciation: Implications for Marine Carbon Cycling and Prospects for Regional Radiocarbon Calibrations, Paleoceanography and Paleoclimatology, 34, 1807–1815, 2019.

Soulet, G., Skinner, L. C., Beaupré, S. R., and Galy, V.: A Note on Reporting of Reservoir ^{14}C Disequilibria and Age Offsets, Radiocarbon, 58, 205–211, 2016.

Southon, J., Noronha, A. L., Cheng, H., Edwards, R. L., and Wang, Y.: A high-resolution record of atmospheric ^{14}C based on Hulu Cave speleothem H82, Quaternary Science Reviews, 33, 32–41, 2012.

Stuiver, M., and Polach, H. A.: Discussion: Reporting of ^{14}C Data, Radiocarbon, 19, 355–363, 1977.

Tschumi, T., Joos, F., and Parekh, P.: How important are Southern Hemisphere wind changes for low glacial carbon dioxide? A model study, Paleoceanography and Paleoclimatology, 23, https://doi.org/10.1029/2008PA001592, 2008.

Tschumi, T., Joos, F., Gehlen, M., and Heinze, C.: Deep ocean ventilation, carbon isotopes, marine sedimentation and the deglacial CO_2 rise, Climate of the Past, 7, 771–800, 2011.

Usoskin, I. G., Hulot, G., Gallet, Y., Roth, R., Licht, A., Joos, F., . . . Khokhlov, A.: Evidence for distinct modes of solar activity, Astronomy & Astrophysics, 562, 1–4, 2014.

Wagner, G., Beer, J., Masarik, J., Muscheler, R., Kubik, P. W., Mende, W., . . . Yiou, F.: Presence of the solar de Vries cycle (~205 years) during the last ice age, Geophysical Research Letters, 28, 303–306, 2001.

Wallmann, K., Schneider, B., and Sarnthein, M.: Effects of eustatic sea-level change, ocean dynamics, and nutrient utilization on atmospheric pCO_2 and seawater composition over the last 130 000 years: a model study, Climate of the Past, 12, 339–375, 2016.

Yiou, F., Raisbeck, G. M., Baumgartner, S., Beer, J., Hammer, C., Johnsen, S., . . . Yiou, P.: Beryllium 10 in the Greenland Ice Core Project ice core at Summit, Greenland, Journal of Geophysical Research: Oceans, 102, 26783–26794, 1997.

Formatted: German (Switzerland)

Formatted: Bibliography,References, Indent: Left: 0 cm, Hanging: 1.27 cm

Deleted: ¶

Deleted: ↵ ↵ ¶

Formatted: Font: 12 pt

Formatted: Normal, Line spacing: single, Don't keep with next

Table 1. Summary of model scenarios considered in this study. Initial conditions refer to the boundary conditions used for the precursor spin-up simulation needed to initialize the transient simulation. These correspond either to preindustrial (PI) or last glacial conditions. The paleoclimate forcing fields, i.e., Orb-GHG-Ice, are reconstructed changes in orbital parameters (Berger, 1978), greenhouse gas radiative forcing based on reconstructed atmospheric greenhouse gas histories (Köhler et al., 2017), and varying ice sheet extent scaled using the global benthic δ^{18}O stack of Lisiecki and Stern (2016). Numbers refer to the scale factor values applied to the tunable model parameters τ (wind stress scale factor), K_V (vertical diffusivity), k_w (gas transfer velocity), rr ($CaCO_3$-to-POC export ratio), and ℓ_{POC} (POC remineralization length scale) at the last glacial maximum (LGM). These values were chosen in order to achieve an atmospheric CO_2 concentration close to the LGM level, and are varied over time using the global benthic δ^{18}O stack. See Roth et al. (2014) for the Bern3D model parameter set. In all scenarios, the fully coupled model configuration, including the major global carbon reservoirs (atmosphere, terrestrial biosphere, ocean, and sediments), is used.

Scenario	Initial conditions	Paleoclimate forcing	Tunable parameters: scale factor at LGM				
			τ	K_V	k_w	rr	ℓ_{POC}
MOD	PI	-	-	-	-	-	-
PAL	Glacial	Orb-GHG-Ice	-	-	-	-	-
CIRC	Glacial	Orb-GHG-Ice	0.4	0.4	-	-	-
VENT	Glacial	Orb-GHG-Ice	0.4	0.4	0.4	-	-
VENTx	Glacial	Orb-GHG-Ice	0.4	0.4	0.0	-	-
BIO	Glacial	Orb-GHG-Ice	-	-	-	0.8	1.2
PHYS-BIO	Glacial	Orb-GHG-Ice	0.7	0.7	0.7	0.7	-
PHYS-BIOx	Glacial	Orb-GHG-Ice	0.8	0.8	0.8	0.8	1.2

Deleted: ¶

Deleted: ¶

Table 2. Production rate estimates in relative units inferred from three fundamentally different reconstruction methods: geomagnetic field data from marine sediments, ^{10}Be and ^{36}Cl measurements in polar ice cores, and model-based deconvolution of atmospheric $\Delta^{14}C$. Laj00, Laj04, Now13, and Chn18 refer to the paleointensity-based reconstructions of Laj et al. (2000), Laj et al. (2004), Nowaczyk et al. (2013), and Channell et al. (2018), respectively. Adp18 refers to the ice-core ^{10}Be-based reconstruction of Adolphi et al. (2018). Int13 and Hul18 refer to the model-based reconstructions from this study, using the IntCal13 calibration curve (Reimer et al., 2013) and the new Hulu Cave $\Delta^{14}C$ dataset (Cheng et al., 2018). The bold numbers show the mean production rates during the last glacial (50 to 18 kyr BP).

	Mean production rate (relative units)						
Time (kyr BP)	Laj00	Laj04	Now13	Chn18	Adp18	Int13	Hul18
50 to 42	1.08	1.04	1.12	1.08	1.01	1.23	1.14
42 to 37	1.57	1.56	1.71	1.36	1.44	1.45	1.67
37 to 32	1.19	1.09	1.35	0.98	1.10	1.25	1.28
32 to 22	1.22	1.15	1.29	0.92	0.99	1.31	1.31
22 to 18	1.31	1.20	1.17	0.81	0.98	1.11	1.11
50 to 18	**1.25**	**1.18**	**1.31**	**1.01**	**1.08**	**1.28**	**1.29**

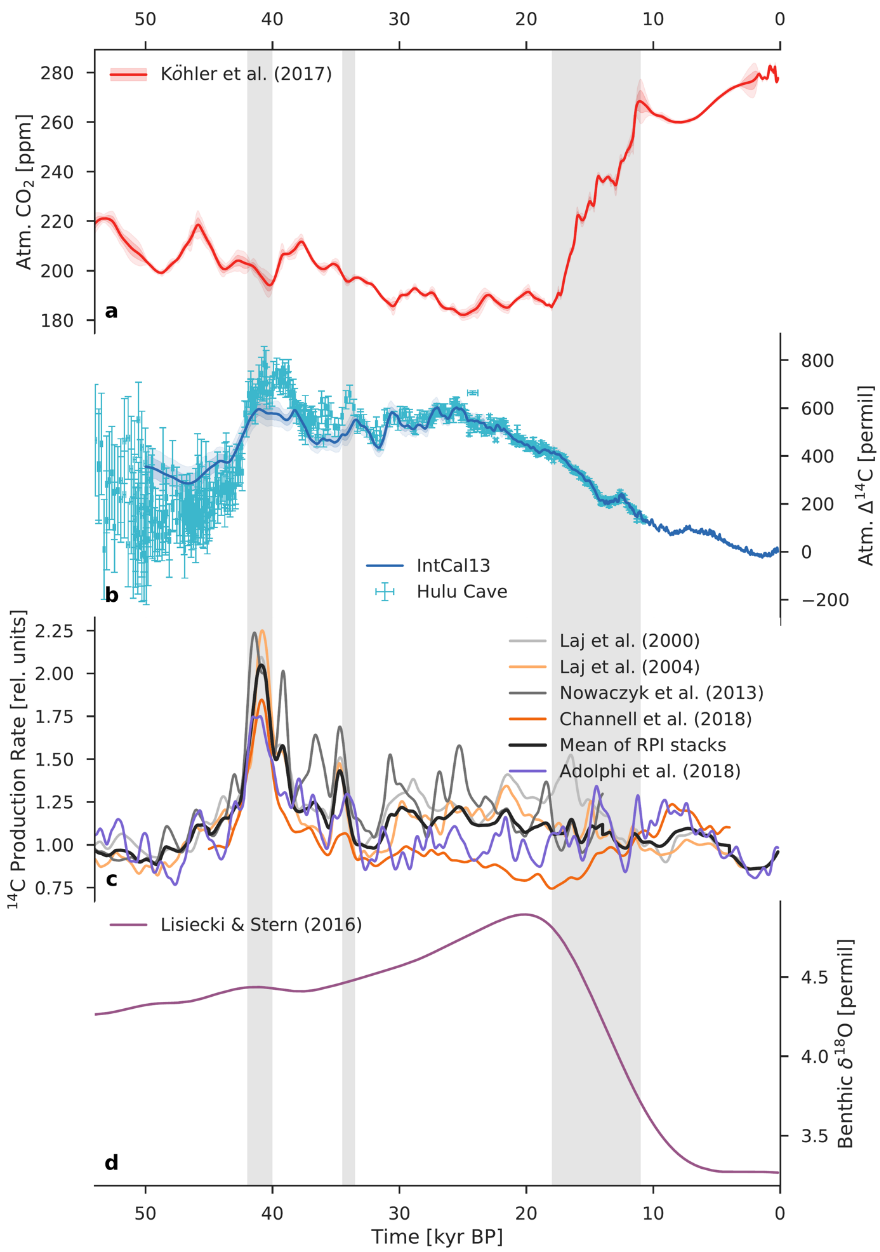

Köhler et al. (2017)
Atm. CO_2 [ppm]
a
IntCal13
Hulu Cave
Atm. $\Delta^{14}C$ [permil]
b
Laj et al. (2000)
Laj et al. (2004)
Nowaczyk et al. (2013)
Channell et al. (2018)
Mean of RPI stacks
Adolphi et al. (2018)
^{14}C Production Rate [rel. units]
c
Lisiecki & Stern (2016)
Benthic $\delta^{18}O$ [permil]
d
Time [kyr BP]

Fig. 1. Comparison of various paleoclimate records for the last 54 kyr. (a) Atmospheric CO_2 from the data compilation of Köhler et al. (2017). The light red envelope shows the uncertainty (2σ). (b) Atmospheric $\Delta^{14}C$ reconstructed from ^{14}C measurements on tree rings, plant macrofossils, speleothems, corals, and foraminifera. The light blue envelope shows the uncertainty (2σ) in the IntCal13 calibration curve (Reimer et al., 2013), whereas the Hulu Cave data (Cheng et al., 2018) are shown with error bars (1σ). Hulu Cave data are consistent with IntCal13 between ~10.6 and 33.3 kyr BP. For both records $\Delta^{14}C$ values were adjusted to the presently accepted value of the radiocarbon half-life (5700 years). (c) ^{14}C production rate in relative units reconstructed from paleointensity data (Laj et al., 2000; Laj et al., 2004; Nowaczyk et al., 2013; Channell et al., 2018) and from polar ice-core ^{10}Be fluxes (Adolphi et al., 2018). The heavy dark gray line is the mean paleointensity-based ^{14}C production rate. (d) Global benthic $\delta^{18}O$ stack, a proxy for ice volume, from Lisiecki and Stern (2016). Three vertical light gray bars indicate the Laschamp excursion (~41 kyr BP), when the Earth's geomagnetic dipole field intensity was close to zero, the Mono Lake geomagnetic excursion (~34 kyr BP), and the last glacial termination (~18 to 11 kyr BP), respectively.

Deleted:

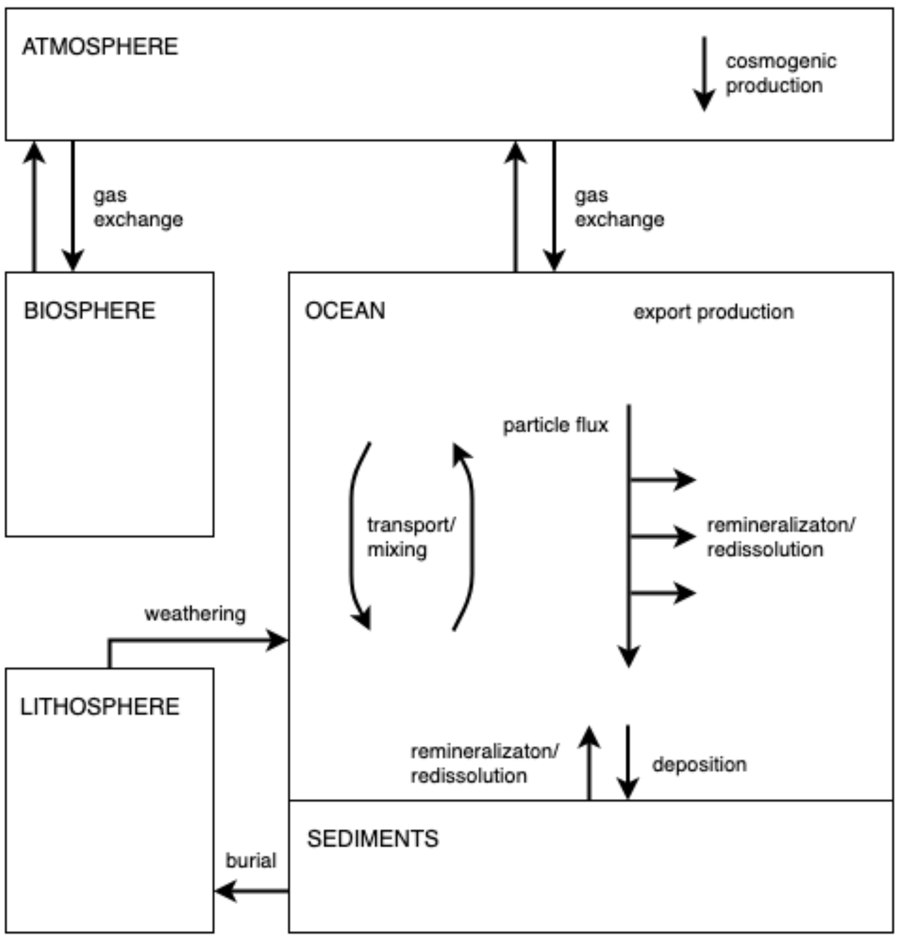

Fig. 2. Schematic diagram of the Bern3D carbon cycle model. The fully coupled model includes the major global carbon reservoirs (atmosphere, terrestrial biosphere, ocean, and sediments) and the exchange fluxes between them. Biogeochemical processes, namely, air-sea gas exchange, biological export production, and particle flux through the water column, are parameterized by refined OCMIP-2 formulations. Details concerning the model are provided in Sect. 2 and Appendix A.

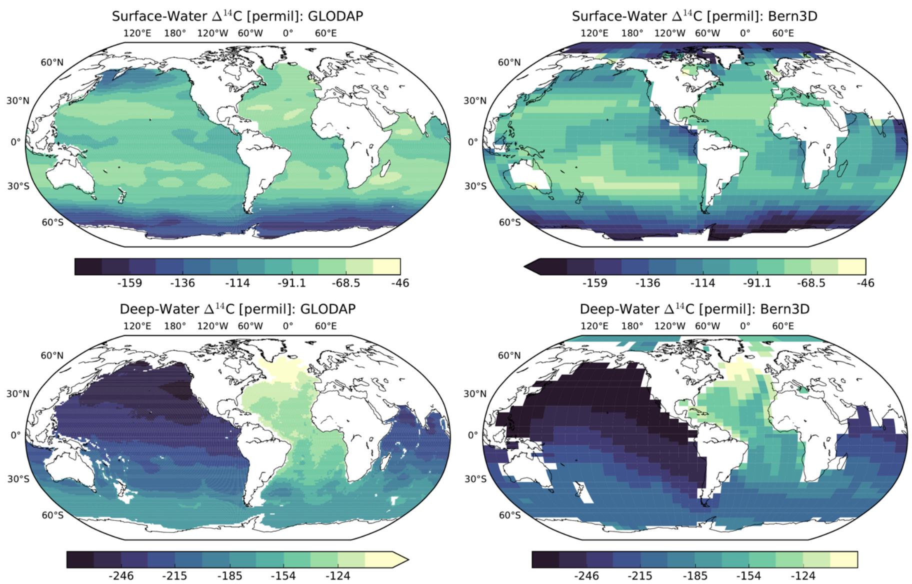

Fig. 3. Steady-state distribution of $\Delta^{14}C$ in the surface (≤ 100 m) and deep (≥ 1500 m) ocean for the preindustrial control run (right), compared to the distribution of $\Delta^{14}C$ based on the Global Ocean Data Analysis Project (GLODAP).

Deleted: >

Deleted: <

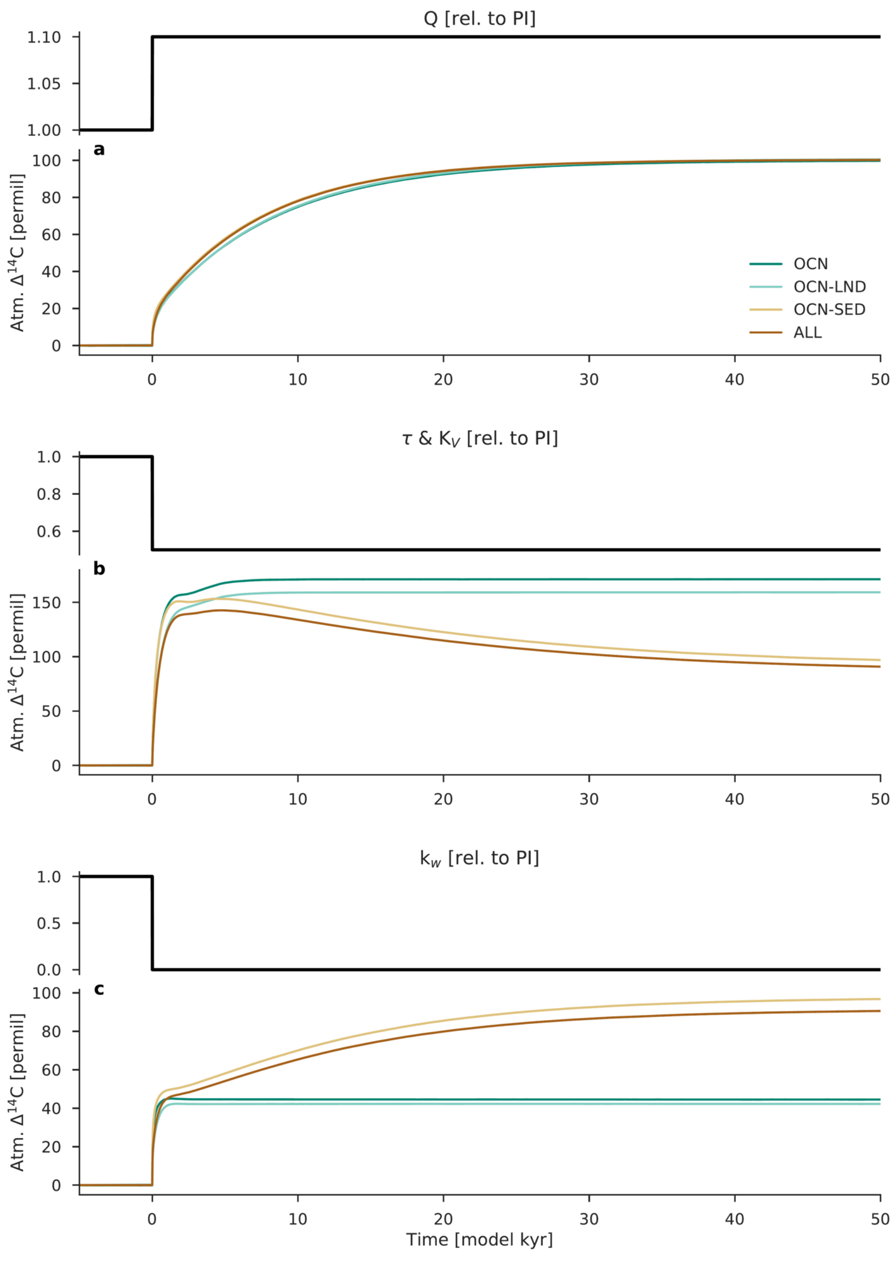

Q [rel. to PI]
a
OCN
OCN-LND
OCN-SED
ALL
Atm. Δ14C [permil]
τ & K_V [rel. to PI]
b
k_w [rel. to PI]
c
Time [model kyr]

Fig. 4. Response of atmospheric $\Delta^{14}C$ to step changes in ^{14}C production, followed by step changes in the tunable model parameters of the ocean carbon cycle. (a) ^{14}C production Q is increased at time 0 from 100 to 110 percent of its preindustrial value ("higher production" scenario). (b) Wind stress scale factor τ and vertical diffusivity K_V are decreased at time 0 from 100 to 50 percent of their preindustrial values ("reduced deep ocean ventilation" scenario). (c) Gas transfer velocity k_w is decreased at time 0 from 100 to 0 percent of its preindustrial value at the north (> 60°N) and south (> 48°S) poles ("enhanced permanent sea ice cover" scenario). Four model configurations are considered. The dark turquoise line shows the model results using the atmosphere–ocean (OCN) configuration, the light turquoise line is the atmosphere–ocean–land (OCN-LND) configuration, the light brown line is the atmosphere–ocean–sediment (OCN-SED) configuration, and the dark brown line is the atmosphere–ocean–land–sediment (ALL) configuration.

1757

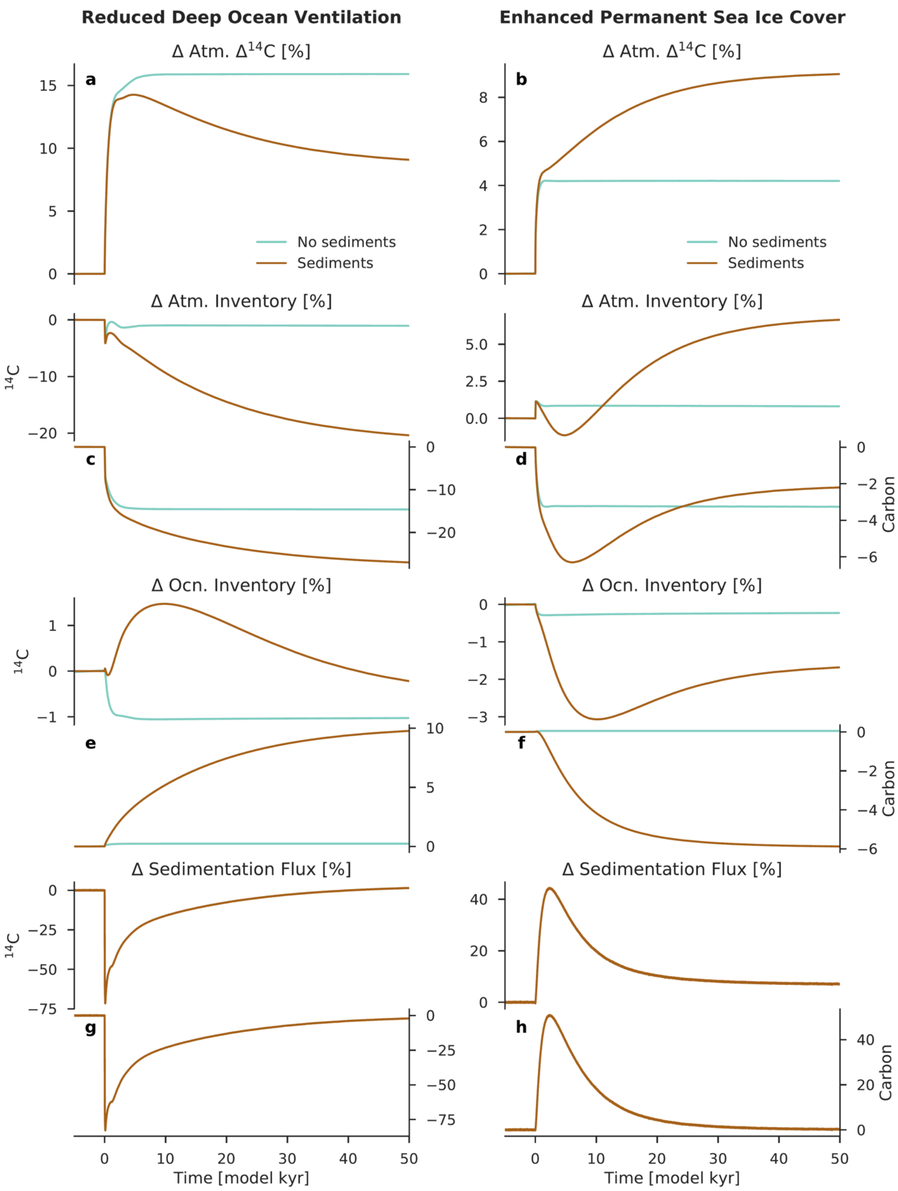

Reduced Deep Ocean Ventilation
Enhanced Permanent Sea Ice Cover
Δ Atm. Δ14C [%]
Δ Atm. Inventory [%]
Δ Ocn. Inventory [%]
Δ Sedimentation Flux [%]
No sediments
Sediments
14C
Carbon
Time [model kyr]

Fig. 5. Changes in carbon reservoir sizes and the sedimentation flux for the scenarios "reduced deep ocean ventilation" (left) and "enhanced permanent sea ice cover" (right). The change in atmospheric $\Delta^{14}C$ is also shown (a, b). Anomalies are expressed here as differences relative to the preindustrial steady state (in percent). Turquoise lines show the model results using configuration OCN-LND (without sediments) and brown lines are configuration ALL (with sediments). The y-axis on the left-hand side of each panel refers to changes in the ^{14}C inventory, whereas the y-axis on the right-hand side of each panel refers to changes in the carbon inventory or flux.

Deleted: no

Deleted: model includes

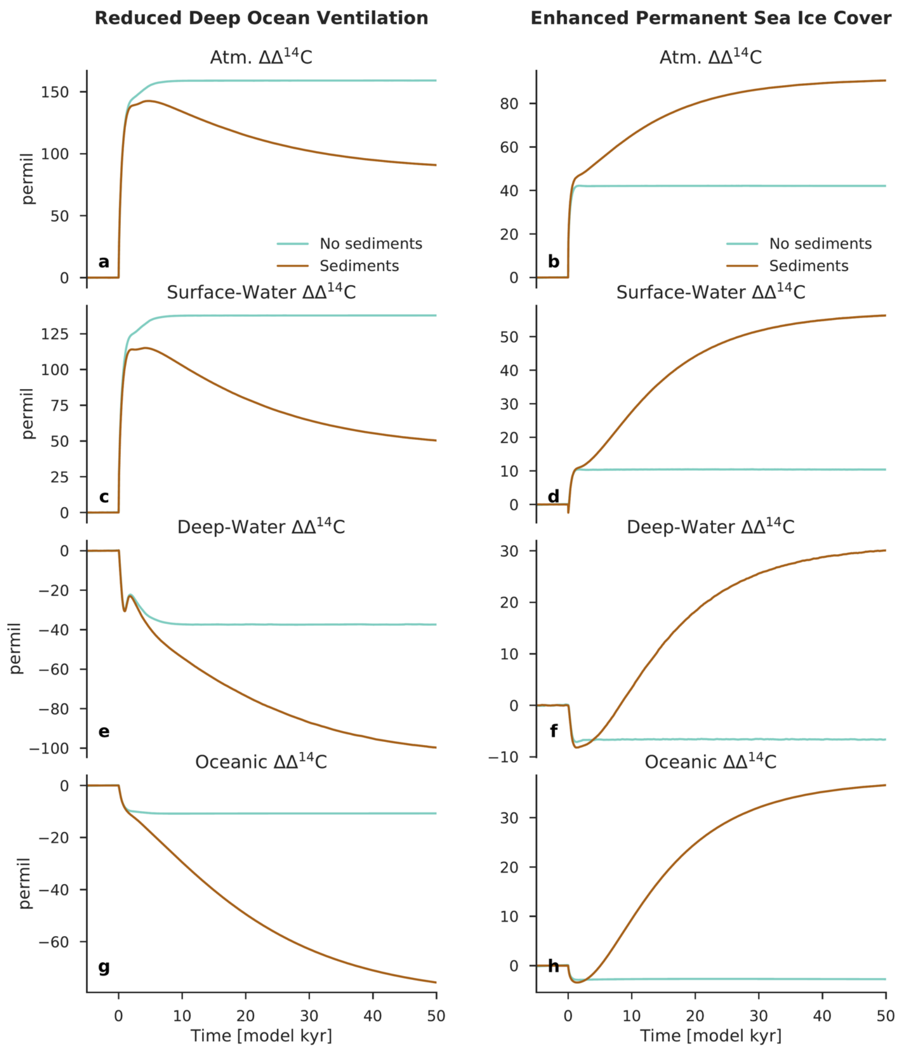

Fig. 6. Change in $\Delta^{14}C$ for the atmosphere, surface ocean, deep ocean, and global ocean for the scenarios "reduced deep ocean ventilation" (left) and "enhanced permanent sea ice cover" (right). Anomalies are expressed here as differences relative to the preindustrial steady state (in permil). Turquoise lines show the model results using configuration OCN-LND (without sediments) and brown lines are configuration ALL (with sediments).

Deleted: no

Deleted: model includes

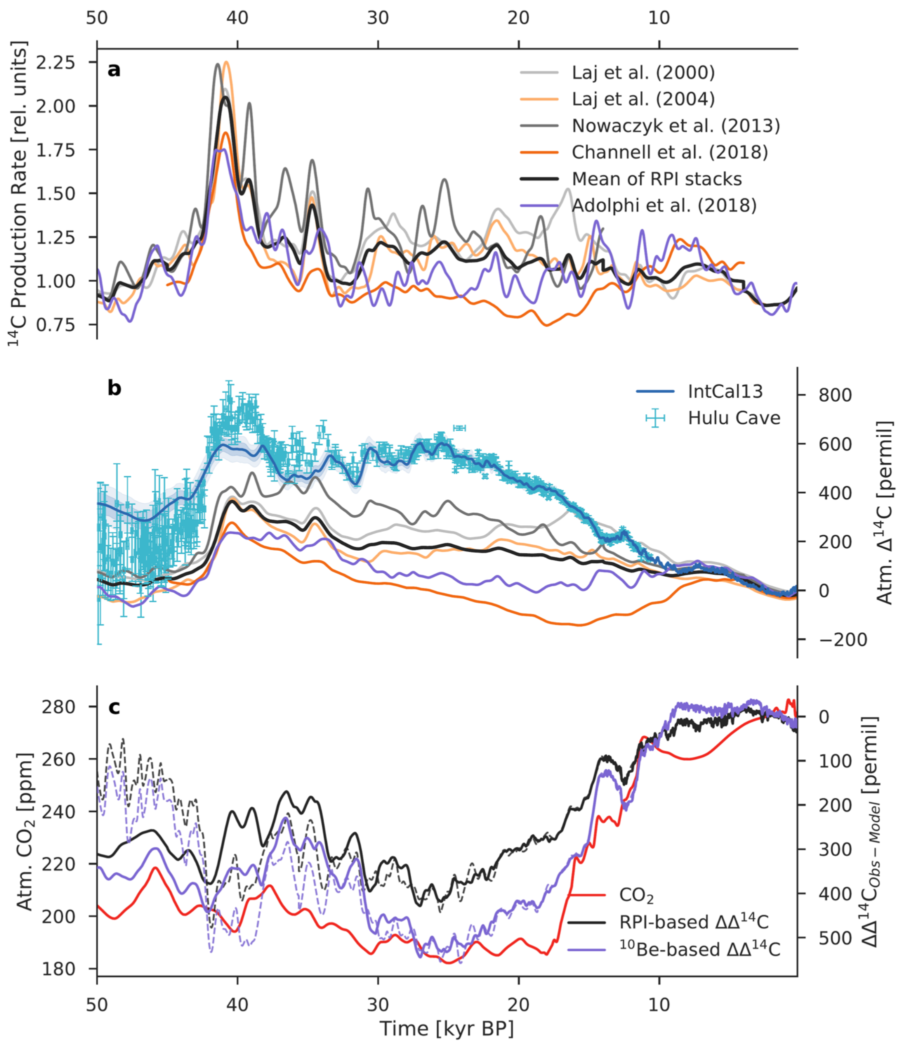

Fig. 7. Component of atmospheric Δ^{14}C variability caused by production changes alone. (a) Relative ^{14}C production rate as inferred from paleointensity data (gray) and from polar ice-core ^{10}Be fluxes (purple). The heavy dark gray line is the mean paleointensity-based ^{14}C production rate. (b) Modelled Δ^{14}C records based only on ^{14}C production changes, compared with the reconstructed IntCal13 and Hulu Cave Δ^{14}C records. The modelled records are given by scenario MOD that assumes a constant preindustrial carbon cycle. (c) Difference between reconstructed Δ^{14}C and model-simulated Δ^{14}C using averaged paleointensity data (RPI-based $\Delta\Delta^{14}$C; gray) and the ice-core ^{10}Be data of Adolphi et

al. (2018) (^{10}Be-based $\Delta\Delta^{14}$C; purple), compared with the atmospheric CO_2 record (red). Solid lines show the IntCal13–model difference, whereas dashed lines show the Hulu–model difference. The $\Delta\Delta^{14}$C curve indicates changes in Δ^{14}C that can be attributed to some combination of carbon cycle changes, uncertainties in the reconstruction of the ^{14}C production rate, and uncertainties in the IntCal13 and Hulu Cave Δ^{14}C records.

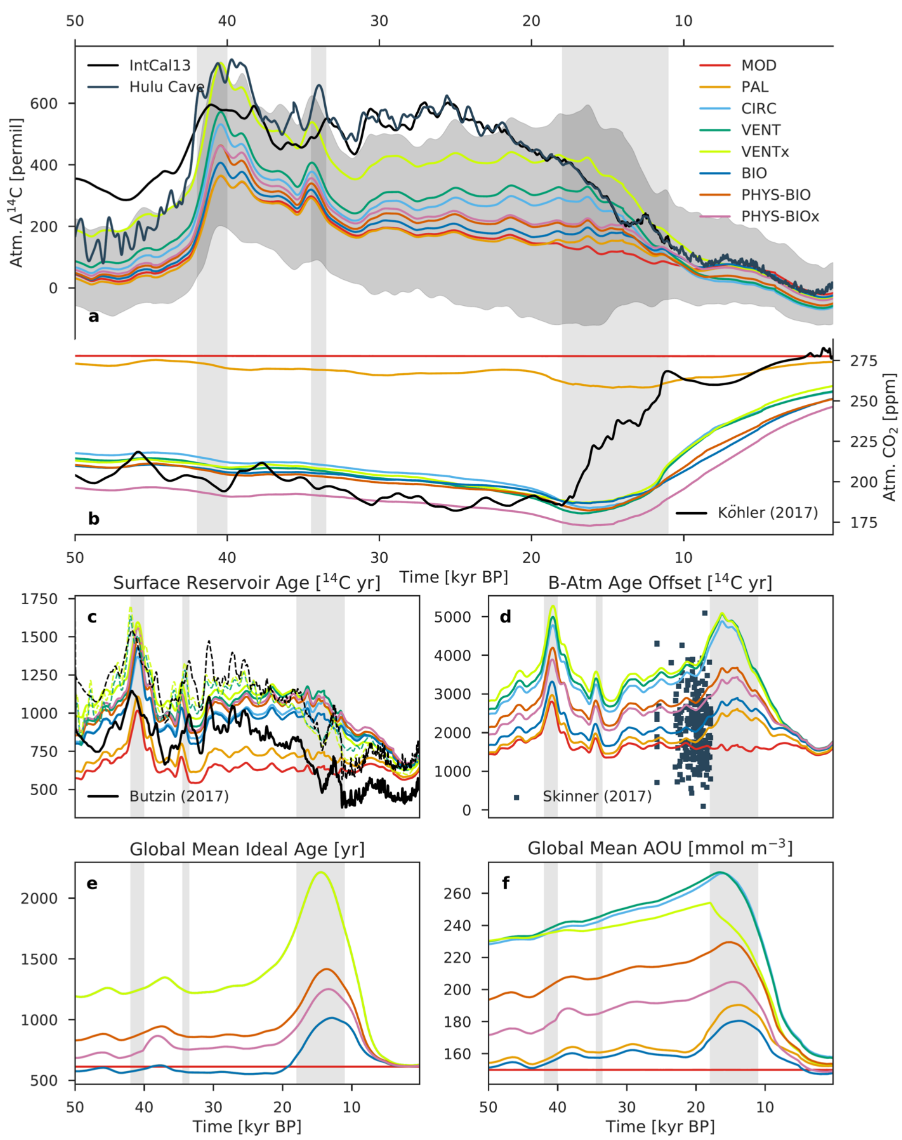

Fig. 8. Modelled records of atmospheric (a) $\Delta^{14}C$ and (b) CO_2, compared with their reconstructed histories (black and dark blue lines). Also shown are modelled records of the global average (c) surface reservoir age and (d) B-Atm ^{14}C age offset, compared with a recent compilation of LGM marine radiocarbon data (dark blue squares) by Skinner et al.

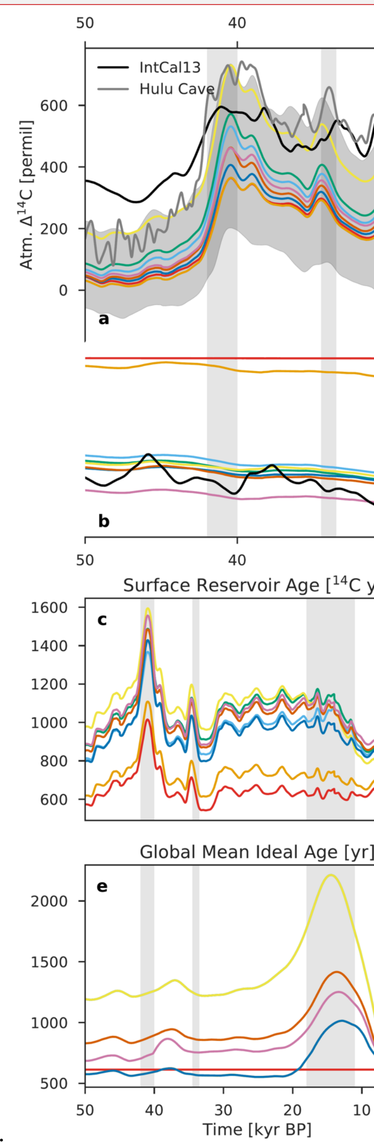

Deleted:

Deleted: atmospheric

Deleted: gray

Deleted: ,

(2017) and model-based surface reservoir age estimates between 50°N and 50°S (solid black line) and across all latitudes (dashed black line) from Butzin et al. (2017), as well as (e) ideal age and (f) apparent oxygen utilization (AOU). Colored lines show the results of model runs using the mean paleointensity-based ^{14}C production rate and the eight different carbon cycle scenarios described in Sect. 2.4 and Table 1. The gray envelope in (a) shows the uncertainty (2σ) from all production rate reconstructions and carbon cycle scenarios, providing a bounded estimate of $\Delta^{14}C$ change. The dashed colored lines in (c) show the surface reservoir age results from VENT and VENTx where atmospheric $\Delta^{14}C$ and CO_2 are prescribed. Radiocarbon ventilation ages are expressed here as radiocarbon reservoir age offsets following Soulet et al. (2016) which are used extensively by the radiocarbon dating community.

Deleted: ,

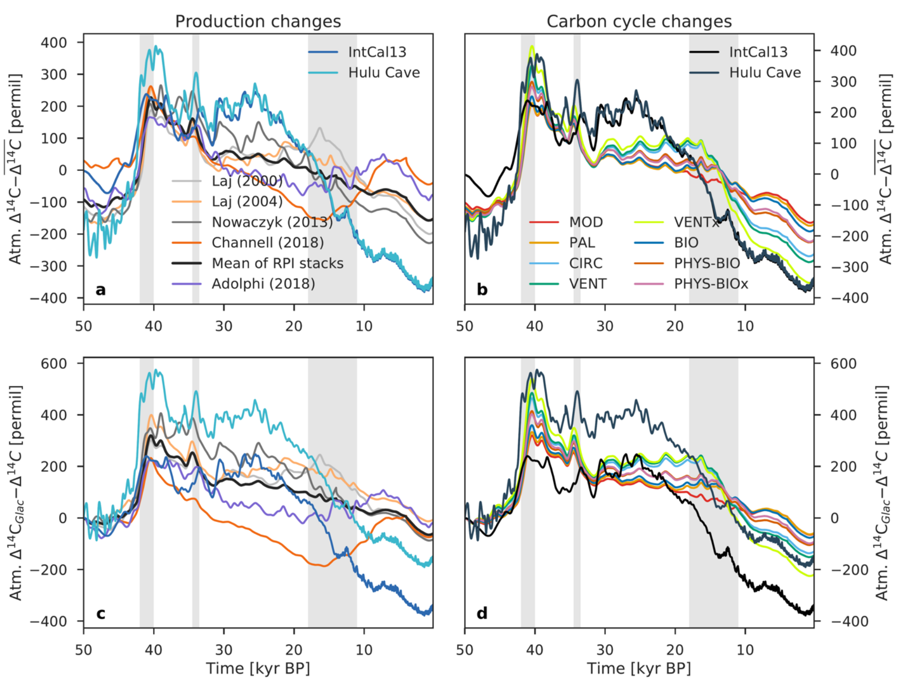

Fig. 9. Comparison of atmospheric $\Delta^{14}C$ variability caused by changes in the ocean carbon cycle (b, d) with production-driven changes in atmospheric $\Delta^{14}C$ using scenario MOD (a, c). For the analysis of carbon cycle changes, only the results of model runs using the mean paleointensity-based ^{14}C production rate are shown. The $\Delta^{14}C$ records in the upper panel (a, b) have been detrended by removing the mean, whereas the lower panel (c, d) shows $\Delta^{14}C$ anomalies expressed as differences relative to the $\Delta^{14}C$ value at 50 kyr BP. Three vertical light gray bars indicate the Laschamp (~41 kyr BP) and Mono Lake (~34 kyr BP) geomagnetic excursions, and the last glacial termination (~18 to 11 kyr BP).

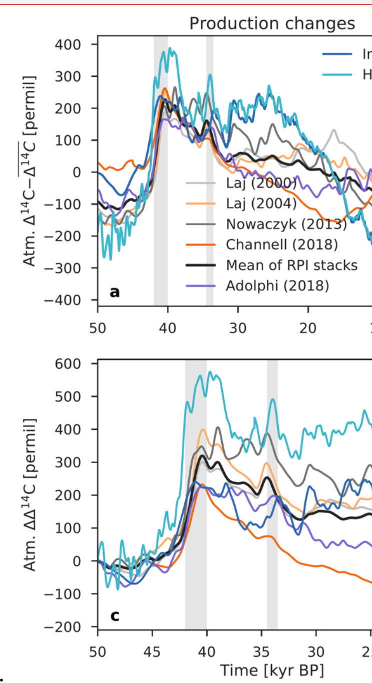

Deleted:

Deleted: to

Deleted: e

Deleted: , only for the portion of the record older than 18 kyr BP…

Deleted: Two

Deleted: .

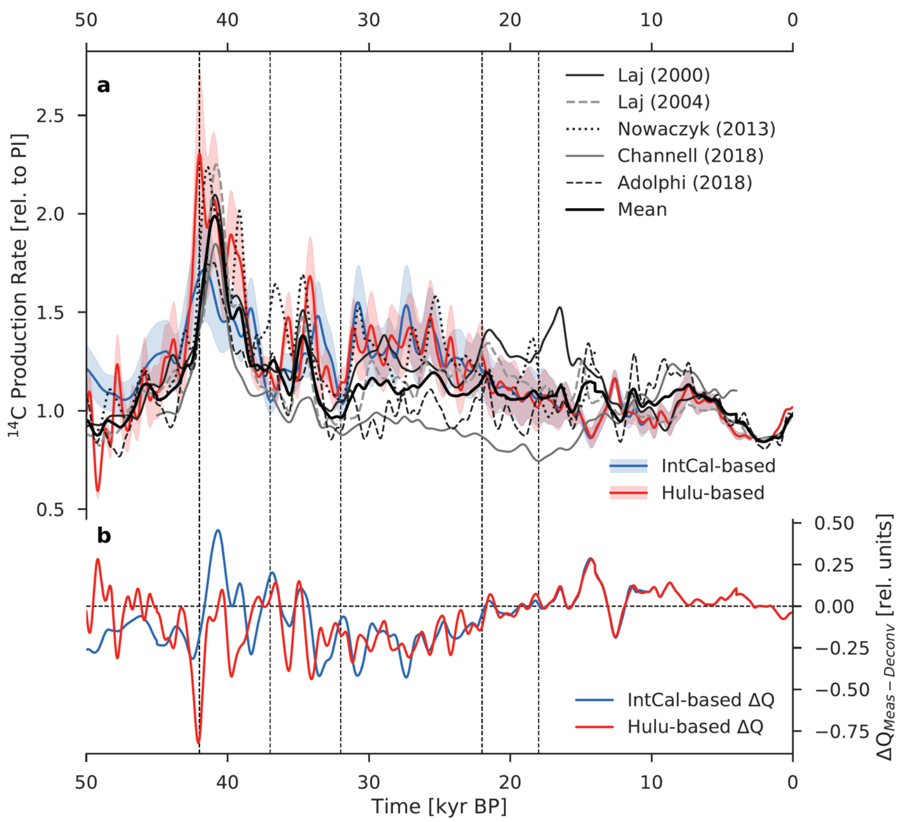

Fig. 10. Comparison of ^{14}C production rate estimates inferred from a deconvolution of the atmospheric Δ^{14}C record and from paleointensity and ice-core ^{10}Be data. (a) ^{14}C production rate calculated as the sum of the modelled air-sea and atmosphere-land $^{14}CO_2$ fluxes and the reconstructed change in the atmospheric ^{14}C inventory and loss of ^{14}C due to radioactive decay (see Eq. [2]). Model-based $^{14}CO_2$ fluxes were obtained by forcing the Bern3D carbon cycle model with reconstructed variations in atmospheric Δ^{14}C and CO_2 as well as seven different carbon cycle scenarios. Results of model runs using the IntCal13 calibration curve are shown in the light blue envelope (2σ), whereas the light red envelope (2σ) shows the results from simulations using the composite Hulu Cave (10.6 to 50 kyr BP) and IntCal13 (0 to 10.6 kyr BP) Δ^{14}C record. The heavy black line is the mean of five available production rate reconstructions: Laj et al. (2000), Laj et al. (2004), Nowaczyk et al. (2013), Channell et al. (2018), and Adolphi et al. (2018). (b) Difference between the mean of the measurement-based production rate estimates (heavy black line) and estimates based on the deconvolution of the IntCal13 (IntCal-based ΔQ; blue) and Hulu Cave (Hulu-based ΔQ; red) Δ^{14}C data.

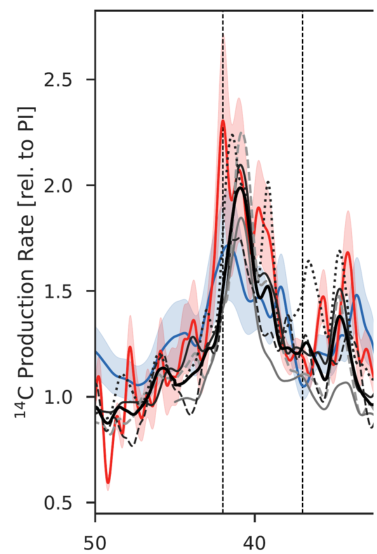

Deleted:

Deleted: Model-based

Deleted: rate in relative units compared with

Formatted: Font: Not Bold

Deleted: -based and

Deleted: -based estimates

Formatted: Font: Not Bold

Deleted: Here, the

Formatted: Font: Not Bold

Deleted: ^{14}C production rate is inferred from an atmospheric radiocarbon budget, using the Bern3D carbon cycle model

Deleted: forced

Deleted: .

Deleted: and seven carbon cycle scenarios

Deleted: . T

Deleted: obtained

Deleted: the

Formatted: Font: Not Bold

Deleted: ¶
¶
¶
¶
¶
¶

... [6]

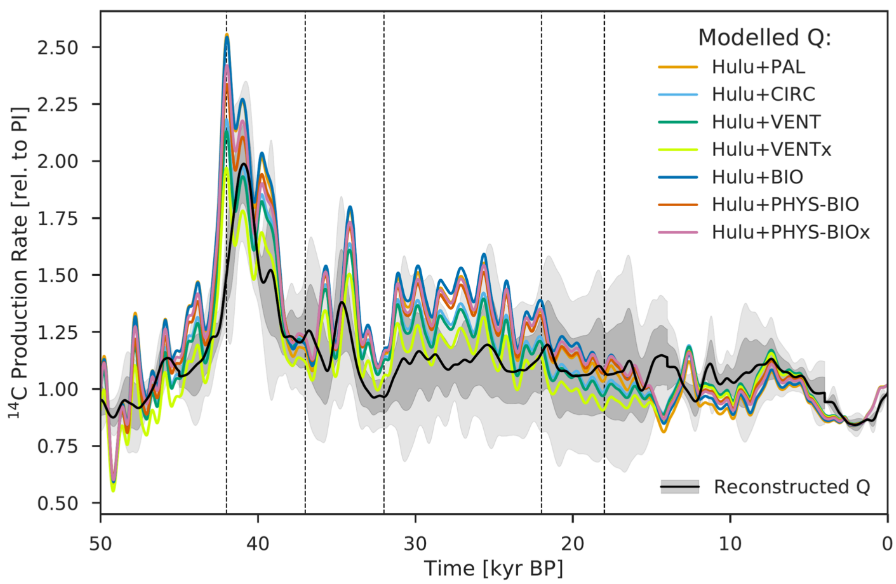

Fig. 11. Relative ^{14}C production rate as inferred from the Bern3D model under seven carbon cycle scenarios (see Sect. 2.4). Estimates shown here are based on the composite Hulu Cave and IntCal13 Δ^{14}C record. The black line is the mean of the five production rate reconstructions shown in Fig. 10; the gray envelope shows its uncertainty (2σ).

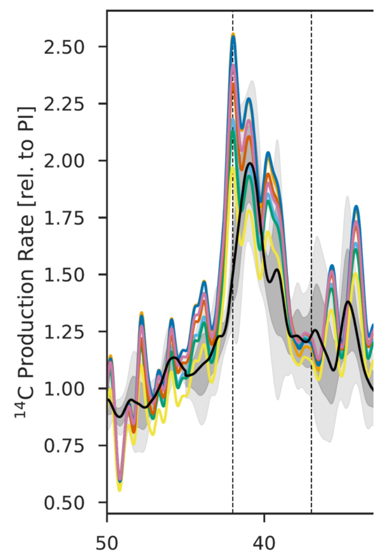

Deleted:

Deleted: obtained by

Deleted: available

Deleted: Fig. 10

Page 16: [1] Deleted	Dinauer, Ashley Marie (STUDENTS)	27/03/2020 19:30:00

Page 16: [1] Deleted	Dinauer, Ashley Marie (STUDENTS)	27/03/2020 19:30:00

Page 16: [2] Deleted	Dinauer, Ashley Marie (STUDENTS)	29/03/2020 13:55:00

Page 16: [2] Deleted	Dinauer, Ashley Marie (STUDENTS)	29/03/2020 13:55:00

Page 16: [3] Deleted	Dinauer, Ashley Marie (STUDENTS)	29/03/2020 13:49:00

Page 16: [3] Deleted	Dinauer, Ashley Marie (STUDENTS)	29/03/2020 13:49:00

Page 16: [3] Deleted	Dinauer, Ashley Marie (STUDENTS)	29/03/2020 13:49:00

Page 16: [3] Deleted	Dinauer, Ashley Marie (STUDENTS)	29/03/2020 13:49:00

Page 16: [3] Deleted	Dinauer, Ashley Marie (STUDENTS)	29/03/2020 13:49:00

Page 16: [3] Deleted	Dinauer, Ashley Marie (STUDENTS)	29/03/2020 13:49:00

Page 16: [4] Deleted	Dinauer, Ashley Marie (STUDENTS)	05/05/2020 16:48:00

Page 16: [4] Deleted	Dinauer, Ashley Marie (STUDENTS)	05/05/2020 16:48:00

Page 16: [4] Deleted	Dinauer, Ashley Marie (STUDENTS)	05/05/2020 16:48:00

Page 16: [4] Deleted	Dinauer, Ashley Marie (STUDENTS)	05/05/2020 16:48:00

Page 16: [4] Deleted	Dinauer, Ashley Marie (STUDENTS)	05/05/2020 16:48:00

Page 16: [4] Deleted	Dinauer, Ashley Marie (STUDENTS)	05/05/2020 16:48:00

Page 16: [4] Deleted	Dinauer, Ashley Marie (STUDENTS)	05/05/2020 16:48:00

Page 16: [4] Deleted	**Dinauer, Ashley Marie (STUDENTS)**	**05/05/2020 16:48:00**

Page 16: [4] Deleted	**Dinauer, Ashley Marie (STUDENTS)**	**05/05/2020 16:48:00**

Page 16: [4] Deleted	**Dinauer, Ashley Marie (STUDENTS)**	**05/05/2020 16:48:00**

Page 16: [5] Deleted	**Dinauer, Ashley Marie (STUDENTS)**	**04/04/2020 13:04:00**

Page 16: [5] Deleted	**Dinauer, Ashley Marie (STUDENTS)**	**04/04/2020 13:04:00**

Page 16: [5] Deleted	**Dinauer, Ashley Marie (STUDENTS)**	**04/04/2020 13:04:00**

Page 16: [5] Deleted	**Dinauer, Ashley Marie (STUDENTS)**	**04/04/2020 13:04:00**

Page 16: [5] Deleted	**Dinauer, Ashley Marie (STUDENTS)**	**04/04/2020 13:04:00**

Page 16: [5] Deleted	**Dinauer, Ashley Marie (STUDENTS)**	**04/04/2020 13:04:00**

Page 16: [5] Deleted	**Dinauer, Ashley Marie (STUDENTS)**	**04/04/2020 13:04:00**

Page 16: [5] Deleted	**Dinauer, Ashley Marie (STUDENTS)**	**04/04/2020 13:04:00**

Page 16: [5] Deleted	**Dinauer, Ashley Marie (STUDENTS)**	**04/04/2020 13:04:00**

Page 16: [5] Deleted	**Dinauer, Ashley Marie (STUDENTS)**	**04/04/2020 13:04:00**

Page 16: [5] Deleted	**Dinauer, Ashley Marie (STUDENTS)**	**04/04/2020 13:04:00**

Page 16: [5] Deleted	**Dinauer, Ashley Marie (STUDENTS)**	**04/04/2020 13:04:00**

Page 16: [5] Deleted	**Dinauer, Ashley Marie (STUDENTS)**	**04/04/2020 13:04:00**

Page 16: [5] Deleted	**Dinauer, Ashley Marie (STUDENTS)**	**04/04/2020 13:04:00**

Page 16: [5] Deleted	**Dinauer, Ashley Marie (STUDENTS)**	**04/04/2020 13:04:00**
Page 16: [5] Deleted	**Dinauer, Ashley Marie (STUDENTS)**	**04/04/2020 13:04:00**
Page 16: [5] Deleted	**Dinauer, Ashley Marie (STUDENTS)**	**04/04/2020 13:04:00**
Page 16: [5] Deleted	**Dinauer, Ashley Marie (STUDENTS)**	**04/04/2020 13:04:00**
Page 16: [5] Deleted	**Dinauer, Ashley Marie (STUDENTS)**	**04/04/2020 13:04:00**
Page 16: [5] Deleted	**Dinauer, Ashley Marie (STUDENTS)**	**04/04/2020 13:04:00**
Page 16: [5] Deleted	**Dinauer, Ashley Marie (STUDENTS)**	**04/04/2020 13:04:00**
Page 16: [5] Deleted	**Dinauer, Ashley Marie (STUDENTS)**	**04/04/2020 13:04:00**
Page 16: [5] Deleted	**Dinauer, Ashley Marie (STUDENTS)**	**04/04/2020 13:04:00**
Page 48: [6] Deleted	**Dinauer, Ashley Marie (STUDENTS)**	**05/04/2020 16:48:00**